

**MEMBRANE- BASED SEPARATION OF OIL-WATER EMULSIONS: EFFECT OF
SURFACTANTS AND SALINITY**

By

Charifa Ale Hejase

A DISSERTATION

Submitted to
Michigan State University
in partial fulfillment of the requirements
for the degree of

Environmental Engineering – Doctor of Philosophy
Environmental Science and Policy – Dual Major

2020

ABSTRACT

MEMBRANE -BASED SEPARATION OF OIL-WATER EMULSIONS: EFFECT OF SURFACTANTS AND SALINITY

By

Charifa Ale Hejase

In the last decade, oil-water separation has gained global interest due to the large volumes of oily wastewater produced by various industries (e.g. food and beverage, metal and machining, pharmaceuticals) and the frequent oil spill accidents. Oil pollution is not only a pressing environmental problem, but it can also adversely impact human health due to contaminated water resources and crop production. Compared to other de-oiling technologies, membrane filtration offers several advantages including high quality permeate and ease of operation. To improve the feasibility of membranes for oil-water separation, a thorough understanding of oil deposition at the membrane surface during separation is needed to both optimally design and operate such processes.

In this dissertation, Direct Observation Through the Membrane (DOTM) technique was employed to visualize oil drops in real-time at the membrane surface under conditions of hydrodynamic shear. This work was complemented by modeling of oil-membrane interactions and bench-scale crossflow filtration tests to gain quantitative understanding of oil droplet deposition on porous ultrafiltration (UF) and salt rejecting nanofiltration (NF) membranes. Experimental variables included surfactant type, salt type and concentration, and membrane material as well as pore size. Membrane fouling by emulsified oil was found to be a strong function of surfactant type. Visualization tests revealed that the worst type of fouling was observed when droplet coalescence resulted in contiguous oil films sealing large areas of the membrane. The visualization work was

supplemented by deposition kinetics model that describes the three distinct stages of UF membrane fouling: (1) droplet deposition when the membrane surface is oil-free; (2) droplet deposition when membrane is coated by droplets; and (3) surface coalescence of droplets resulting in film formation. Nanofiltration of highly saline oil-water emulsions revealed that NF membrane fouling by emulsified oil enhances concentration polarization of rejected salt. However, headloss analysis showed that over the longer term, the additional hydraulic resistance due to a layer of oil droplets on the membrane surface became the dominant fouling mechanism.

For both NF and UF membranes, when droplet-membrane interactions were favorable, this scenario led to formation and growth of surface films. These findings call for membrane materials or coatings that stunt the movement of the three-phase contact line to prevent oil film formation and spreading over the membrane surface. From the process engineering perspective, membrane surface sealing by oil films can be effectively managed by a hydraulic flush at zero transmembrane pressure.

Finally, to achieve pipe parity, oil-water separation technologies need to consider legislature and regulations as well as environmental and social impacts (i.e. public perception).

Copyright by
CHARIFA ALE HEJASE
2020

This dissertation is dedicated to my nieces,
Leila and Rachelle.

ACKNOWLEDGMENTS

The completion of this journey could not have been possible without the support of so many people whose names may not all be enumerated. Their contributions are sincerely appreciated and gratefully acknowledged.

First and foremost, I express my sincerest gratitude and profound respect to my advisor, Dr. Volodymyr Tarabara, who has helped encourage me during all stages of graduate school with great patience and immense care. I met Dr. Tarabara as an undergraduate student in his CE 272 class and I was drawn to his passion and devotion for his research work. I am particularly grateful for his understanding, emphasis on collaboration, and encouragement to publish journal papers and attend conferences. Thank you for your guidance and support.

Second, I would like to express my deepest appreciation to my dissertation committee, Dr. André Bénard, Dr. Annick Anctil, and Dr. Wei Zhang, for their thoughtful guidance and valuable insights along the way. This guidance committee always raised key questions and gave valuable input that forced me to think about my research work from different angles. I'm also extremely grateful to Dr. Merlin Bruening for our many technical discussions during the early stages of my PhD journey.

To the Tarabara group former and current members, thank you for the supportive and friendly work environment. Particularly I would like to thank Dr. Emily Tummons for her advice and protocol expertise. I am also grateful to Dr. Christopher Crock, who introduced me to research as an undergraduate student. Thank you all for the stimulating discussions, your positive attitudes, and friendships that will last beyond MSU.

A word of appreciation goes to our collaborators at Singapore Membrane Technology Centre and HTW Berlin particularly Dr. Jia Wei Chew.

I also want to acknowledge the great faculty and staff members in the Department of Civil and Environmental Engineering. My appreciation goes to Dr. Susan Masten for her excellent lectures and Dr. Annick Ancil for introducing me to the area of life cycle assessment. Many thanks to Lori Larner, Laura Post, and Joseph Nguyen for their administrative and technical support.

Finally, and most importantly, I'm extremely grateful to my parents, Ale and Layla, for their unconditional love, prayers, and sacrifices to educate me and provide me with a better future. To my brothers, Jose, Hussein, and Ahmad, thank you for being my backbone and best friends. Finally, to our newest family members, Leila and Rachelle, thank you for always putting a smile on my face.

TABLE OF CONTENTS

LIST OF TABLES.....	xi
LIST OF FIGURES.....	xii
KEY TO SYMBOLS.....	xvii
CHAPTER ONE	1
OVERVIEW.....	1
CHAPTER TWO.....	3
Membrane-based separation of oily wastewater*.....	3
Abstract.....	3
2.1. Introduction	4
2.1.1. Oily wastewater: Sources, quantities and composition	6
2.1.2. Regulations for discharging oily wastewater	7
2.1.3. Oily wastewater treatment: Conventional technologies.....	8
2.2. Membrane technology for oil-water separation	10
2.2.1. Commercially-available membranes for oily industrial wastewater	11
2.2.2. Membrane modules	15
2.2.3. Hybrid membrane processes	18
2.2.4. Economics of membrane-based treatment of oily wastewater.....	20
2.3. The challenges of membrane operation	21
2.3.1. Mechanisms of membrane fouling by oil.....	21
2.3.2. Mitigating membrane fouling by oil: An overview of methods	23
2.3.2.1. Materials science approach: Making membranes resistant to fouling	24
2.3.2.2. “Damage-control” approach: Devising effective methods of membrane cleaning.....	27
2.3.3. Quantifying the extent of membrane fouling	29
2.3.3.1. Permeate flux	29
2.3.3.2. Selectivity	31
2.3.4. Evaluating the fouling potential of the feed solution.....	33
2.3.4.1. Silt Density Index (SDI)	33
2.3.4.2. Modified Fouling Index (MFI) and Combined Fouling Index (CFI).....	34
2.3.4.3. Applicability of SDI, MFI, and CFI to quantifying membrane fouling by oil- water emulsions.....	36
2.4. Understanding membrane fouling by oily wastewater: Measurement approaches and techniques	37
2.4.1. Offline Measurement.....	37
2.4.1.1. Direct Observation through Membrane (DOTM) and other microscopy- based techniques.....	37
2.4.1.2. Optical Coherence Tomography (OCT).....	39
2.5. Conclusions.....	40

CHAPTER THREE	43
Membrane fouling by surfactant-stabilized oil-water emulsions: Effect of emulsion stability and salinity	43
3.1. Introduction	43
3.2. Materials and Methods	48
3.2.1. Reagents.....	48
3.2.2. Emulsion preparation	48
3.2.3. Emulsion characterization	49
3.2.4. Membranes used in DOTM tests. Characterization	49
3.2.5. Direct observation through the membrane (DOTM) system.....	49
3.3. Results and Discussion	50
3.3.1. Characteristic of oil-water emulsions	50
3.3.1.1. Droplet size distribution.....	51
3.3.1.2. Interfacial tension.....	52
3.3.2. Membrane characterization.....	54
3.3.2.1. Contact angle measurements	54
3.3.3. DOTM tests with oil-in-water emulsions	57
3.3.3.1. Effect of surfactant type on UF membrane fouling by emulsified oil	57
3.3.3.2. Effect of salt type on UF membrane fouling by emulsified oil.....	59
3.5. Conclusions.....	66
APPENDIX	67
CHAPTER FOUR.....	79
Nanofiltration of saline oil-water emulsions: Combined effect of salt concentration polarization and fouling by oil*	79
Abstract.....	79
4.1. Introduction	80
4.2. Approach.....	83
4.2.1. Background.....	83
4.2.2. Quantifying separate contributions of membrane fouling and osmotic pressure to permeate flux decline	85
4.3. Materials and Methods	87
4.3.1. Reagents.....	87
4.3.2. Oil-water emulsion preparation and characterization	87
4.3.3. Crossflow filtration system	88
4.3.4. Experimental protocol	89
4.4. Results and Discussion	90
4.4.1. Oil-water emulsions: Droplet size and interfacial tension	90
4.4.2. Determining concentration dependence of NF transport coefficients.....	91
4.4.2.1. NaCl reflection coefficient, σ , as a function of NaCl concentration.....	91
4.4.2.2. NaCl permeability coefficient, B, as a function of NaCl concentration.....	92
4.4.3. Oil fouling experiments: Permeate flux and salt rejection at different ionic strengths	94
4.4.4. Headloss analysis. Implications for practice.....	98
4.4.4.1. Instantaneous flux decline	98

4.4.4.2 Headloss analysis: Relative contributions fouling and osmotic pressure to flux decline.....	101
4.4.4.3. Implications for practice	101
4.5. Conclusions.....	103
APPENDIX.....	106
CHAPTER FIVE	112
Public perception of oil spills and pipelines	112
5.1. Introduction	112
5.2. Methods	113
5.2.1. Survey Design.....	113
5.2.2. Data Analysis.....	114
5.3. Results and Discussion	116
5.3.1. Summary Statistics	116
5.3.2. Knowledge-based Questions	116
5.3.3. Vignette.....	120
5.3.4. Willingness to Pay (WTP)	121
5.3.5. Behavioral Intention Questions	121
5.3.6. Vignette and Behavioral Intention Questions	122
5.4. Conclusions.....	123
APPENDIX.....	125
CHAPTER SIX	128
Overarching conclusions and future work	128
REFERENCES.....	131

LIST OF TABLES

Table 1. Technologies commonly used for treating oily wastewater	9
Table 2. Commercial membranes designed and marketed for oil-water separation applications	12
Table 3. Membrane type and module for oil-water separation	17
Table 4. Eight DOTM tests carried out with Anopore membranes (nominal pore diameter of 0.02 μm)	50
Table 5. Distinct fouling patterns observed in DOTM tests as a function of surfactant and salt types	65
Table 6. Chi-squared test for knowledge-based question outcome as a function of education level	119
Table 7. Spearman’s rank-order correlation (significant associations are in bold)	122
Table 8. Questions assessing knowledge related to energy (the correct answer is shown in bold along with the percentage of respondents for each option)	126
Table 9. Vignette related to an oil pipeline in the respondent’s state	127
Table 10. Attitudes and risk perception associated with oil spills (all items were set to 1-Strongly Disagree, to 7-Strongly Agree scale)	127
Table 11. Willingness to pay to switch to “greener” source of energy	127
Table 12. Proposed experiments	129

LIST OF FIGURES

- Figure 1.** Number of publication for each technology from 1988 to 2018. The data was extracted from Web of Science on December 7, 2018, with the keywords of “oil AND wastewater AND (technology)”..... 5
- Figure 2.** Direct Observation through the Membrane (DOTM) Setup 38
- Figure 3.** (a) The OCT system that gives a 3D tomographic image of the scanned region (b), which can be further analyzed to identify the feed-membrane interface (c) and layers parallel to the feed-membrane interface to detect fouling (d) [87]. 40
- Figure 4.** Effect of salt type on droplet size in hexadecane-water emulsions stabilized by Triton (a) and CE9500 (b). Lines are added to guide the eye. The corresponding number-based DSDs are shown in Figure 11..... 52
- Figure 5.** Effect of surfactant and salts in the continuous phase on a) the interfacial tension of hexadecane-water emulsions and b) hexadecane contact angles on 0.02 μm Anopore membrane..... 56
- Figure 6.** Transmembrane pressure buildup during constant flux DOTM tests with Triton- and Corexit-stabilized emulsions (Tests 1 and 5; Table 4). The size bars in DOTM images correspond to 30 μm 59
- Figure 7.** Transmembrane pressure buildup during constant flux in DOTM experiments with Triton- and Corexit-stabilized hexadecane-in-water emulsions as a function of type of salt in the continuous phase: a) NaCl (Tests 2 and 6; Table 1) and b) MgSO₄ (Tests 3 and 7). 62
- Figure 8.** Transmembrane pressure buildup during constant flux in DOTM experiments with Triton- and Corexit-stabilized hexadecane-in-water emulsions in model sea water (Tests 4 and 8; see Table 1). The size bars in DOTM images correspond to 30 μm 64
- Figure 9.** Fraction of the Anopore membrane area blocked by oil as a function of time for Triton (A) and CE9500 (B) – stabilized hexadecane-water emulsions. 65
- Figure 10.** Effect of surfactant type on volume-based (a) and number-based (b) droplet size distribution in hexadecane-water emulsions. Lines are added to guide the eye. ... 69
- Figure 11.** Effect of salt type on the number-based droplet size distributions stabilized by Triton (a) and CE9500 (b). Lines are added to guide the eye. Fig. 4 shows the corresponding volume-based distribution..... 70

Figure 12. Transient behavior of oil droplets at the surface of Anopore membrane ($d_{\text{pore}}=0.02 \mu\text{m}$) during crossflow ultrafiltration of hexadecane-water emulsions stabilized by different surfactants: Triton (A-D) and CE9500 (E-H). Each row represents a separate DOTM experiment and each column corresponds to the same filtration time to aid with direct comparison of fouling patterns. 71

Figure 13. Effect of NaCl addition on fouling behavior of hexadecane-water emulsions. Each row represents a separate DOTM experiment: Test 2 (A, B); Test 6 (C, D). Each column corresponds to the same filtration time (1 min, 30 min). 72

Figure 14. Effect of MgSO₄ addition on fouling behavior of hexadecane-water emulsions. Each row represents a separate DOTM experiment: Test 3 (A, B); Test 7 (C, D). Each column corresponds to the same filtration time (1 min, 30 min). 73

Figure 15. Effect of IO on fouling behavior of hexadecane-water emulsions. Each row represents a separate DOTM experiment: Test 4 (A, B); Test 8 (C, D). Each column corresponds to the same filtration time (1 min, 8 min). 74

Figure 16. (video 1) DOTM Test 1 with HW-Triton emulsion. The recording starts 1 min into the test. Collective movement of droplets and detachment are observed at timestamps ~2 s, ~6 s, ~11 s, ~15 s, ~17 s, ~24 s, ~27 s and 33 s into the video. 75

Figure 17. (video 2) DOTM Test 1 with HW-Triton emulsion. The recording starts 3600 s (60 min) into the test. Survey of the membrane surface shows full coverage by clusters of small oil droplets and occasional larger ones. 75

Figure 18. (video 3) DOTM Test 5 with HW-CE9500 emulsion. The recording starts 1 min into the experiment. Coalescence events are observed at time stamps of ~1 min 44s, 1 min 50 s, and 1 min 57 s into the video. 75

Figure 19. (video 4) DOTM Test 5 with HW-CE9500 emulsion. The recording starts 14 min into the experiment. Coalescence events are observed at time stamps of ~1 min 5 s and 1 min 7 s into the video. 75

Figure 20. (video 5) DOTM Test 5 with HW-CE9500 emulsion. Membrane survey shows that the majority of the membrane is covered with a dark veil along with clusters of small oil droplets and large droplets. The membrane coverage by oil was sparse as some areas remained oil-free. 76

Figure 21. (video 6) DOTM Test 2 with HW-Triton-NaCl emulsion. The recording starts 13 min into the DOTM test. Multiple coalescence events were observed at the following timestamps ~12 s, ~17 s and ~46 s. 76

Figure 22. (video 7) Membrane survey 61 min into DOTM Test 2 shows that the membrane is completely covered by a monolayer of oil droplets. 76

Figure 23. (video 8) DOTM Test 6 with HW-CE9500-NaCl emulsion. Membrane survey conducted 61 min into the experiment shows a monolayer coverage of droplets. 76

Figure 24. (video 9) DOTM Test 3 with HW-Triton-MgSO₄ emulsion. The recording starts 11 min into the experiment. Coalescence was observed at the following timestamps ~4 s, ~6 s, ~8 s, ~ 11 s, ~18 s, ~42 s, ~44 s, and ~46 s..... 77

Figure 25. (video 10) Membrane survey 61 min into DOTM Test 3 shows that the membrane is covered with clusters of small droplets along with larger ones. Many areas of the membrane remained oil-free and available for water permeation..... 77

Figure 26. (video 11) DOTM Test 7 with HW-CE9500-MgSO₄ emulsion. The recording starts 3 min in to the experiment. 77

Figure 27. (video 12) DOTM Test 7 with HW-CE9500- MgSO₄ emulsion. The membrane was surveyed 60 min into the experiment showing complete oil coverage by a monolayer of droplets. 77

Figure 28. (video 13) DOTM Test 4 with HW-Triton-IO emulsion. The recording starts 36 min in to the experiment. Multiple coalescence events were observed at the following timestamps ~2 s, ~8 s, ~18 s, ~25 s, ~30 s, ~48 s, ~55 s, ~1 min 1 s, ~1 min 15 s, ~1 min 25 s, ~1 min 34 s, ~1 min 46 s, ~1 min 55 s and ~2 min 1 s. 2 min in to the video, droplet deformation is observed..... 78

Figure 29. (video 14) DOTM Test 4 with HW-Triton-IO emulsion. The recording starts 40 min into the experiment. 78

Figure 30. (video 15) DOTM Test 8 with HW-CE9500-IO emulsion. The recording starts 15 min into the experiment. Droplet coalescence was followed by droplet deformation and film formation..... 78

Figure 31. (video 16) DOTM Test 8 with HW-CE9500-IO emulsion. The recording starts 17 min into the experiment. Oil film quickly grew and spread over the entire focus area. 78

Figure 32. Dependence of NaCl reflection coefficient of an NF270 membrane on the osmotic pressure differential. Different segments of the dependence correspond to tests with different initial feed concentrations, C_{f0} , of NaCl. Results of replicate measurements with different initial feed concentrations, C_{f0} , of NaCl. Results of replicate measurements with two other NF270 membranes are shown in Appendix, Figure 24. 93

Figure 33. NaCl permeability coefficient of NF270 membrane during salt conditioning tests with different initial feed concentrations C_{f0} , of NaCl and different concentration polarization conditions. The dashed red line is the asymptote to which $B(t)$ dependence appears to converge. Each test was terminated once a steady state permeate flux was achieved: $dJ/dt < 0.02 \text{ min}^{-1}$ 93

Figure 34. Permeate flux behavior in crossflow nanofiltration tests with SDS-stabilized saline emulsions of hexadecane as a function of NaCl concentration (100 mM, 469 mM, or 1711 mM). The experiments were performed at $\Delta P = 200 \text{ psi}$ (1.38 MPa) and with a constant with a constant crossflow velocity ($v_{cf} = 0.1 \text{ m/s}$). Initial permeate fluxes and hydraulic resistance of clean membranes for all filtration tests are given in Appendix. Different symbols of the same shade correspond to different tests (each test was performed in duplicate)..... 96

Figure 35. Steady state values of the observed (a) and intrinsic (b) rejection of NaCl by NF270 in conditioning tests (feed: NaCl and SDS) and in fouling tests (feed: NaCl, SDS, hexadecane). Lines are added to guide the eye. The (very weak) dependence of R_{obs} and R_{int} on time is shown in Appendix, Figure 27..... 96

Figure 36. Headloss distribution across four different sources of hydraulic resistance in nanofiltration tests with SDS-stabilized saline emulsions of hexadecane as a function of NaCl concentration: a) 100 mM; (b) 469 mM; and (c) 1711 mM. 100

Figure 37. Volume-based (a) and number-based (b) droplet size distributions of SDS-stabilized hexadecane-in-water emulsion in the presence of salt (100 mM NaCl, 469 mM NaCl, or 1711 mM NaCl). The volume-based median diameter increased with an increase in the ionic strength from 20 μm to 32 μm to 49 μm for the HD-0.1SDS-100NaCl, HD-0.1SDS-469NaCl, and HD-0.1SDS-1711NaCl emulsions, respectively. 106

Figure 38. Permeate flux (a), intrinsic rejection of NaCl (b), and observed rejection of NaCl (c) by NF270 as functions of NaCl concentration in the feed. 107

Figure 39. Dependence of reflection coefficient on NaCl concentration at the membrane surface 108

Figure 40. Dependence of NaCl reflection coefficient of NF270 membrane on the osmotic pressure differential. Different segments of the dependence correspond to tests with different initial feed concentrations, C_{f0} , of NaCl. The two graphs are for two replicate measurements with two different NF270 membranes. The dependence for another NF 270 membrane is shown in Figure 16. 109

Figure 41. Dependence of NaCl reflection coefficient of NF270 membrane on the osmotic pressure differential. The power law provides the best fit (dashed red line). The data represent a merged dataset recorded in three separated tests with different NF270 membranes. Data set for each membrane consists of segments corresponding to different feed concentrations of NaCl (Figure 24)..... 110

Figure 42. Permeate flux change during conditioning and fouling stages at $\Delta P = 200$ psi (1.38 MPa) and $C_{f0} = 100$ mM NaCl..... 111

Figure 43. Observed and intrinsic rejections of NaCl by NF270 for SDS-stabilized hexadecane-in-water emulsion at different ionic strengths..... 111

Figure 44. Number of respondents as a function of correct answers (n=630)..... 118

KEY TO SYMBOLS

J	volumetric permeate flux
ΔP	transmembrane pressure differential
μ	dynamic viscosity of the permeating solution
$\Delta\pi$	osmotic pressure differential across the membrane
σ	reflection coefficient
R_m	hydraulic resistance of the clean membrane
R_f	added resistance to the permeate flux due to fouling
i	van't hoff's factor
R	ideal gas constant
T	temperature of the solution
C_m	concentration of solute in the immediate vicinity of the membrane surface
C_p	concentration of solute in the permeate
C_f	concentration of solute in the feed
k_{cp}	mass transfer coefficient
Sc	schmidt number
D	solute diffusion coefficient
d_h	hydraulic diameter of the crossflow channel
Re	reynolds number
J_s	solute flux across the membrane
B	solute permeability coefficient

R_{obs} observed salt rejection

R_{int} intrinsic salt rejection

CHAPTER ONE

OVERVIEW

Membrane-based separation is the most cost-effective technology capable of removing micron-sized oil droplets. For stable oil-in-water emulsions (droplet size in the 1 to 10 μm range), ultrafiltration (UF) and tight microfiltration (MF) are effective choices. However, if the wastewater is saline (e.g. produced water), nanofiltration (NF) and reverse osmosis (RO) can be employed. Membrane fouling by emulsified oil is the major drawback that has limited the broader acceptance of membranes. Oil droplets, which can deform and coalesce, challenge the available knowhow on membrane fouling. The motivation for this research is to understand the effects of surfactants and salinity on the underlying mechanisms of membrane fouling by emulsified oil. The rest of this dissertation is organized as follows.

Chapter 2 gives a comprehensive overview of the state of the knowledge concerning the mechanisms of membrane fouling by emulsified oil. It also identifies the knowledge gaps and provides a perspective on possible future research directions. A manuscript based on this Chapter was published in *Water Research* journal.

Chapter 3 represents a real-time direct visualization UF study that was complemented by a deposition kinetics model to elucidate the stages of membrane fouling by emulsified oil. This study investigated the effects of surfactant type and salinity on oil fouling behavior. A manuscript based on this Chapter is in preparation for submission to the *Journal of Membrane Science*.

Chapter 4 represents the first mechanistic study of NF membrane fouling by model saline emulsions. The study investigated how the interaction of emulsified oil and dissolved species in the vicinity of a nanofiltration membrane affects permeate flux and selectivity of separation. Individual contributions of membrane fouling and concentration polarization to the overall flux decline were identified. The approach was based on measuring membrane transport coefficients and their dependence on the concentration of salt. A manuscript based on this Chapter was published in the *Journal of Membrane Science* on September 1, 2020.

Chapter 5 presents the results of a national survey conducted to examine the public's knowledge about oil spills and their stance on pipelines.

Finally, in chapter 6, we conclude by summarizing our presented work and highlighting future research directions.

CHAPTER TWO

Membrane-based separation of oily wastewater*

*Published on June 1, 2019, *Water Res.*, DOI: 10.1016/j.watres.2019.03.021

Abstract

The large volumes of oily wastewater generated by various industries, such as oil and gas, food and beverage, and metal processing, need to be de-oiled prior to being discharged into the environment. Compared to conventional technologies such as dissolved air flotation (DAF), coagulation or solvent extraction, membrane filtration can treat oily wastewater of a much broader compositional range and still ensure high oil removals. In the present review, various aspects related to the practical implementation of membranes for the treatment of oily wastewater are summarized. First, sources and composition of oily wastewater, regulations that stipulate the extent of treatment needed before discharge, and the conventional technologies that enable such treatment are appraised. Second, commercially available membranes, membrane modules, operation modes and hybrids are overviewed, and their economics are discussed. Third, challenges associated with membrane filtration are examined, along with means to quantify and mitigate membrane fouling. Finally, perspectives on state-of-the-art techniques to facilitate better monitoring and control of such systems are briefly discussed.

2.1. Introduction

Oil-water mixtures are found in many industrial processes, and can take the form of a product, a by-product or a waste stream. Whether the goal is for recovering the oil for economic gains or removing the oil phase for environmentally friendly disposal, the separation of the oil and other immiscible components is necessary. Environmental regulations governing the discharge of oily wastewater have become increasingly stricter, with country-specific regulatory limits on the maximum oil concentration of generally within the 5 to 40 mg/L range [1]. The oil phase in wastewater can exist in three forms, classified based on the size of the oil droplets [2], namely, free oil ($> 150 \mu\text{m}$), dispersed oil (20 to 150 μm), and emulsified oil ($< 20 \mu\text{m}$). The choice and performance of oil-water separation techniques depend not only on oil droplet size, but also on other considerations, such as oil concentration and chemical composition. Membrane filtration is a promising technology for separating oil droplets smaller than $\sim 10 \mu\text{m}$ [3]. Notably, the increasing interest in the employment of membrane filtration for the treatment of oily wastewater is evident in the significant increase in the number of publications over the last three decades (1988-2018), vis-à-vis more conventional methods, as depicted in **Figure 1**. Correspondingly, a review of the advances to date on this topic is warranted.

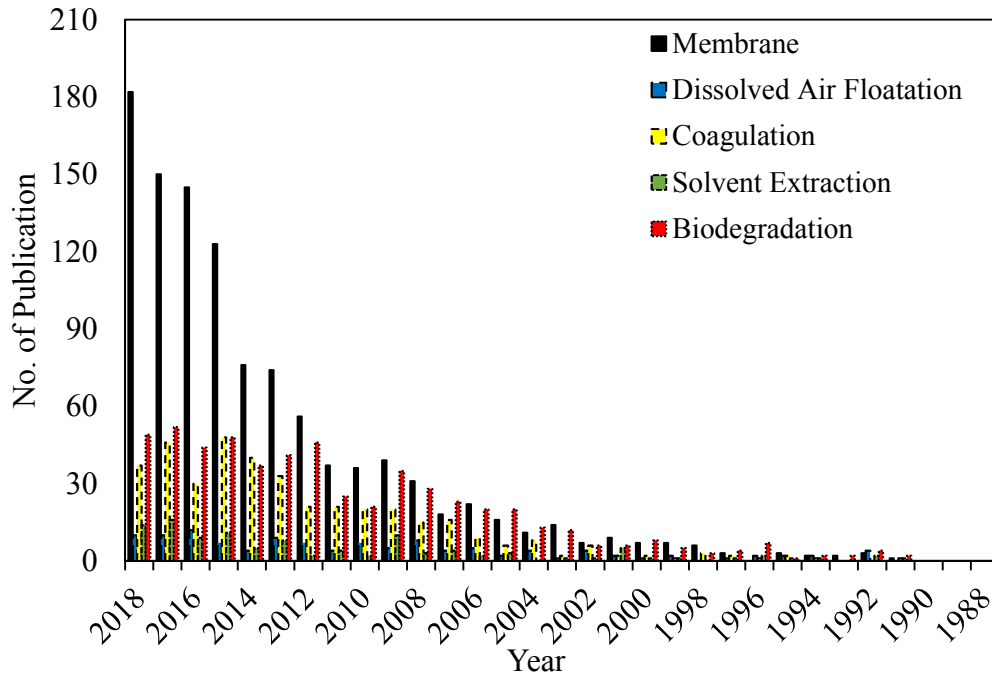


Figure 1. Number of publication for each technology from 1988 to 2018. The data was extracted from Web of Science on December 7, 2018, with the keywords of “oil AND wastewater AND (technology)”.

Unfortunately, membrane fouling is a major drawback that reduces productivity and increases operational costs of membrane filtration. Many efforts have been dedicated to understanding the mechanisms of membrane fouling, and to develop methods to effectively monitor and mitigate membrane fouling. The focus of the review is on the practical aspects of applying pressure-driven membranes to the treatment of oily wastewaters, highlighting the requirements, recent development, drawbacks and corresponding mitigation strategies.

In the first section of this chapter, we review the common sources and properties of oily wastewater, the discharge regulations, as well as technologies that have been used to treat oily wastewater. In the subsequent section, the advantages of using membranes for the treatment of oily wastewater commercially will be reviewed along with the related

challenges and counter-measures. In the final section, we review the state-of-the-art technologies of monitoring and mitigating membrane fouling, and discuss the potential of membranes for the treatment of oily wastewater.

2.1.1. Oily wastewater: Sources, quantities and composition

Oily wastewater is a by-product generated by many industries including oil and gas, food and beverage, shipping and maritime, tanning, textile, and metal and machining [2, 4]. Oily wastewater not only adversely affects the environment if not adequately treated, but also represents a substantial economic loss if the oil is not recovered.

Oil-water separation has received renewed interest with the recent developments in the fossil fuel sector, particularly for the treatment of produced water, which is oily wastewater stream from the oil and gas extraction operations [1, 2]. Produced water is generated from onshore as well as offshore wells. The global produced water generated is approximated at 250 million barrels/day for every 80 million barrels/day of oil produced, with 800 million m³ of produced water were discharged from offshore facilities throughout the world in 2003 alone [5, 6]. The treatment of the enormous volume of produced water is important from both an environmental perspective to reduce water consumption and minimize waste disposal, and also from an economic perspective as expenses on water management can account for 5% - 15% of drilling costs [5, 6]. Other than oil, complex constituents in produced water include many type of chemicals, such as linear chain hydrocarbons, aromatic hydrocarbons (benzene, toluene, and xylene), metals, naturally occurring radioactive material (NORM), and additive chemicals such as corrosion

inhibitors and emulsion destabilizers [2, 4, 5]. The composition of produced water as well as its physical and chemical properties are generally site-specific [5].

In the food, drink and milk industry, water is a significant component in most products [7], and also is involved in many steps and processes, such as washing, rinsing, mixing, pasteurizing, etc. [8]. Because the amount of oily wastewater produced is also large, the implementation of means for reuse is cost-effective due the economies of scale [9]. Most of the oil waste comes from meat, poultry, seafood and dairy, thus the wastewater typically has a very high content of organic carbon.

Another major producer of oily wastewater is the metal processing industry where cutting oil is used as a coolant and flushing fluid [2, 10]. Cutting oils are emulsions consisting of oil, water and additives such as fatty acids, surfactants, heavy metals and biocides [11]. The oil content in such waste streams is too low for it to be incinerated, yet they are too toxic to be treated biologically.

In summary, oily wastewater from various industries tends to be of very complex and varied compositions, which complicates the selection of an appropriate treatment technology and calls for context-specific treatment solutions.

2.1.2. Regulations for discharging oily wastewater

The direct discharge of oily wastewater into the environment without proper treatment can have grave consequences, including the disruption of the aqueous ecosystem, pollution of the groundwater or drinking water resources, and endangering human health [12]. Region-specific regulations have been introduced to enforce the treatment of oily wastewater prior to its discharge to the environment. In the North Sea

region, Oslo-Paris (OSPAR) convention regulates that the upper limit for the discharge of oil content in the wastewater is 30 mg/L [13]. According to the Paris convention, the upper limit of oil content to be discharged to the sea is 40 mg/L for the offshore fields and 5 mg/L for the on-land fields [14]. In the U.S., the Environmental Protection Agency (EPA) stipulates a maximum oil content of 72 mg/L for any 24 hour period and 45 mg/L over a 30 days period [15].

Other studies reported on regulations with similar limits of oil concentration that can be released into the open water, e.g., maximum oil content of 40 mg/L, typical range around 10-15 mg/L [4, 16]. In Norway, the limit on the oil concentration allowed to be discharged into the sea from an offshore installation to the Norwegian Continental Shelf was reduced from 40 to 30 mg/L as of 2007, which implies the increased stringency in the quality of the discharge. In China, the upper limit for oil concentration in the discharged wastewater is 10 mg/L [12]. These regulations compel an urgent need for developing technologies that can reach these treatment goals cost-efficiently. The common technologies for treating oily waste water are discussed in the next section.

2.1.3. Oily wastewater treatment: Conventional technologies

An overview of the common technologies used in treating oily wastewater is provided in Table 1, along with the oil concentration ranges in the feed and the removal effectiveness [1, 6, 17]. Each method has its own challenges in treating oily wastewater.

Table 1. Technologies commonly used for treating oily wastewater

No.	Method	Brief description	Feed Oil Concentration	Extent of Oil Removal in Effluent Concentration	Ref.
1	Dissolved Air Floatation (DAF)	Removal of oil by attachment to micron-size bubbles and floatation	500 ppm	95% removal	[18]
2	Fentone Process	Poly-ferric sulfate used as a coagulant	12,000 mg/L	65.8% removal	[19]
3	Coagulation	Adding Coagulant to create oil-contained flocs that sink	7,000-15,000 ppm	93% removal	[18]
4	Solvent Extraction	Removal of free oil or dissolved oil in lighter hydrocarbon solvent	5,410 ppm	90% removal	[18]
5	Froth Floatation	Separation of oil by mixing with surfactant, and aerated in a stirrer to float oil-saturated bubbles	25,000-50,000 ppm	55% removal	[18]
6	Biodegradation	Degradation of oil by microorganisms	10,000 ppm	98% degradation	[20]
7	Adsorption	Usage of porous	1,040-1,710 ppm	67% removal	[24]

2.2. Membrane technology for oil-water separation

Membrane-based separation is the most cost-effective solution for removing oil droplets smaller than $\sim 10 \mu\text{m}$ [21]. The amount of oil in the emulsified fraction can be significant, making the removal of these droplets a prerequisite for meeting environmental regulations. Separation methods based on the oil/water density differential (e.g., settling, flotation, hydrocyclone) require an exceedingly long retention time for the removal of emulsified oil, while chemical treatment (e.g., fentone process, coagulation) may not effectively de-stabilize oil-in-water emulsions particularly when the emulsified oil is finely dispersed [22]. Compared to the conventional methods, membrane filtration offers several advantages that include higher quality permeate, lower space footprint, more straightforward automation, no need for extraneous chemicals and therefore reduced waste, and lower energy input [4, 23-25]. These advantages, coupled with the ability of membranes to reject other pollutants present in the feed, make membranes competitive with the more traditional technologies.

As with all membrane filtration processes, the key drawback that limits the broader implementation of membrane-based oil-water separations is membrane fouling [2], which is the cumulative deposition of the feed constituents like oil on the surface of the membrane and inside the pores that results in a decline in the permeate flux and quality. Other limitations of membrane technology include lower throughput (e.g., much lower than that of hydrocyclones) and relatively higher capital costs.

Given that membrane-based separation is most effective for the oil droplet size range of 1 - 10 μm , ultrafiltration (UF) and tighter microfiltration (MF) are the more relevant choices [26]. However, if the wastewater is saline and desalination is an accompanying treatment

goal, employing reverse osmosis (RO) and nanofiltration (NF) can allow for a single-step processing of such waste streams [2]. Membrane distillation (MD) also shows promise [27-30]. In this section, commercially-available membranes are discussed, followed by membrane modules, then batch and continuous modes. The last two sub-sections focus on hybrid or integrated membrane processes and the economics of the membrane process.

2.2.1. Commercially-available membranes for oily industrial wastewater

The membrane-based processing of oily wastewaters, sometimes combined with conventional methods, has been successfully implemented in more than 3000 polymeric UF/MF installations and over 75 inorganic/ceramic ones worldwide since 20 years ago [2]. According to a report by Grand View Research Inc., the global market for the treatment of produced water, which is the major wastewater in the oil and gas industry, reached \$5.81 billion in 2015, of which 46.8% was for secondary separation technologies including membrane-based techniques [31]. Several companies such as Osmonics, Koch, Alcoa, Veolia and Filtration Solution Inc. offer commercial membranes for oil-water separation. Table 2 presents a list of some of the membranes available on the market currently.

Table 2. Commercial membranes designed and marketed for oil-water separation applications

Manufacturer	Filtration type	Configuration	Pore size / MWCO	Membrane material	Specific water flux, L/(m ² ·h.bar)	Ref.
Osmonics	UF	Spiral Wound	0.01 µm	Chemically modified PAN	-	[32]
Filtration Solution Inc.	UF	Spiral Wound	0.01 µm	Chemically modified PAN	-	[32]
Clean Water Tech PTE, Ltd	UF	Hollow Fiber	0.01 to 0.1 µm	Hydrophilic PAN	13-20	[33]
Veolia Water Technologies	UF	Tubular	0.1 µm	TiO ₂	-	[34]
Koch	UF	Hollow Fiber	50 kDa	Polysulfone	-	[35]
Hydranautics	RO	Spiral Wound	-	Composite polyamide	0.54	[33]

Osmonics and Filtration Solutions Inc. offer spiral wound ultrafiltration membrane modules to concentrate oily wastewater streams: M-Series UltraFiloc and SHP series membranes, respectively [32, 36]. Both membranes are made from a chemically modified polyacrylonitrile (PAN) and designed to protect the membrane from fouling by “free” oil and from degradation by solvents. To minimize fouling, these membranes have been engineered to be extremely hydrophilic (i.e., water contact angle of 4°) relative to the conventional polyvinylidene difluoride (PVDF) and polysulfone (PS) membranes that are hydrophobic [36]. In addition, both membranes can operate at temperatures of up to 50 °C, and can withstand pH values in the range from 2 to 10 for continuous operation and from 3 to 9 for when Cleaning-In-Place (CIP) is incorporated into the process. Typical permeate fluxes are 8 to 34 L/(m²·h) for the M-Series Ultrafiloc membranes and 17 to 43 L/(m²·h) for the SHP series membranes [32, 36].

Numerous membrane companies offer integrated treatment systems to process oily industrial wastewater. Akvola Technologies established a flotation-filtration system (akvoFloat) that can lower both energy consumption and footprint [37] of treatment. The system consists of two stages that are integrated in the same tank. The first stage is flotation whereby the suspended oil is carried to the surface by bubbles with the aid of the Akvola MicroBubble Generator, which induces fine gas bubbles using low pressure air, nitrogen, ozone or carbon dioxide (CO₂). The role of the microbubbles is to attach to the oil droplets and particles, which are carried to the surface and then continuously skimmed off. The second stage entails membrane-filtration with submerged ceramic membranes ($d_{pore} = 0.2 \mu\text{m}$) positioned below the float layer [37].

CDM Smith is currently marketing a hybrid system to treat produced water containing up to 20,000 mg/L of total dissolved solids. This system combines several commercially available technologies, namely, microfiltration (MF), ion exchange, UV disinfection and reverse osmosis (RO). The pretreatment consists of filtering the feed solution through prefiltration (cartridge filter with a nominal pore size of 1 to 3 μm) to remove particulates, followed by ion exchange to remove polycations, and then UV disinfection to reduce bacterial activity. Finally, the water undergoes a multi-stage RO process, employing a combination of low-pressure RO (capable of achieving 85% recovery) and seawater RO membranes (80% water recovery) [38].

Veolia Water Technologies offers a produced water system OPUS[®] (Optimized Pretreatment and Unique Separation) technology, which consists of multiple treatment processes, namely, chemical softening via Multiflo[®] with filtration, followed by ion exchange, then RO. The pretreatment processes before the RO step are designed to reduce the hardness and suspended solids in the feed solution, eliminating the potential for precipitative and colloidal fouling of the RO membranes [34].

Clean Water Tech Pte Ltd provided a UF hollow fiber membrane with pore size ranged from 0.01 to 0.1 μm , which was made from hydrophilized polyacrylonitrile (Ultra-Flo U630C). The pH range that this membrane could tolerate was 2 - 12, and the maximum feed pressure and temperature possible were respectively 3.5 bar and 50 °C. In addition, a RO composite polyamide spiral wound membrane (SWC3+) from Hydraunatics could handle feeds with pH ranged from 3 – 10, and maximum operating pressure and temperature of 83 bar and 45 °C, respectively [33].

These examples of commercially available membranes indicate the practical feasibility of such processes. In the last two decades, the focus on the treatment of oily wastewater has made available membranes that can withstand reasonable ranges of temperature, pressure and pH to cater to the complexities of such feeds.

2.2.2. Membrane modules

Different kinds of membrane types and modules and system have been employed in oil-water separation processes (

Table 3). The common module designs are flat sheet, spiral wound, tubular, capillary, and hollow fiber, with flat sheet and tubular being more popular.

Flat sheet modules are commonly employed in research laboratories for bench-scale experimentation. The advantages include relative simplicity of module design and operation, and availability of wide range of pore sizes (spanning RO, NF, UF and MF). However, one of the key advantages is that the membrane area per unit module volume is low and thereby less feasible for commercial implementation because of the larger footprint necessary. Nonetheless, flat sheet membranes form the basis for the dominant RO module, namely, the spiral wound membrane (SWM) module, which is a stack of flat-sheet membranes, with spacers between the sheets, rolled and placed inside a cylindrical case. Such a packing method significantly enhances the availability of membrane area per unit module volume for filtration. Tubular membranes, capillary and hollow fiber membranes differ by the lumen size (inner lumen diameters greater than 0.635 cm, between 0.1 to 0.635 cm, and between 0.025 to 0.1 cm, respectively). Most of the ceramic membranes, which have greater mechanical strength as well as chemical and thermal

stability, are tubular. The drawback is the limited availability of such membranes to only UF and MF. One of the chief advantages of hollow fiber membranes is the greatest membrane area per unit volume vis-à-vis tubular and flat sheet ones, which is giving this membrane type more attention in the membrane community.

Table 3. Membrane type and module for oil-water separation

No.	Module	Type	Material	Ref.
1	Tubular	MF	Carbon	[39]
2	Tubular	MF	Ceramic	[14]
3	Tubular	MF	Alumina	[40]
4	Flat Sheet	MF	PVDF	[41]
5	Flat Sheet	MF	PTFE / PVDF	[42]
6	Tubular	MF	α -Alumina	[4]
7	Tubular	MF	Alumina	[43]
8	Tubular	MF	PVDF / PS	[44]
9	Tubular	MF	GO - Alumina	[45]
10	Flat Sheet	MF	Nylon	[46]
11	Disk Shaped	MF	Ceramic	[16]
12	Hollow Fiber	UF	S-PPSU	[47]
13	Tubular	UF	Ceramic	[48]
14	Flat Sheet	UF	Cellulose / PS	[49]
15	Flat Sheet	UF	Polysulfone	[50]
16	Flat Sheet	FO ⁶	Cellulose Triacetate	[51]
17	Flat Sheet	FO	Polysulfone	[52]
18	SWM	RO	Polymer type	[53]
19	Flat Sheet	RO	Polyamide / Polydopamine	[54]
20	Flat Sheet	NF	PVDF / PDMS	[55]
21	Flat Sheet	NF	Polyamide	[56]
22	Flat Sheet	UF	Polysulfone	[56]
23	Flat Sheet	NF-RO	Polyester-Polysulfone	[25]

2.2.3. Hybrid membrane processes

Oily wastewater can have a very complex composition and contain suspended and dissolved species that differ in concentration, size, charge and density. In order to achieve a sustainable membrane-based separation of oily wastewater, it is often necessary to integrate the membrane unit with other membranes, whether in batch or continuous processes as described previously, or other conventional unit processes. Such integration may ease the foulant load on the membrane thereby mitigating membrane fouling and prolonging the membrane lifetime.

Membrane fouling can be mitigated using adequate pretreatment. Different physical, biological, and chemical methods have been used for the pretreatment of oily wastewater; these include gas sparging [57, 58], coagulation [59], flocculation [60], centrifugation [59], electrocoagulation [61], acidification [62], cartridge pre-filtration [59], dissolved air flotation (DAF) [18], activated carbon adsorption [63] as well as separation by larger pore size membranes such as UF [64-66] and MF [67].

Karakulski and Morawski employed an integrated membrane system based on UF and NF to treat waste oil-water emulsion from a cable factory [59]. UF with 100 kDa MWCO membranes resulted in 99% rejection of suspended solids, and retention of oil and lubricants. The resulting UF permeate was further purified by NF to reject the remaining pollutants and reduce the content of copper ions (i.e., dominant constituent in the oily wastewater from the cable factory). Another study proposed a hybrid system that used flocculation as a pretreatment [60]. By coupling this pretreatment with the downstream MF with a 0.2 μm pore size zirconia membrane, the permeate flux was increased and permeate quality improved in comparison with MF alone.

One study utilized adsorption with membrane-filtration for treating oily wastewater and demonstrated that the integration increased the permeate quality and reduced membrane fouling [68]. Powdered activated carbon (PAC) and natural zeolite were compared in terms of the effectiveness as adsorbents at the MF pretreatment stage. Total organic carbon (TOC) removal was up to 99.5% and 99.9% respectively for PAC and zeolite, with the latter performing better due to the higher oil adsorption rate and thereby lower fouling of the MF membrane. In another study on treating industrial oily wastewater with 550 mg(oil)/L of oil and 6500 mg(COD)/L, coagulation coupled with MF was used as a pretreatment step for UF [69]. Polyaluminum chloride was the coagulant used in combination with a ceramic 0.2 μm pore size MF membrane, followed by a PVDF UF membrane unit. The results demonstrated that the UF permeate flux increased 2.5 times compared to the process without pretreatment. The entire integrated system achieved up to 95.2% of COD reduction and 98.5% oil removal, which was much better than what could be accomplished with the standalone units or with any other couplings. Other types of coagulation have also been integrated with membrane units, an example of which is electrocoagulation (EC) with RO [70]. In this study with feeds containing 1000 mg(oil)/L, EC functioned as a pretreatment step using either AC or DC current, after which the effluent was left in a sedimentation tank for 5 minutes before going through the RO unit. While EC gave 92% reduction of COD, which was sufficient alone to meet the current regulations for discharge to the sea, the subsequent RO unit achieved 100% removal of COD.

Membrane technology complements rather than replaces the conventional methods for treating oily wastewater to achieve a higher quality product sustainably. The

integration of membrane-based and other methods harnesses the advantages and also circumvents the shortcomings of each.

2.2.4. Economics of membrane-based treatment of oily wastewater

As mentioned earlier, membrane technology is economically advantageous for oily wastewater treatment compared to the other conventional technologies. Based on the numbers available in literature, the cost of membrane-based treatment was estimated to be ~ \$1-3/m³ [2, 71], which compares favorably with that for is \$3.65/m³ cost of treatment by Dissolved Air Floatation (DAF). The cost inevitably depends on the source of the oily wastewater, since each industry has unique blends of oil and grease as well as other foulants specific to the process. For example, the total cost (including costs of membranes, labor, electricity, cleaning and maintenance) of treating oily wastewater from the fatty acid industry was \$2.65/m³ [72], that from the railroad industry was \$1.03-1.48/m³, while that for the metalworking wastewater using UF was \$2.8/m³ [71]. In another study using MF, Nandi and coworkers estimated that the annual cost of the membrane-based treatment for oily wastewater with an oil concentration of 50 mg/L could be as little as \$0.098/m³ for treating feeds at 100 m³/day [73]. Clearly, the cost of membrane-based treatment of oily wastewater is quite varied, but is nevertheless lower than that for conventional technologies. Moreover, more recently, the cost of membrane-based treatment has been slashed due to improvements in membrane fabrication and operation. As a benchmark, the total water treatment cost by RO desalination was around \$0.5/m³, whereas that by the conventional thermal process was in the range of \$0.8-

1.1/m³ [74]. As another benchmark, the total cost for treating a secondary agriculture-based effluent stream was around \$0.15-0.42/m³ [75].

2.3. The challenges of membrane operation

2.3.1. Mechanisms of membrane fouling by oil

The key obstacle that hinders the widespread implementation of membrane technology for oil-water separation is membrane fouling. Notably, the underlying mechanisms of membrane fouling by emulsified oil remains poorly understood, for example, the conditions under which the accumulated oil forms compressible cakes or contiguous films are unclear. Several studies have analyzed permeate flux decline during the filtration of oil-in-water emulsions and used blocking filtration laws (one of the first reports was by Hermia [76]) to explain the mechanisms of membrane fouling by oil [44, 77-81]. Two studies [73, 77] showed that membrane fouling by oil is due to cake formation whereby multiple layers of oil form a secondary membrane on the membrane surface. Other researchers linked membrane fouling by oil to intermediate pore blocking whereby the membrane is fouled by early stages of cake filtration and complete pore blocking [73, 77, 81]. Six out of the seven aforementioned studies applied the blocking filtration laws to crossflow filtration, although the Hermia blocking laws [76] do not take into account the back-transport of particles away from the membrane surface and only account for spherical, non-deformable particles. Oil droplets, which can both deform and coalesce, are unique foulants that challenge the available knowhow on fouling.

Another study investigated the fouling of NF and UF membranes using hexadecane-in-water emulsions stabilized by different surfactants, namely, a non-ionic surfactant

(Triton X-100), anionic surfactant (sodium dodecylbenzenesulfonate; DDBS) and cationic surfactant (cetyltrimethylammonium bromide; CTAB) [56]. Experiments with surfactant-stabilized emulsions and pure surfactant solutions indicate that emulsified oil rather than free surfactants is responsible for the increase in the TMP. UF crossflow filtration tests revealed that emulsions stabilized by CTAB quickly fouled the negatively charged polysulfone UF membrane due to electrostatic attraction between surfactant-stabilized oil droplets and the membrane. In contrast, membrane fouling was less severe in experiments with DDBS- and Triton-stabilized emulsions. In NF filtration tests, fouling increased exponentially regardless of the type of surfactant used to stabilize the emulsion [56]. For both UF and NF processes, fouling experiments and theoretical calculations indicated that cake layer formation underlies the initial membrane fouling by emulsified oil. However, depending on the type of emulsion and membrane, once the pressure drop across the cake layer reached a critical value, oil droplets can wet the membrane surface and lead to irreversible membrane fouling.

In a different study, He et al. conducted a set of constant permeate flux fouling experiments with PVDF MF membranes using multiple feed solutions, namely, latex bead suspension soybean, motor and crude oil-in-water emulsions [82]. The fouling tests were performed under the same hydrodynamic conditions and with the same membrane where the fouling propensity only depended on membrane-foulant and foulant-foulant interactions. The TMP profiles for motor and crude oil-in-water emulsions, which fouled more severely, exhibited slow TMP increase in the early stage, followed by an abrupt increase due to inhomogeneous fouling, and then the TMP eventually reached a pseudo steady-state with cake filtration as the operative fouling mechanism. The results also

revealed that foulants with higher zeta potential have lower fouling propensity. Subsequently, the same group investigated the impact of permeate flux on membrane fouling [83]. Constant permeate flux tests with soybean and crude oil-in-water emulsions and PVDF MF membranes showed that above the threshold flux, TMP profile develops over three distinct stages: initial gradual TMP increase, followed by a TMP jump, and then a pseudo-steady state TMP, which corresponds to the critical pressure of the oil layer [82].

Membrane fouling is inherently a complex phenomenon, and the fouling by oil droplets further augments the complexity due to unique phenomena such as coalescence [84], moving cake layer, thinner but denser cake, viscous effects, better predictability by the DLVO (Derjaguin-Lewis-Verwey-Overbeek) rather than XDLVO (i.e., extended DLVO) model [85], effect of different surfactants [86], and internal membrane pore fouling despite the oil droplets being larger than the membrane pore [87]. While membrane fouling studies are abundant in the literature, the understanding on oil foulants remain comparatively limited. More studies on mechanistically understanding membrane fouling by oil is needed, particularly in view of the recent studies that have collectively shown oil to be distinctive from other particulate foulants.

2.3.2. Mitigating membrane fouling by oil: An overview of methods

This section introduces three main approaches to membrane fouling control and describes case studies to illustrate how each approach is applied in the context of oil-water separation.

2.3.2.1. Materials science approach: Making membranes resistant to fouling

An effective approach to reduce membrane fouling by oil is to increase the hydrophilicity of the membrane surface [62, 88, 89]. Water adsorption onto a hydrophilic surface restricts its interactions with oil and limits fouling with the hydration layer serving as an entropic barrier for oil attachment [62, 88]. Numerous techniques have been used to increase the hydrophilicity of membranes by either blending common membrane polymers with hydrophilic additives (e.g. hydrophilic polymers, amphiphilic copolymers, and inorganic nanoparticles) or altering the membrane surface properties via chemical or physical post-modification (e.g. surface coating and surface graft polymerization) [62].

The incorporation of polyethylene glycol polymer chains alone or among copolymer blends is a common method for increasing surface hydrophilicity. Chakrabarty et al investigated the performance of four types of polysulfone (PS) UF membranes in the process of separating synthetic emulsions of crude oil in water under crossflow conditions [50, 90]. PS membranes were fabricated using different casting mixtures of N-methyl pyrrolidone (NMP), polyvinylpyrrolidone (PVP) and poly (ethylene glycol), which led to different membrane morphologies. The four membranes successfully rejected ~ 90% of the oil and the oil concentration in the permeate was below 10 mg/L, which met discharge requirements. In another study, Chen et al. modified the hydrophilicity of an ultrafiltration membrane by blending amphiphilic copolymers (Pluronic F127) with poly(ether sulfone) (PES) to separate oil-water emulsions. PES/Pluronic F127 membranes exhibited higher permeate flux and better antifouling property compared to the bare PES membrane [91]. While addition of hydrophilic polymers improves the fouling resistance of membranes, the introduction of hydrophilic polymers can lead to defects in the membrane, resulting in a

breakdown of the membrane under high TMP [92]. The modification of commercial membranes to become more hydrophilic for anti-fouling characteristics to enhance oily wastewater treatment has been enabled by Osmonic, Filtration Solution Inc., and Clean Water Pte. Ltd., which offer hydrophilized polyacrylonitrile (PAN) as the membrane material, under different brand names (Section 2.2.1).

The usage of nanomaterials to improve membrane performance has also emerged in recent years. Zhan et al. used a halloysite nanotubes (HNTs) intercalated graphene oxide (GO) coating on a porous poly(arylene ether nitrile) nanofibrous support layer, which was further enhanced with another layer of mussel-inspired polydopamine (PDA) coating [93]. This combination gave superior performance of more than 99% oil rejection and high permeate flux of 1130.56 l/m²h for the gravity-driven filtration of a feed containing oil emulsion, because the nanotubes provided more water channels for permeation, and the hydrophilic PDA increased water flux and also rejected oil more effectively. Nano-sized polydopamine (nanocluster) coating was also employed by Wang et al. on a electrospun nanofibrous (ENF) membrane constructed from the cross-linking of polyacrylonitrile and hyperbranched polyethyleneimine (PAN/HPEI) [94]. The resulting membrane gave a high permeate flux of 1600 l/m²h and oil rejection of 98.5% also for gravity-driven filtration. Li et al. surface-modified a commercial PTFE membrane by using a polydopamine layer infused with nano-microsphere and hydrophilic carboxyl groups in a tetrahydrofuran (THF)-Tris buffer mixture [95]. The membrane exhibited rejection of up to 99% and permeate flux of around 2000 l/m²h for feeds containing various oils and surfactants. Another new trend for oil-water separation is the surface modification of an inorganic mesh, rather than polymer or ceramic membrane. Hou et al. had nano-sized

nickel particle coating on a stainless steel mesh, which was made by using electrodeposition in deep eutectic solvent (DES) composed by choline chloride (ChCl) – ethylene glycol (EG) to separate oil and water [96]. Such modified meshes expressed superhydrophilicity and underwater superoleophobicity characteristics, which made the oil-water separation excellent for various oils (such as silicon oil, corn oil and crude oil). For feeds containing oil emulsion, the modified mesh was altered further by more electrodeposition to reduce the pore size of the mesh from 14 μm to 4 μm improve the rejection of the micron-sized oil droplets. The permeate flux of this gravity driven process was around 300 $\text{l/m}^2\text{h}$, but rejection was poor. Another study had a stainless steel mesh coated with copper via electrodeposition to make a hydrophilic membrane, which was modified further by applying dodecanethiol to make the membrane became superhydrophobic [97]. Both membranes were used concurrently in the filtration setup, such that water permeated through the superhydrophilic membrane and oil permeated through the superhydrophobic membrane, giving high permeate flux and separation efficiency greater than 99.8%.

Though the reported performances are excellent for such modified membranes, the practicality for commercial implementation has to be critically assessed. Firstly, the longer-term durability of such coatings particularly in the presence of cross-flow in practical operations. Most of these membranes and meshes were tested using gravity-driven filtration, which is not congruent with the presence of a continuous tangential shear on the membrane surface that may wash away the coatings with time. The hydrodynamic stability, on top of thermal and chemical stability, of such membranes needs to be addressed. Secondly, quite a number of such studies focused on treating feeds with free

oil (i.e., droplets larger than 150 μm), which is more effectively separated by other means like hydrocyclones [2]. Thirdly, the uniformity of such modification across larger membranes has to be assessed, particularly because membrane fouling is a self-accelerating process.

2.3.2.2. “Damage-control” approach: Devising effective methods of membrane cleaning

Different cleaning procedures have been proposed and employed in practice to remove foulants from the membrane surface and/or from within membrane pores. Based on the nature of the cleaning methods, they can be classified as hydraulic, chemical and mechanical.

Hydraulic cleaning methods rely on water flushes, water back-flushes, and periodic TMP relaxation [98]. One of the studies employed hydraulic cleaning methods (back-flushing and cross-flushing) to clean UF and NF membranes fouled by hexadecane-in-water emulsions stabilized by Triton X-100, CTAB and DDBS [56]. The results showed that hydraulic cleaning can be used to recover membrane flux when operating below a critical pressure drop across the cake layer. However, once the membrane is wetted by oil, hydraulic cleaning is not effective at restoring the permeate flux.

Hydraulically irreversible fouling calls for the application of a more aggressive cleaning strategy such as chemical cleaning. The chemicals include aqueous solutions at extreme pH (alkaline or acidic, depending on the predominant foulant) and oxidizing compounds (e.g., hypochlorite) [99, 100]. Aggressive chemical cleaning gradually degrades membrane materials, accelerates membrane aging and shortens membrane’s lifespan [100]. Another study employed two chemical cleaning techniques to remove oil

adsorbed onto a PVDF UF membrane [101], namely, (i) washing with a micellar solution consisting of a surfactant (SDS) and an alcohol in water (pentan-1-ol); and (ii) immersion of the fouled membrane in a HCl-NaCl-gasoline aqueous solution. Both could restore the properties of the membranes to 97% of the initial permeability. Zhang et al. evaluated cleaning strategies for removing crude oil from a polyamide NF membrane using flux measurements, salt rejection experiments, atomic force microscopy (AFM), contact angle measurements and ATR-FTIR. The results indicated that optimal cleaning consisted of two stages: cleaning with an alkaline (pH 11) solution of 0.05% EDTA, 0.2% sodium pyrophosphate and 0.2% SDS for 0.5 h, followed by an HCl solution (pH of 2) for 0.5 h. The cleaning approach recovered permeate flux without damaging the membrane [102].

Mechanical cleaning methods include air flushing, ultrasound, vibrational cleaning and sponge ball cleaning [4]. Juang and Lin used a horn ultrasonicator to recover permeate flux of a UF membrane used to filter water-in-oil emulsions [103]. Experiments explored the effects of sonicator tip position, ultrasonic power, and solution properties such as percentage of emulsification and volumetric ratio of emulsions to the external aqueous phase. The results demonstrated that the membrane lifespan could be prolonged with careful control of the ultrasonic intensity, such as below about 80 W/cm², due to the trade-off between the higher fouling mitigation efficiency and the higher degradation of organics associated with a higher power. One of the commercial membrane modules which include both chemical and hydraulic cleaning via the cleaning-in-place (CIP) method is CeraMem® from Veolia Water Tech [34]. Chemical cleaning is done using a combination of caustic soda, citric acid and sodium hypochlorite, while hydraulic cleaning by backwash. Another chemical cleaning bench-scale study was done

at the Qatari LNG Plant by Suez Water Technologies & Solutions, USA. A sequence of cleaning by hypochlorite and then followed by citric acid was found to be adequate to recover the flux in membrane bioreactors [104].

Due to the deformability of oil droplets and the propensity to form a contiguous film, cleaning the membrane fouled with oil is more difficult than that fouled with rigid particulates. Hydraulic cleaning is effective for external fouling (i.e., fouling on the membrane surface) but not irreversible fouling. On the other hand, chemical cleaning is more effective due to its capability to remove irreversible fouling as well. Past studies indicate that cleaning, whether physical or chemical, cannot recover the membrane performance totally, so effective membrane fouling mitigation is essential to prolong filtration and delay cleaning as much as possible.

2.3.3. Quantifying the extent of membrane fouling

2.3.3.1. Permeate flux

Membrane separation is characterized in terms of permeate flux and selectivity. When the feed is ultrapure water, the hydraulic resistance of the membrane, R_m (m^{-1}), can be obtained using Darcy's equation [98]:

$$J_0 = \frac{\Delta P}{\mu R_m} \quad (1)$$

where J_0 is volumetric permeate flux membrane ($\text{m}^3/\text{m}^2 \cdot \text{s}$), ΔP is the transmembrane pressure differential (Pa), and μ is the dynamic viscosity of the permeating solution ($\text{Pa} \cdot \text{s}$).

When the feed contains components other than water, Eq. (1) needs to be modified to include the osmotic pressure differential across the membrane, $\Delta\pi$ (Pa) and added resistance to the permeate flux due to fouling, R_f (m^{-1}):

$$J = \frac{\Delta P - \sigma \Delta \pi}{\mu(R_m + R_f)} \quad (2)$$

where σ is the reflection coefficient.

For the permeate flux to occur in the direction from the feed to the permeate side of the membrane, the pressure exerted across the membrane needs to be larger than the osmotic pressure. The osmotic pressure can be calculated using van't Hoff's equation (3):

$$\Delta \pi = i \cdot R \cdot T \cdot (C_m - C_p) \quad (3)$$

where i is the van't Hoff's factor (unitless), R is the ideal gas constant ($J/mol \cdot K$), T is the temperature of the solution (K), C_m (mol/L) is the concentration of solute in the immediate vicinity of the membrane surface and C_p (mol/L) is the solute concentration in the permeate. Rejected solutes form a mass transfer boundary layer adjacent to the feed face of the membrane. This effect, known as concentration polarization, describes how C_m relates to the concentration of the bulk feed, C_f . Thin film theory can be used to predict C_m in terms of C_f , permeate flux J and mass transfer coefficient k_{cp} (m/s):

$$\frac{c_m - c_p}{c_f - c_p} = e^{\left(\frac{J}{k_{cp}}\right)} \quad (4)$$

The mass transfer coefficient k is given by a ratio of the diffusion coefficient of the solute (m²/s) to the thickness of the boundary layer (m). The latter can be predicted based on the Sherwood correlations available for membrane channels of several geometries (e.g. flat slit, tubular, hollow fibers) commonly employed in membrane systems [105].

Eq. (2) can be recasted as the energy balance equation (e.g., [106]) to illustrate the individual contributions of osmotic pressure and hydraulic resistance of the deposited oil layer to the permeate flux decline:

$$\frac{\Delta P_m(t)}{TMP} + \frac{\Delta P_d(t)}{TMP} + \frac{\Delta \pi_m(t)}{TMP} = 1 \quad (5)$$

2.3.3.2. Selectivity

The selectivity of the membrane is important in conferring the rejection needed to ensure the purity of the retentate and/or permeate. In the membrane-filtration of oily water, the selectivity of the membrane can be represented by the percentage rejection (R), which is quantified by factoring the difference of oil concentrations at the feed (C_f) and the permeate (C_p) sides [16, 47]:

$$R (\%) = \left(\frac{C_f - C_p}{C_f}\right) \times 100\% \quad (6)$$

A trade-off inevitably exists between permeability and selectivity. On the one hand, larger pore sizes give higher permeability but lower selectivity. On the other hand, smaller

pore sizes give lower permeability but higher selectivity. To this end, researchers have continuously striven to push the limits of both permeability and selectivity simultaneously.

As fouling progresses, oil rejection or selectivity deteriorates [3]. Oil, unlike other rigid colloidal foulants, can deform and penetrate through the membrane pores and thereby reduces the permeate quality [107]. Penetration of the oil occurs only if the TMP is high enough to overcome the critical pressure, which is based on the Young-Laplace equation and developed to describe the penetration of the oil droplet or oil film into the pores [108]. In the presence of the typical cross flow implemented to mitigate fouling, the permeation of the oil is not only dependent on TMP alone, but also on the force balance between permeation and drag force from the cross-flow shear. Darvishzadeh et al. subsequently extended the simulation study to incorporate this shear effect for an oil droplet pinned on the pore entrance [107], and considered many parameters that can affect the permeation of the oil droplet, such as droplet to pore size ratio, surface tension and viscosity ratio. Experimentally, one study found that, increasing the cross-flow velocity (CFV) decreased then increased oil rejection [109]. This is because the cross flow has the twin effects of enhancing permeation due to the higher pressure and also enhancing coalescence to form a secondary membrane that resists permeation. In another experimental study, as the TMP increased, the flux increase accelerated pore blockage and thereby decreased oil rejection [110]. Clearly, the trade-off between permeability and selectivity has to be considered, with particular consideration of the deformation and coalescence of the oil droplets.

2.3.4. Evaluating the fouling potential of the feed solution

Several indices have been devised to quantify the fouling propensity of the membrane feed. The indices can be obtained in simple tests by following standard testing procedures and can help with the choice of the suitable membrane type.

2.3.4.1. Silt Density Index (SDI)

The Silt Density Index (SDI) is a common method used to quantify the fouling propensity of feed water. The test procedure involves measuring the time needed for 500 ml of the feed solution to pass through a 0.45 μm microfiltration membrane at 30 psi (~207 kPa) [111]. After 15 minutes of filtration, the time required to filter the same volume is recorded. Conventionally, the measurement is taken over a period of 15 min, but when the solution has high fouling properties, the 15-min time interval can be shortened to 10, 5 or 3 min. SDI can be calculated using the following equation:

$$\text{SDI} = \frac{100}{t} \cdot \left(1 - \frac{t_i}{t_f}\right) \quad (7)$$

where t is the total filtration duration, t_i is the time at the start of the filtration, and t_f is the final time to filter 500 ml of sample after 15 minutes. SDI is not a sensitive fouling index since it is a static measurement of resistance at preset time intervals (i.e., only based on initial and final measurements) and does not measure the rate of change of resistance during the filtration test. In addition, it only measures the fouling rate associated with particles larger than 0.45 μm , although RO fouling can be caused by particles much smaller than 0.45 μm [112]. The standard blocking method of fouling was

found to be the more dominant fouling mechanism during the SDI measurement, but was not in a good agreement with the base assumption of the SDI measurement of total rejection of the colloidal particles. The question regarding of the applicability of SDI also revolved around the fact that fouling is affected by many factors, which include both membrane and colloidal characteristics. Ghaffour et al. [113] found that the variability of the SDI values between two MF membrane with similar mean pore sizes of 0.45 μm was due to differences in membrane thickness and pore size distribution. The thinner membrane gave a higher permeate flux, which brought more particles to the membrane and increased the fouling extent, and thus the SDI value. A similar result was reported by Alhadidi et al regarding the effect of membrane properties on the SDI value [114]. In their study, eight different membranes with similar mean pore sizes were employed to study the variance of the SDI values. They proved that the SDI value was affected by factors that affect membrane resistance like pore size and shape, bulk and surface porosity, thickness, morphology, surface roughness and also zeta potential. These results suggest that SDI is not the best parameter for characterizing the potential of fouling from the feed water, but it is still one of the most popular means due to its simplicity. Other fouling indices such as Modified Fouling Index (MFI) and Combined Fouling Index (CFI) have been proposed as more accurate fouling metrics than SDI.

2.3.4.2. Modified Fouling Index (MFI) and Combined Fouling Index (CFI)

The Modified Fouling Index (MFI) is a dynamic index that takes into account the evolution of the cake resistance during the filtration test. MFI is determined using the same equipment (0.45 μm microfiltration membrane) as the SDI, but the volume is recorded every 30 seconds over a 15 minutes filtration period [115]. This fouling index is

based on the concept of cake filtration where the thickness of the cake layer formed at the membrane surface is directly proportional to the filtered volume. The MFI value can be determined from the gradient of the general cake filtration equation for constant pressure in a t/V versus V plot [98]:

$$\frac{t}{V} = \frac{\mu R_m}{\Delta P A} + \frac{\mu \alpha C_f}{2 \Delta P A^2} V \quad (8)$$

Equation 8 can be rewritten as:

$$\frac{1}{Q} = \alpha + MFI \cdot V \quad (9)$$

where V is the filtrate volume, t is the filtration time and α is the specific resistance of the deposited cake.

The assumption implicit in the MFI approach is that cake filtration is the only fouling mechanism [98]. However, other mechanisms often contribute to permeate flux decline (e.g., pore blocking by smaller particles). Thus, both SDI and MFI are deficient in that they do not account for fouling mechanisms occurring when smaller particles are present in the feed. Therefore, SDI and MFI underestimate the extent of fouling that would be observed in practice with UF, NF and RO membranes.

Unlike SDI and MFI, the Combined Fouling Index (CFI) estimates the potential RO/NF fouling due to various fouling mechanisms by combining MFI values obtained from individual MFI tests. Choi et al. used three different membranes (hydrophilic MF, hydrophobic MF and hydrophilic UF) to measure MFI [116] and calculated CFI by assuming a linear combination of the three MFI values:

$$CFI = \omega_1 M_1 + \omega_2 M_2 + \omega_3 M_3 \quad (10)$$

where M_1 , M_2 and M_3 are the MFI values of the three membranes. The weighing factors ω_1 , ω_2 and ω_3 are calculated based on the flux decline rate (φ) of each membrane, which is defined as [116]:

$$\varphi = \frac{1}{J_o^2} \cdot \left. \frac{dJ}{dt} \right|_{t=0} \quad (11)$$

where J_o is the initial permeate flux and t is the filtration time.

2.3.4.3. Applicability of SDI, MFI, and CFI to quantifying membrane fouling by oil-water emulsions

The fouling indices (SDI, MFI, and CFI) described above are measured using dead-end filtration, but most practical oil-water membrane separations are performed in a crossflow mode. Thus, these fouling indices do not account for the possibility of back-transport due to crossflow. Yet, hydrodynamic conditions can have a profound impact on membrane fouling. For example, membrane fouling by emulsified oil can be mitigated by oil coalescence [84] wherein oil droplets coalesce to reach a critical size and then are swept off the membrane surface by the crossflow shear.

Another concern is the applicability of the same fouling indicator to a variety of oil/water emulsion feed solutions. As described in Section 2.1.1., oily industrial wastewater can vary in composition depending on its source. For instance, produced water may have much higher salinity than oily wastewater produced by food industries. In addition, oil content and droplet size can impact permeate flux decline as increasing oil concentration in the feed can lead to a greater decline in flux. The other limitation is that

MFI and SFI tests use a microfiltration membrane and it is questionable to what extent this membrane can predict the performance of different membranes.

2.4. Understanding membrane fouling by oily wastewater: Measurement approaches and techniques

Significant research efforts have been directed at understanding membrane fouling and development of effective fouling mitigation strategies. The suite of technologies reviewed in this section includes non-invasive and in-situ approaches to assess membrane fouling.

2.4.1. Offline Measurement

Offline measurements have also been used for studying the membrane fouling phenomena. Either a scaled-down version of the process is studied or the membrane is taken offline for measurement of pore size or membrane autopsy after the operation is shut down.

2.4.1.1. Direct Observation through Membrane (DOTM) and other microscopy-based techniques

The direct observation through the membrane (DOTM) technique [84, 86, 117-130] and other microscopic techniques, such as Direct Microscopic Observation (DMO) [131] or Direct Visual Observation (DVO) [132, 133], are based on the usage of light microscopy to directly observe the membrane surface. Firstly introduced by Li et al. [127] as a novel way to study particle deposition on the membrane, the DOTM uses transparent

membranes to enable the visualization of the feed-membrane interface (**Figure 2**). In the other microscopic techniques, non-transparent membranes can be studied of different types (e.g. hollow fiber) [132, 134], materials (e.g. cellulose acetate) [133], and pore sizes (e.g. NF membranes) [131]. The DOTM studies were largely correlated with critical flux [135], which is the permeate flux value below which fouling is negligible. Regarding oil emulsions, DOTM was used by Tummons et al. [84, 130] to study the behavior of deposited oil droplets on the membrane surface. DOTM tests with hexadecane-in-water emulsion stabilized by sodium dodecyl sulfate (SDS) revealed three characteristic stages of membrane fouling by emulsified oil: (1) droplet attachment and clustering, (2) droplet deformation, and (3) droplet coalescence. Visualization by DOTM was complemented with a force balance analysis on an oil droplet pinned on a single pore at the membrane surface. Another study used molecular dynamics simulations and DOTM to explain the coalescence behavior by some oils [86].

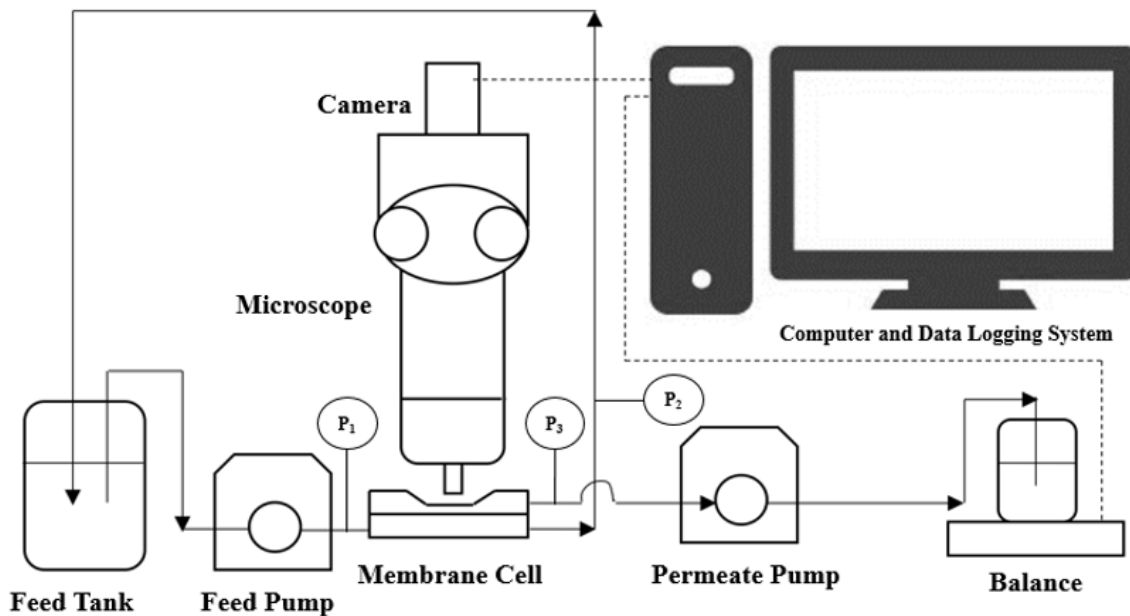


Figure 2. Direct Observation through the Membrane (DOTM) Setup

2.4.1.2. Optical Coherence Tomography (OCT)

Optical Coherence Tomography (OCT) was used initially in the medical field and now commonly in membrane-based filtration processes. OCT is based on light interference generated by a near-infrared light beam, which is split into two channels, with one going to the reference mirror and the other to the membrane cell. In the membrane cell, the light is back-scattered from different media and recombined again with the light from reference mirror, which results in an interference spectrum detected by the spectrometer. The schematic of the OCT is presented in **Figure 3**. By using Fourier Transform Interferogram, the depth information can be known (A-scan), and the collection of these A-scans is known as B-scan, which gives the plane-view of the membrane. Gao and coworkers used OCT to characterize the velocity profile normal to the membrane surface when different orientations of spacers (i.e., 0° , 45° , and 90° to the crossflow) were used [136]. Another study utilized OCT to image biofilms in NF and RO systems, and found that the biofilm was more compact when the permeate flux increased [137]. This indicates that membrane performance deterioration was not only related to biofilm thickness but also the internal biofilm structure. The OCT was also used to study colloidal fouling (silica and bentonite) [138], and internal fouling by oil emulsions [87].

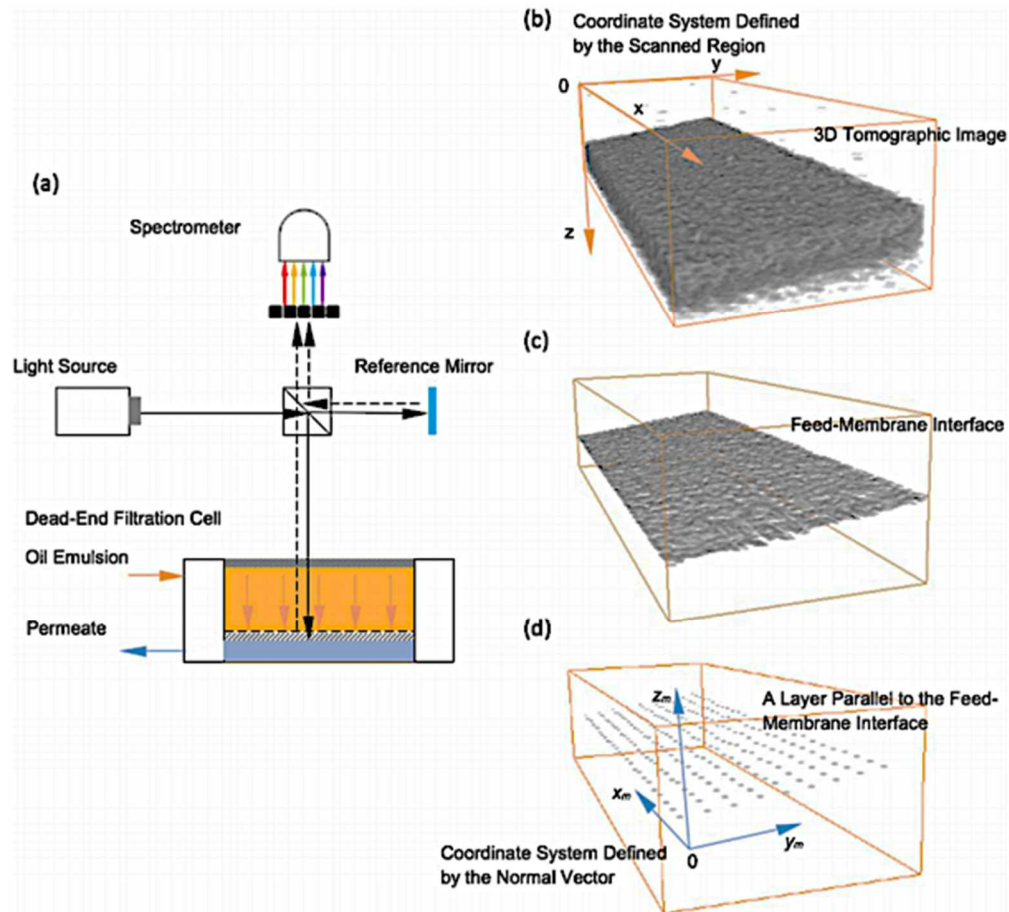


Figure 3. (a) The OCT system that gives a 3D tomographic image of the scanned region (b), which can be further analyzed to identify the feed-membrane interface (c) and layers parallel to the feed-membrane interface to detect fouling (d) [87].

2.5. Conclusions

The abundant oily wastewater would harm the environment if discharged without proper treatment. In view of the urgent need to treat the vast volumes of oily wastewater and the promises of membrane technology playing an important role, a comprehensive review on the practical aspects of membrane-based filtration for oil-water separation was carried out. The present review focuses on practical aspects of applying membrane technology to treatment of oily wastewater. The sources and composition of oily wastewater are appraised. Depending on the source, the composition of oily wastewater

can vary broadly complicating the selection of an appropriate treatment technology. Yet, environmental regulations mandate a certain degree of treatment before the water can be discharging into the environment. Commercially available membrane technologies used to separate oil and water has been used increasingly in the last few years, with ceramic tubular membranes and flat sheet polymeric membranes being most popular. Membrane technology complements rather than replaces the conventional methods for treating oily wastewater to achieve a higher quality product sustainably. The integration of membrane-based and other methods harnesses the advantages and also circumvents the shortcomings of each. The cost of membrane-based treatment of oily wastewater is quite varied, but is generally lower than conventional technologies.

Approaches to mitigating membrane fouling include fouling-resistant membranes, turbulence promoters and membrane cleaning. For the novel membranes, on top on proving superiority in performance, practical issues such as longer-term durability of the coats in the presence of cross-flow, treatment of realistic feeds, and uniformity of modification across large membrane areas have to be addressed too. With respect to turbulence promoters, increasing the shear stress gives better membrane fouling mitigation on one hand, but may affect the membrane integrity on the other hand and thereby reduce rejection. As for membrane cleaning, the deformability of oil droplets and the propensity to form a contiguous film makes total recovery more difficult, so effective membrane fouling mitigation is essential to prolong filtration and delay cleaning as much as possible.

Offline methods to study membrane fouling have been gaining more attention lately. Online means allow for real-time monitoring of practical membrane processes in order to

provide for early warning of membrane fouling. In contrast, offline methods allow for a more in-depth mechanistic understanding of membrane fouling. The discussion of the monitoring methods is concluded by a perspective on the potential of coupling state-of-the-art techniques to facilitate better monitoring and control of membrane fouling by oil.

CHAPTER THREE

Membrane fouling by surfactant-stabilized oil-water emulsions: Effect of emulsion stability and salinity

3.1. Introduction

Oily wastewater is produced by various industries such as oil and gas, food and beverage, metal and machining, and pharmaceuticals [139-142]. One of the largest sources of oily wastewater is produced water (PW), which refers to water trapped in underground formation and is brought to the surface during the oil and gas extraction process. The composition of PW varies considerably as it is related to the chemical characteristics of the geological formation and the hydrocarbon product itself [143, 144]. In addition, PW can include other chemicals that stem from the displacing fluid injected into oil reservoirs [145]. The chemistry of PW is complex and the exact makeup composition is often unknown or proprietary. PW contains dispersed oil, salts, dissolved organics and inorganics, heavy metals as well as chemical additives used to enhance oil recovery (EOR) and prevent operational problems [146]. Such chemicals include surfactants, scale and corrosion inhibitors, and biocides [147].

Over the last decades, many studies have focused on the use of membrane filtration to remove small micron-sized oil droplets from produced water. Nevertheless, the widespread of this technology is still hindered by membrane fouling by emulsified oil. Most the studies related to treating PW have focused on fabricating superoleophobic – superhydrophilic membranes that are resistant to fouling by oil. However, surfactants present in PW can also play an important role in modifying membrane surfaces making

the initial surface chemistry unimportant.

In case of microfiltration (MF) and ultrafiltration (UF) membranes, sieving effect could be neglected due to the small size of surfactant molecules compared to the membrane pore size. Yet, surfactants can adsorb to the membrane surface altering its charge and affinity [148]. The surfactant-membrane interaction is governed by the surfactant type (e.g. charge, structure, concentration), feed composition (e.g. pH, ionic strength, temperature), membrane type (charge, hydrophobicity) and hydrodynamic conditions. Surfactants can form a monolayer, hemi-cylinders, full cylinders, hemi-micelles, spheres, or bilayers on hydrophilic and hydrophobic membrane surfaces [149]. According to Mai et al., depending on the hydrophilicity of the membrane, long chain surfactants can form hemi-cylinders on hydrophobic surfaces and full-cylinders or spheres on hydrophilic surfaces. On the other hand, short chain surfactants form monolayers regardless of the surface hydrophobicity [149].

Numerous studies have evaluated the effect of surfactant type on membrane fouling by emulsified oil [150-156]. Lu et al. studied the influence of surfactant charge on the performance of ceramic UF membranes. Dead-end filtration tests with surfactant-stabilized crude oil and diesel emulsions revealed less irreversible fouling and higher rejection when the surfactant charge of the oil-water emulsion was opposite to that of the membrane [150]. In a different study, Zhu et al. investigated the separation performance of UF and NF membranes when challenged with anionic, cationic, and nonionic-stabilized hexadecane-water emulsions. Constant flux tests with pure surfactant solutions exhibited no change in transmembrane pressure indicating that emulsified oil was solely responsible for the fouling observed in experiments with surfactant-stabilized emulsions.

In UF filtration tests, when the negatively charged polysulfone membrane was challenged with the CTAB-stabilized emulsion, the membrane was rapidly fouled due to the strong electrostatic attraction compared to the less fouling experienced during the crossflow ultrafiltration of SDS and Triton-stabilized emulsions. For NF filtration tests, exponential fouling was exhibited for all three surfactant-stabilized emulsions. Upon the addition of NaCl, there was no significant difference between the surfactants [151].

Dickhout et al. also examined the effects of surfactant type and ionic strength on UF performance. The filtration behavior of hexadecane-water emulsions stabilized by four surfactants, namely, anionic (SDS), cationic (CTAB), non-ionic (Triton), or zwitterionic (DDAPS), were compared. Ionic strength had a profound impact on the filtration behavior of the hexadecane-water emulsion stabilized by the charged surfactants. For SDS-stabilized emulsions, increasing ionic strength led to a higher flux decline due to the formation of a dense cake with low porosity. For CTAB-stabilized emulsions, the effect was less pronounced where increasing ionic strength led to higher surfactant adsorption and oil permeation. The worst type of fouling was observed for the Triton-stabilized emulsions regardless of the ionic strength as it had no effect on the flux decline. For DDAPS-stabilized emulsions, lower flux decline was observed at higher ionic strength [152].

Nagasawa et al. evaluated the fouling propensity of negatively charged ceramic MF membranes by SDS or DTAB- stabilized hexadecane-water emulsions. For small pore sizes, severe fouling was accompanied with excellent oil rejection irrespective of the surfactant type. Surfactant choice became more important when the membrane pore size was comparable to that of the oil droplet size. For SDS-stabilized emulsions, severe flux

decline was observed and complemented with a moderate oil rejection. In case of DTAB-stabilized emulsion, oil droplets deformed resulting in permeation through the membrane [153]. More recently, Virga et al. studied the effect of salinity, surfactant type (anionic, cationic, non-ionic) and concentration to understand the influence of interfacial tension on oil permeation during crossflow filtration of hexadecane-water emulsion. The results indicated that oil retention transited from high to low with decreasing interfacial tension for SDS, CTAB, Triton-stabilized emulsions [154].

Direct observation through the membrane (DOTM) has been employed to elucidate the mechanisms of membrane fouling by emulsified oil [148]. Tummons et al. employed the first application of a direct visualization technique to study the effect of surfactant concentration on oil droplet behavior at the membrane surface in the presence of crossflow. In this study, the evolution of the oil fouling layer was imaged in real-time during microfiltration of SDS-stabilized hexadecane emulsions. DOTM results revealed three distinct stages of membrane fouling: droplet attachment and clustering, droplet deformation, and droplet coalescence followed by the removal of droplets larger than a critical size [157]. In a follow-up study, the effects of anionic surfactant and divalent counterions concentrations on membrane fouling by emulsified oil were investigated. The high ionic strength of divalent cations decreased the solubility of the anionic surfactant as well the interfacial tension and zeta potential of oil droplets promoting coalescence at the membrane surface [158]. Tanudjaja et al. also employed the DOTM technique and observed droplets forming stripes during crossflow microfiltration of Tween-stabilized emulsions. The formation or disappearance of stripes was a strong function of hydrodynamic factors (e.g. permeate drag and crossflow shear), oil-membrane, and oil-

oil interactions [159]. The same group further used the DOTM technique to evaluate the critical flux for various emulsions (i.e. different oil types) and found that the DLVO theory predicts fouling by emulsified oil better than XDLVO [160]. More recently, Tummons et al. used modeling and direct visualization to examine the effects of anionic surfactant and salinity on oil droplet adhesion to model NF membranes. The results indicated that emulsion properties (i.e. electrical charge and stability) together with membrane's affinity for oil govern droplet attachment to the membrane surface [161].

To improve the practical feasibility of membranes for oil-water separation, a thorough understanding of oil deposition at the membrane surface during separation is needed to both optimally design and operate such processes. In this study, we examine the effects of surfactant type (i.e. non-ionic, or a mixture of surfactants) and salinity on ultrafiltration (UF) membrane performance. DOTM was employed to visualize the evolution of fouling for emulsions containing different surfactants and salts. Hexadecane-in-water emulsions were prepared and stabilized by either non-ionic surfactant (Triton X-100) or a mixture of anionic and non-ionic (Corexit EC9500A). Emulsions were characterized in terms of size, interfacial tension, and contact angle with the UF membrane. The emulsion and membrane properties were correlated with the observed oil behaviors and translated into fouling mechanisms.

3.2. Materials and Methods

3.2.1. Reagents

Hexadecane (99%), Triton X-100 (TX-100, laboratory grade), magnesium sulfate heptahydrate ($\text{MgSO}_4 \cdot 7\text{H}_2\text{O}$, $\geq 98\%$), and sodium chloride (NaCl , $\geq 99\%$) were purchased from Sigma-Aldrich. Instant Ocean (IO) sea salt mixture was purchased from Petco. Corexit EC9500A (Nalco Environmental Solutions, LLC) was provided by the National Oceanic and Atmospheric Administration. Corexit EC9500A (hereinafter, CE9500) is a mixture of nonionic surfactants (sorbitan monooleate (Span 80), sorbitan monooleate polyethoxylate (Tween 80), sorbitan trioleate polyethoxylate (Tween 85)) and an anionic surfactant (dioctyl sodium sulfosuccinate (DOSS)) in a solvent that consists of 1-(2-butoxy-1-methylethoxy) propanol and light hydrocarbon distillates [162, 163]. All solutions were prepared using ultrapure water (resistivity of $\sim 18 \text{ M}\cdot\text{cm}$) supplied by a Milli-Q ultrapure water system (Integral 10, Millipore) with a terminal $0.2 \mu\text{m}$ microfilter (MilliPak, Millipore).

3.2.2. Emulsion preparation

Non-saline hexadecane-in-water (HW) emulsions were prepared by dispersing hexadecane at 0.1% v/v ($1000 \mu\text{L/L}$ or 773 mg/L) in 0.1 mM Triton X-100 or 0.001% v/v ($10 \mu\text{L/L}$ or 7.89 mg/L) CE9500 solutions using a digital stand mixer (RW 20 digital dual-range mixer, IKA) at 1000 rpm for 20 min. The surfactant values were below the reported critical micelle concentration (CMC), which is in the 0.2 -0.9 mM range for Triton X-100 [151] and 27-32 mg/L for CE9500 [164].

To prepare the saline HW emulsions, 27.41 g/L of NaCl (469 mM), 6.53 g/L of MgSO_4 (54.3 mM), or 35.79 g/L of Instant Ocean (IO) were added to water along with the

surfactant prior to the addition of hexadecane. In what follows, the emulsions are referred to as HW-X-Y, where X denotes the type of surfactant (Triton, or CE9500) and Y is either NaCl, MgSO₄, or IO.

3.2.3. Emulsion characterization

Light diffraction (Mastersizer 2000, Malvern Instruments) was used to determine the oil droplet size distribution in the bulk for each feed emulsion. A detailed procedure for interfacial tension measurement is described elsewhere [157, 158].

3.2.4. Membranes used in DOTM tests. Characterization

All DOTM tests were conducted with an inorganic anodized alumina (Anopore) ultrafiltration (UF) membranes (Anodisc, Whatman, UK) with a nominal pore diameter of 0.02 μm . The membranes are optically transparent when wet, which made them suitable for DOTM testing. A new membrane was used in each test. The contact angle of hexadecane droplet with the UF membrane in different aqueous solutions of surfactant/salt were performed using a standard goniometer (model 250-F4, rame-hart instrument co.). A detailed procedure for the contact angle measurements is described elsewhere [157, 158].

3.2.5. Direct observation through the membrane (DOTM) system

A detailed description of the DOTM setup has been provided earlier [157, 165]. Briefly, the DOTM system consisted of a microscope (Axio Imager.M1, Zeiss) and a video camera (Digital Color video camera model TK-C921BEG, JVC) that can capture static images and videos. The active membrane area was 7.56 cm² and was located in the middle of the crossflow channel with the permeate side facing the microscope's objective.

The crossflow velocity was adjusted using a feed gear pump (drive model 75211-15, Cole-Parmer) and was set constant at $3.6 \cdot 10^5 \text{ L}/(\text{m}^2 \cdot \text{h})$ (0.1 m/s) in all the tests.

DOTM tests were conducted in a constant flux mode. Throughout each DOTM test, the permeate flux was maintained at a constant value of $52 \text{ L}/(\text{m}^2 \cdot \text{h})$ ($1.4 \times 10^{-5} \text{ m/s}$) using a peristaltic pump (Minipuls 3, Gilson). The buildup of hydraulic resistance due to membrane fouling by oil led to an increase in transmembrane pressure (TMP). At constant flux, TMP increases as hydraulic resistance increases, so fouling was also characterized by an increasing TMP over time. **Table 4** lists the DOTM tests that were conducted to explore the effects of surfactant type and salinity on membrane fouling by emulsified oil.

Table 4. Eight DOTM tests carried out with Anopore membranes (nominal pore diameter of $0.02 \mu\text{m}$).

Surfactant	Salt			
	-	NaCl	MgSO ₄	IO
Triton	Test 1	Test 2	Test 3	Test 4
CE9500	Test 5	Test 6	Test 7	Test 8

3.3. Results and Discussion

3.3.1. Characteristic of oil-water emulsions

Oil droplet behavior at the membrane surface is a function of several variables: droplet size, interfacial tension, type and concentration surfactant, and type and concentration of other dissolved species (e.g. ions) in the continuous phase. In this subsection, we discuss effect of surfactant and salt on two characteristics of emulsion that define its fouling behavior: droplet size and interfacial tension.

3.3.1.1. Droplet size distribution

The type of surfactant had a significant impact on the droplet size distributions (see Appendix, **Figure 10**). Droplets in Triton or CE9500- stabilized hexadecane-water emulsions had a narrow size range. The volume-weighted mean diameter of droplets was 11.1 μm and 18 μm for the HW-Triton, and HW-CE9500 emulsions, respectively. For the non-saline emulsions, the number-based distributions showed that more than 99% of droplets were smaller than 10 μm (see Appendix, **Figure 10**).

In theory, salt in the continuous phase should not interact with non-ionic surfactants. However, other studies have shown that emulsions stabilized by non-ionic surfactants (e.g. Triton X-100 [151, 166, 167] and Tween 20/80 [150, 168, 169]) confer a negative charge due to the specific adsorption of hydroxyl ions at the oil-water interface. The DSD for the HW-Triton-NaCl emulsion couldn't be reliably measured as the required light obscuration ratio was not reached.

The DSD for the CE9500-stabilized hexadecane-water emulsions had a higher tolerance for ionic strength. The DSD for HW-CE9500 emulsion was broad as it included droplets smaller than 1 μm as well as large droplets (>100 μm). The saline CE9500-stabilized emulsions didn't have such large droplets (>50 μm). The volume-based median droplet diameter of droplets decreased with the addition of salt from 15.3 μm to 2.9 μm , 0.4 μm and 10.6 μm for the HW-CE9500, HW-CE9500-NaCl, HW-CE9500-MgSO₄, and HW-CE9500-IO emulsions, respectively. Stabilization by CE9500 dispersed a fraction of oil into submicron droplets. The average droplet size in DI water, \bar{d}_{drop} , was 0.89 μm . As for instant ocean, \bar{d}_{drop} was 0.59 μm and 0.05 μm for the HW-CE9500-MgSO₄ emulsion.

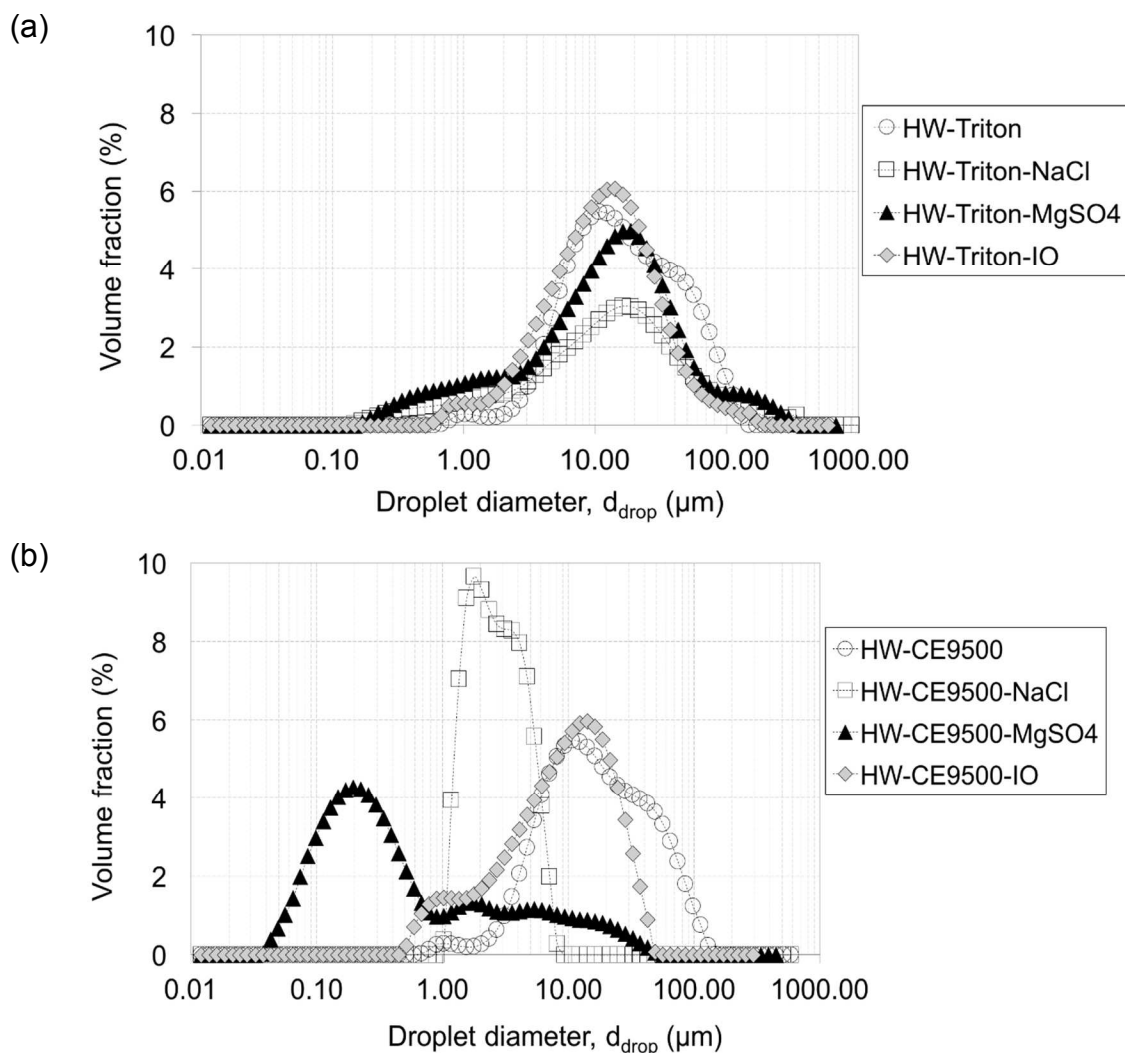


Figure 4. Effect of salt type on droplet size in hexadecane-water emulsions stabilized by Triton (a) and CE9500 (b). Lines are added to guide the eye. The corresponding number-based DSDs are shown in Figure 11.

3.3.1.2. Interfacial tension

Surfactant adsorption leads to a decrease in the interfacial tension of the oil-water emulsion as the interaction between the hydrophilic head group and the surrounding water is much more favorable compared to the interaction of oil and water. Interfacial tension is a key parameter in determining the emulsion stability, the likelihood of droplets deforming, coalescing or breaking up [148]. For charged surfactant head groups, the charge of the surfactant-coated oil droplet inhibits coalescence due to electrostatic

repulsion. **Figure 5a** shows the effects of surfactant type and salt on the interfacial tension of hexadecane-water emulsions.

Several studies have reported that the addition of inorganic salts (i.e. monovalent or divalent) to anionic surfactant solutions can lower their CMC and lead to the precipitation of surfactants in the form of crystals [170-172]. Tummons et al. showed that the addition of MgSO_4 decreases the solubility of SDS and can lead to crystalline precipitates (i.e. magnesium dodecylsulfate salts) [158]. For a mixed surfactant system (anionic and non-ionic), Stellner et al. reported that the counterion concentration necessary to cause precipitation increases with the addition of non-ionic surfactant. Salinity tolerance increases as mixed micelle form, reducing the concentration of anionic surfactant monomers [173].

In our earlier study, the interfacial tension of hexadecane and DI water was measured to be 41.8 mN/m [158]. Triton, the non-ionic surfactant, was able to further stabilize the hexadecane-water emulsion. In the absence of salt, the interfacial tension of HW-Triton was measured to be 18.9 mN/m. The interfacial tension of Triton-stabilized hexadecane droplets didn't significantly change upon the addition of salt.

The CE9500-stabilized hexadecane-water emulsion exhibited the highest interfacial tension in the absence of salt. The addition of 0.001 %v/v CE9500 didn't significantly impact the interfacial tension of the hexadecane-water emulsion. The trend was different than earlier reports with Louisiana sweet crude oil [162] and 1-dodecene [174]. Similar to earlier studies, increasing the ionic strength of the continuous phase led to a decrease in the oil-water interfacial tension [151, 158, 161]. The addition of salt led to a decrease in the interfacial tension of the CE9500-stabilized hexadecane-water

emulsion to an asymptomatic value of approximately 35 mN/m regardless of the salt type and concentration.

This decrease in interfacial tension is due to charge screening, which allows more surfactant to adsorb to the droplet surface. With the lower interfacial measurements, as expected, salt shifted the size distribution of the suspended droplets to smaller sizes. However, an opposite trend was observed for the HW-CE9500-IO, where the addition of salt produced larger droplets.

3.3.2. Membrane characterization

In this subsection, we will discuss the effect of surfactant and salt on the wettability properties of the UF membrane.

3.3.2.1. Contact angle measurements

Figure 5b summarizes the hexadecane contact angle data for the UF Anopore membrane in twelve different aqueous solutions containing different surfactant types and salts.

In the absence of surfactant, the contact angle of hexadecane on the Anopore membrane was measured to be 151°. Upon the addition of the non-ionic surfactant, membrane hydrophilicity increases due to the adsorption of surfactants on the membrane surface and at the oil/water interface, which adds electrostatic and steric forces between the droplets and the membrane surface reducing their interaction [175]. Pichot et al. [176] observed an increase in the contact angle of oil with increasing surfactant concentration until a critical concentration was reached. Zhu et al. [151] also showed that the addition of TX-100 increased the contact angle of hexadecane with UF membrane from 102° to 121°, respectively.

This UF membrane can be classified as “oleophobic” as the average contact angle ranged between 133° and 158°. For Triton, we predicted that the hexadecane contact angle data won't be influenced by ionic strength. However, even though Triton is a non-ionic surfactant, it still carries a negative charge because of the hydroxyl ions that associate with the hydrophilic head of the surfactant molecule. The hexadecane contact angle on the UF membrane in Triton solution decreased upon the addition of salt. At the highest ionic strength, we expect the negatively charged oil droplets to interact more favorably with the membrane, allowing more spreading of the oil droplet. Unlike other surfactants, CE9500 decreased the oleophobicity of the UF membrane. However, the addition of salt compensated and made the membrane less oleophobic.

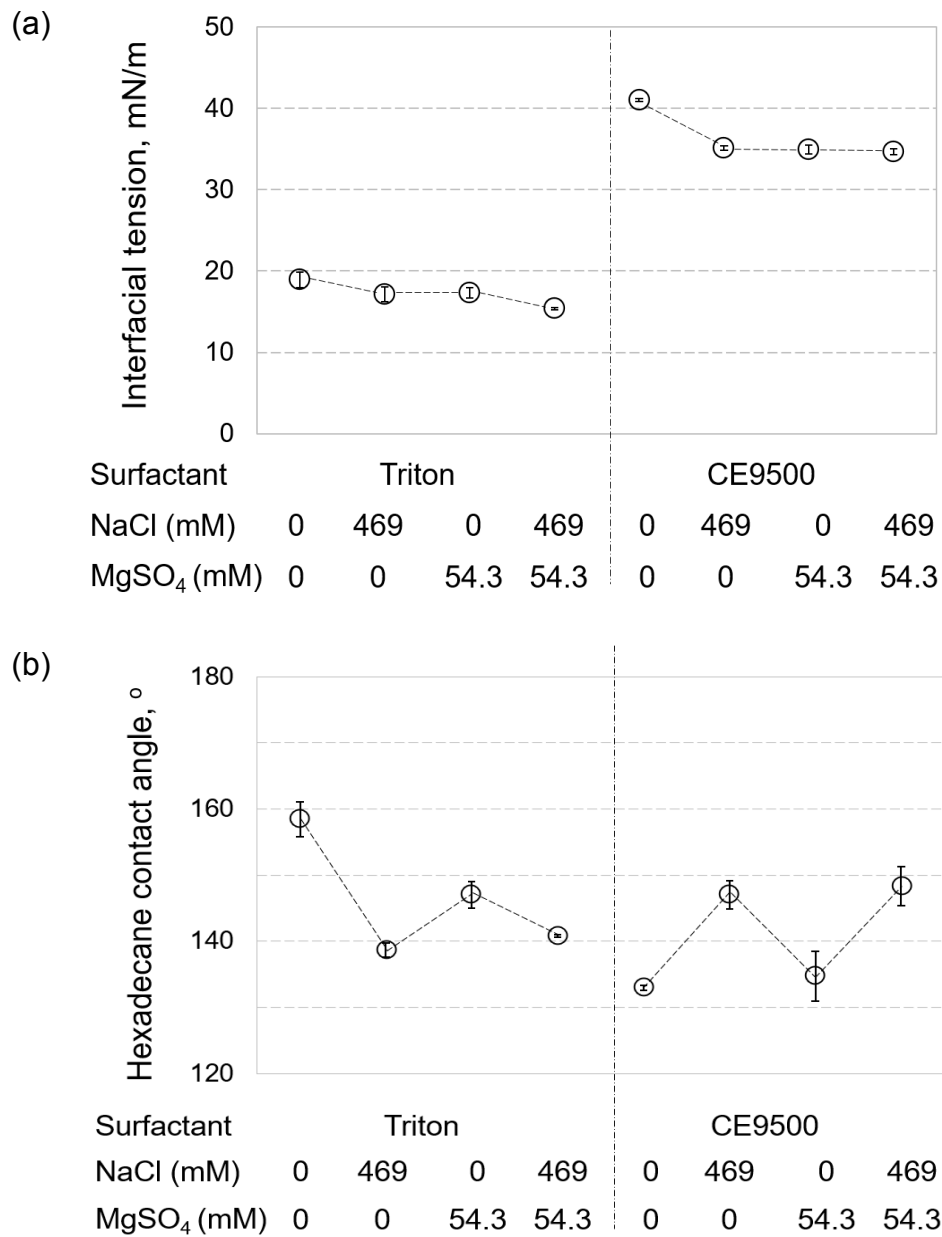


Figure 5. Effect of surfactant and salts in the continuous phase on a) the interfacial tension of hexadecane-water emulsions and b) hexadecane contact angles on 0.02 μm Anopore membrane.

3.3.3. DOTM tests with oil-in-water emulsions

3.3.3.1. Effect of surfactant type on UF membrane fouling by emulsified oil

The type of surfactant dictates the droplet-droplet and droplet-membrane interactions. Fig. S3 shows the interaction of hexadecane droplets with the UF Anopore membrane ($d_{pore} = 0.02 \mu m$). Each of the two rows represent a separate DOTM experiment with an emulsion stabilized by a certain surfactant (Triton or CE9500). The images in each column correspond to the same filtration time into the DOTM test allowing for direct comparison of fouling patterns.

The observed droplet population on the membrane surface in each of the two DOTM tests (HW-Triton and HW-CE9500) was consistent with DSD and interfacial tension measurements. Droplets in the HW-Triton emulsion were the smallest due to the lower interfacial tension (18.9 mN/m) compared to droplets in HW-CE9500 emulsions (41.1 mN/m).

During DOTM Test 1 (See Appendix, **Figure 12**), small droplets of the HW-Triton emulsion rapidly attach to the membrane surface at the beginning of the filtration test forming small clusters. Larger droplets continued to move along the membrane in the crossflow direction. Droplets of the HW-Triton emulsion had a distinct behavior where droplets collectively flowed across the membrane surface and in many events, didn't firmly attach. The high stability of the emulsion and the oleophobicity of the membrane minimized coalescence as droplet-droplet collision typically led to detachment (Video 1). Ten minutes into the test, oil droplets form a layer in the upper and bottom of the focus area with a crevasse of oil-free membrane in-between, where larger droplets continue to flow and small droplets later deposited (**Figure 12**). Within 20 mins, the membrane was

completely covered with a monolayer of small oil droplets, but no coalescence events were observed. The transmembrane pressure was monitored during the constant flux DOTM test and the pressure data correlated with the qualitative DOTM results. Once the membrane focus area was completely covered with oil (20 mins into the test), there was a continual increase in transmembrane pressure over time (**Figure 6**). A survey carried out 60 min into the test showed that most of the membrane was covered with clusters of small oil droplets and occasional large ones (Video 2).

During the early stages of DOTM Test 5 (**Figure 12**), large droplets attach to the membrane surface and droplet deformation was observed. The HW-CE9500 emulsion employed in DOTM Test 5 was less stable (higher interfacial tension) compared to the Triton-stabilized hexadecane-water emulsion. The stronger affinity observed for droplet-membrane interaction coupled with the favorable droplet-droplet interaction led to faster fouling including an early onset for coalescence. Droplet coalescence occurred within two minutes of the DOTM test, where two droplets that encountered each other coalesced (Video 3). As the test continued, more coalescence events were observed. The membrane facilitated coalescence where both droplets remained attached to the membrane surface (Video 4). Droplets coalescing and remaining attached to the membrane surface led to an increase in transmembrane pressure (**Figure 6**). A survey was conducted 60 min into the test showing that the majority of the membrane was covered with a dark veil, few large droplets, and clusters of small droplets (Video 5).

Table 5, column 1, summarizes the characteristic fouling patterns for hexadecane-water emulsion as a function of surfactant type.

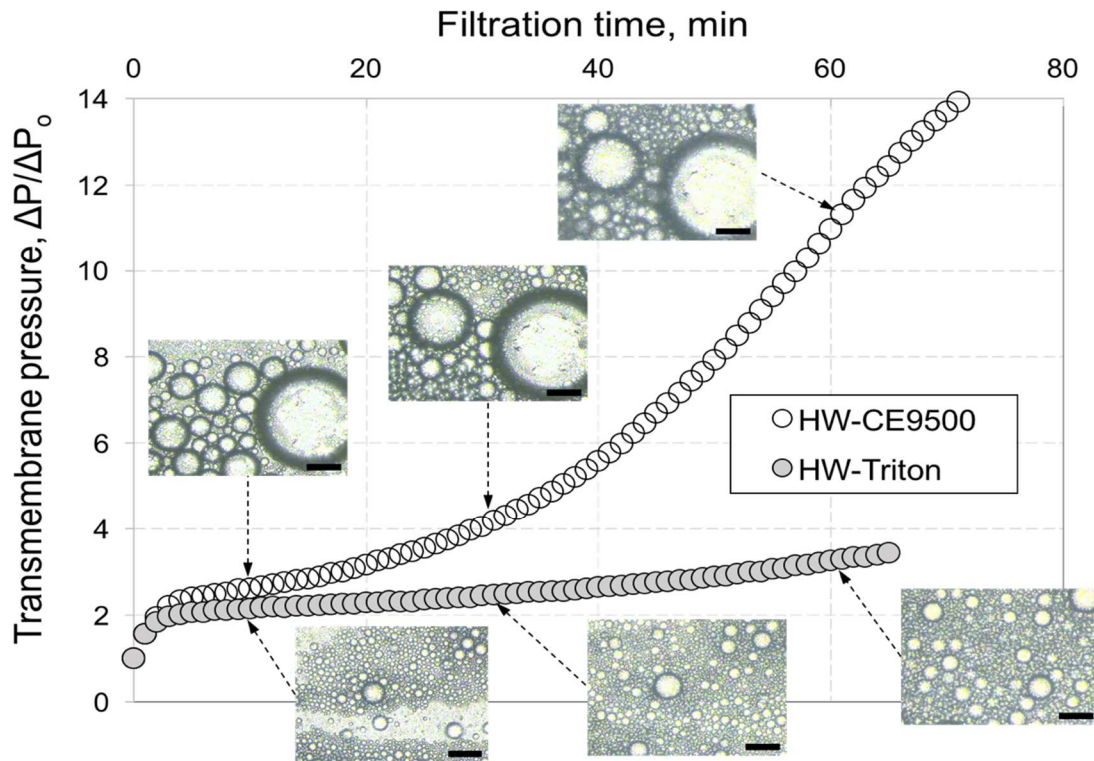


Figure 6. Transmembrane pressure buildup during constant flux DOTM tests with Triton- and Corexit-stabilized emulsions (Tests 1 and 5; Table 4). The size bars in DOTM images correspond to 30 μm .

3.3.3.2. Effect of salt type on UF membrane fouling by emulsified oil

3.3.3.2.1. Effect of NaCl

Incorporation of NaCl to the HW-Triton emulsion led to further droplet attachment to the UF Anopore membrane (**Figure 13** compared to **Figure 12**). This additional oil deposition can be explained by the decrease in the hexadecane contact angle with the UF membrane upon NaCl addition (from 158.5° to 138.7°). Despite the low interfacial tension of the HW-Triton-NaCl emulsion, the Anopore membrane facilitated surface coalescence unlike when the membrane was challenged with the HW-Triton emulsion

(Video 6). A survey 60 mins into the DOTM test showed complete coverage of the membrane by a monolayer of oil droplets (Video 7).

In DOTM Test 6, the Anopore membrane allowed the attachment of the HW-CE9500-NaCl droplets within minutes (see Appendix, **Figure 13**). The lower interfacial tension and droplet size distribution explains the smaller droplets sizes observed during the filtration test. Within eleven minutes, the membrane focus area was completely covered with clusters of oil droplets. Occasional coalescence between a flowing droplet and an attached droplet occurred, but was immediately followed by detachment. Similar to DOTM Test 2, a survey conducted 61 mins into the test, showed a monolayer layer of small oil droplets with no clean membrane area left (Video 8).

Regardless of the surfactant, the presence of NaCl had a similar impact on the fouling of UF membrane by the hexadecane-water emulsion. In both DOTM tests, the membrane was covered with a monolayer of oil droplets. **Figure 7a** shows that the TMP vs time profiles during each of the DOTM tests. During the early stage of DOTM Test 2, the initial jump in transmembrane pressure is attributed to the additional droplet deposition in DOTM Test 2 compared to Test 6.

Table 5, column 2, summarizes the effect of NaCl on the observed fouling patterns for hexadecane-water emulsions stabilized by various surfactants.

3.3.3.2.2. Effect of MgSO₄

The addition of the divalent cation salt had a similar impact to NaCl on the HW-Triton emulsion. Despite the high hexadecane contact angle (147°) with the Anopore membrane, droplets of the HW-Triton-MgSO₄ emulsion immediately attached to the membrane surface (See Appendix, **Figure 14**). In addition, the high stability of the HW-Triton-MgSO₄

emulsion didn't prevent coalescence from occurring. Throughout DOTM Test 3, multiple coalescence events were observed between an attached droplet and a flowing droplet. Coalescence was followed by detachment where the resulting droplet reached a critical size and was swept off by the crossflow shear (Video 9). At the end of the test, a survey of the membrane showed clusters of small oil droplets, a few large droplets that aren't firmly attached to the membrane surface and areas of clean membrane. The survey indicated that membrane coverage by oil droplets was less compared to DOTM tests 1 and 2 (Video 10).

When the Anopore membrane was challenged with the HW-CE9500-MgSO₄ emulsion, droplets rapidly attached to the membrane surface, where small droplets formed clusters (**Figure 14**). A video taken 3 min into DOTM Test 7 (Video 11) showed how oil droplets get jammed at the edge of the membrane focus area. Additional droplets attached forming a monolayer. A survey conducted 60 min into the test, showed that the membrane was completely covered with oil droplets (Video 12).

The formation of a monolayer of oil didn't lead to an increase in TMP as shown in **Figure 7b**. The TMP over time profiles for both surfactants in the presence of NaCl or MgSO₄ were identical. **Table 5**, column 3, summarizes the effect of MgSO₄ on the fouling behavior of Triton or CE9500-stabilized emulsions.

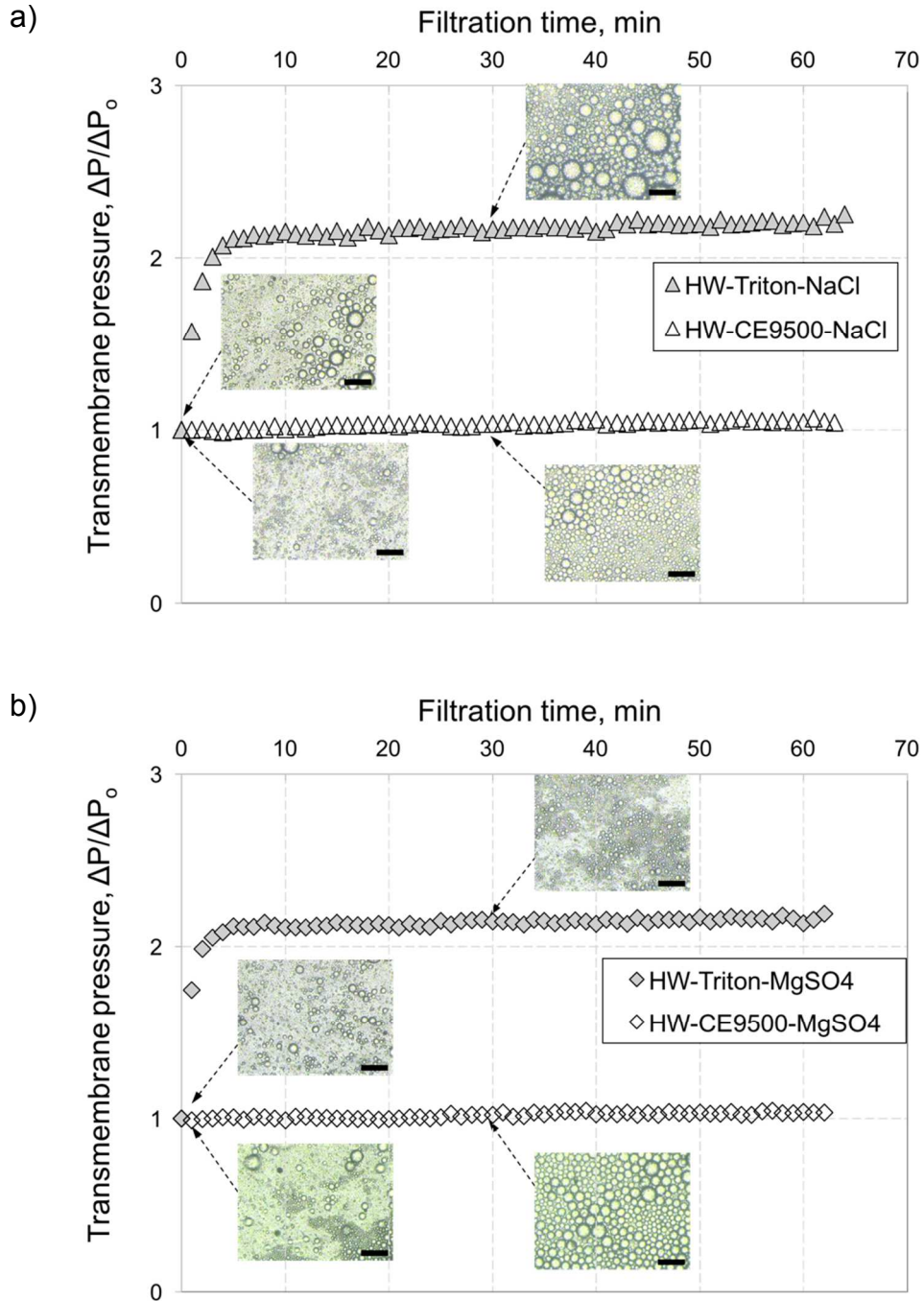


Figure 7. Transmembrane pressure buildup during constant flux in DOTM experiments with Triton- and Corexit-stabilized hexadecane-in-water emulsions as a function of type of salt in the continuous phase: a) NaCl (Tests 2 and 6; Table 1) and b) MgSO₄ (Tests 3 and 7).

3.3.3.2.3. Effect of Instant Ocean

With the addition of instant ocean to the HW-Triton emulsion, droplets rapidly attached to the membrane surface and formed clusters within one min of DOTM Test 4 (See Appendix, **Figure 15**). During the first twenty minutes of DOTM test 4, multiple coalescence events were observed between attached droplets and were typically followed by detachment. However, 37 min into the experiment, coalescence led to droplet deformation and eventually a film formation (Video 13). As the test continued, more coalescence occurred and the membrane was predominately covered with films (Video 14). A survey carried out at the end of the DOTM test showed that the membrane was covered with contiguous oil films with no oil-free areas available for water permeation.

When the Anopore membrane was challenged with the HW-CE9500-IO emulsion, minimal droplet attachment was observed in the early stages of DOTM Test 8 (**Figure 15**). As the test continued, additional droplet deposited on the membrane surface covering most of the focus area. Within fifteen minutes (Video 15), the membrane was covered with deformed droplets which eventually coalesced into an oil film covering the entire focus area (Video 16). In DOTM Test 8, it only took 14 min for the Anopore membrane to be covered with oil films compared to at least 40 min in DOTM Test 4.

The pressure data corroborates the DOTM results (**Figure 8**). The abrupt increase in TMP for the HW-CE9500-IO emulsion at ~14 min is consistent with our observations of oil droplet deformation followed by film formation. For DOTM Test 4, the increase in TMP wasn't until 26 min later, the time it took for the Anopore membrane to be covered with oil films.

Table 5, column 4, summarizes the effect instant ocean sea salt mixture on the characteristic fouling patterns observed during DOTM tests for the different emulsions.

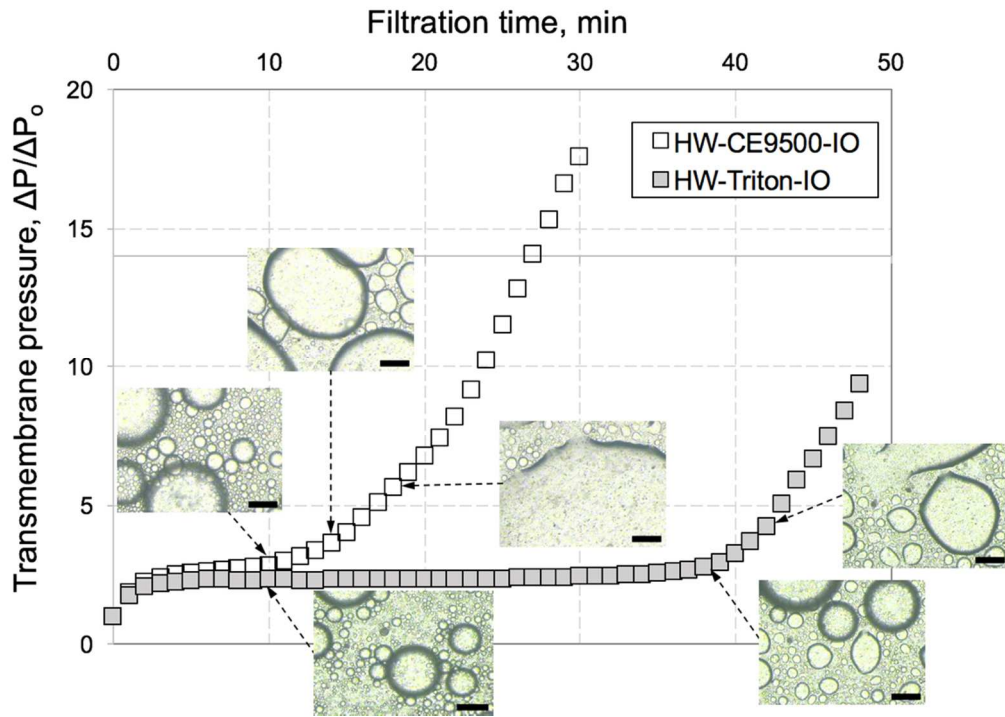


Figure 8. Transmembrane pressure buildup during constant flux in DOTM experiments with Triton- and Corexit-stabilized hexadecane-in-water emulsions in model sea water (Tests 4 and 8; see Table 1). The size bars in DOTM images correspond to 30 μm .

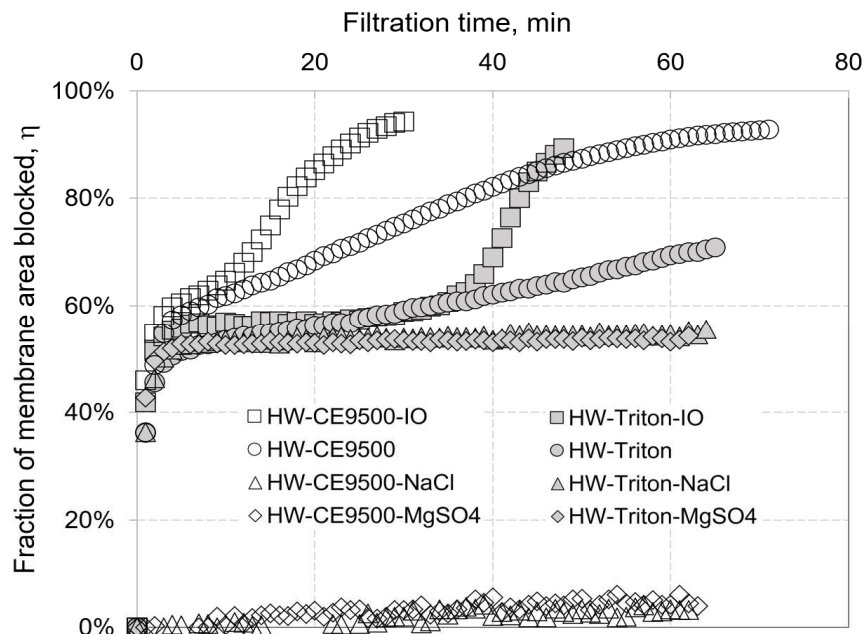


Figure 9. Fraction of the Anopore membrane area blocked by oil as a function of time for Triton (A) and CE9500 (B) – stabilized hexadecane-water emulsions.

Table 5. Distinct fouling patterns observed in DOTM tests as a function of surfactant and salt types

Surfactant	Salt			
	none	NaCl	MgSO4	Instant Ocean
Triton	-Formation of monolayer of oil -No coalescence observed	Formation of monolayer of oil with no areas of clean membrane	-Coalescence followed by detachment -Formation of monolayer of oil with no areas of clean membrane	Deformation and oil film formation at later stages
CE9500	- Multiple coalescence events between attached droplet -Dark veil	Membrane covered with monolayer of oil with oil-free areas	Membrane completely covered with a monolayer of oil	Rapid formation of oil films

3.5. Conclusions

In summary, membrane fouling by emulsified oil is controlled by the surfactant type. In the absence of salt, the stable droplets of the Triton-stabilized emulsion packed tightly together and formed a monolayer of oil droplets. The worst type of fouling was observed for the CE9500-stabilized emulsions where droplets immediately coalesced and remained attached to the membrane surface. In addition, during later stages of filtration, a “veil” covered most of the membrane focus area.

Consistent with earlier studies [151, 153], the addition of NaCl reduced the electrostatic repulsion between droplets and quenched the difference between surfactants. In this case, regardless of the surfactant type, hexadecane oil droplets formed a monolayer on the membrane surface. In the presence of divalent counterions, the fouling behavior of Triton and CE9500-coated droplets on the UF membrane was similar where a monolayer of oil was formed.

Despite the high stability of the emulsions prepared in instant ocean, oil droplets of the Triton and CE9500- stabilized emulsions deposited on the membrane surface and formed contiguous oil films that sealed large areas of the membrane surface.

APPENDIX

APPENDIX

A1. Droplet Size Distribution Analysis

The volume-based median droplet diameter was 8.8 μm for the HW-Triton emulsion and 15.3 μm for the HW-CE9500 emulsion. The corresponding number-based mean diameters were 0.9 μm , 0.8 μm and 0.8 μm (Fig. 10).

The addition of salt led to an increase in the volume-weighted mean diameter of droplets from 11.1 μm for the non-saline emulsion to 24.6 μm and 16 μm for the HW-Triton-MgSO₄ and HW-Triton-IO emulsions, respectively. The corresponding number-based mean diameters were 0.2 μm , 0.8 μm , and 0.9 μm (Fig. 11).

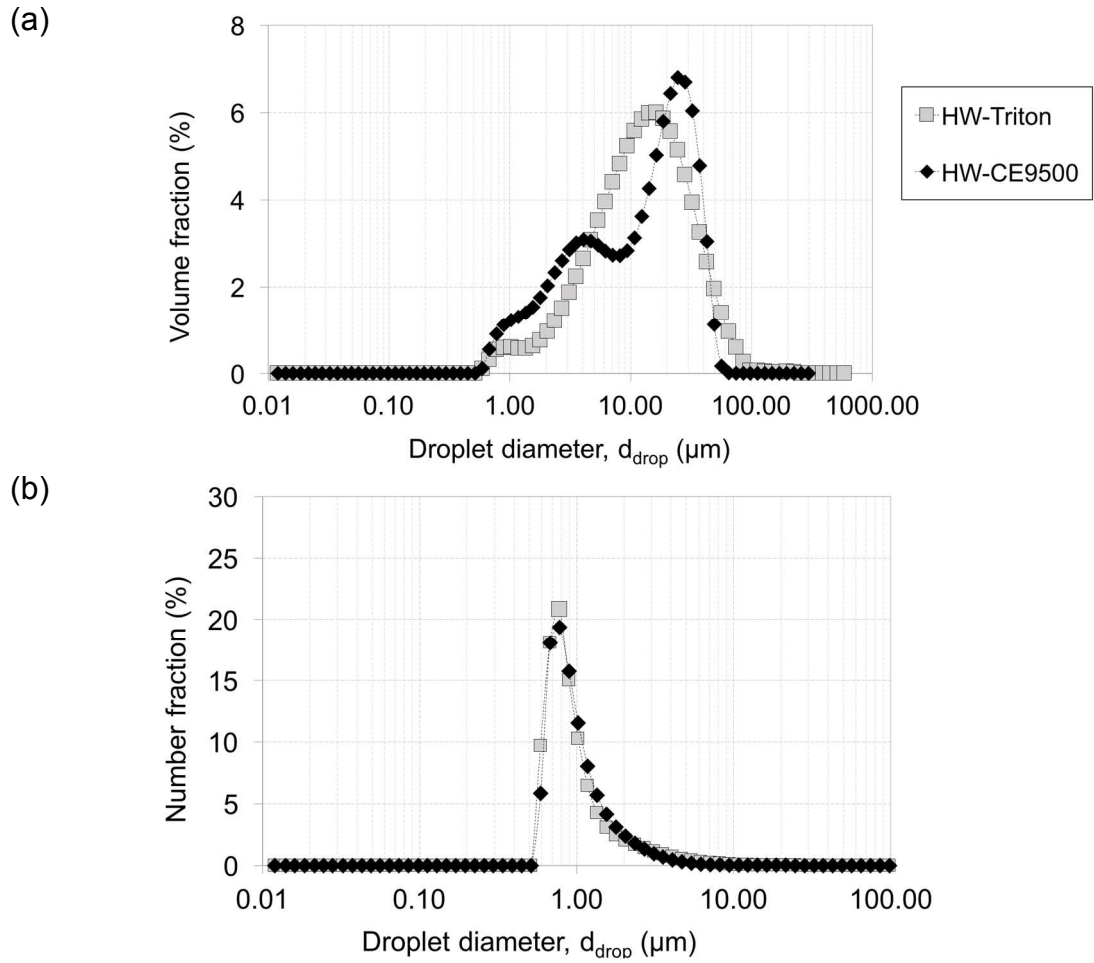


Figure 10. Effect of surfactant type on volume-based (a) and number-based (b) droplet size distribution in hexadecane-water emulsions. Lines are added to guide the eye.

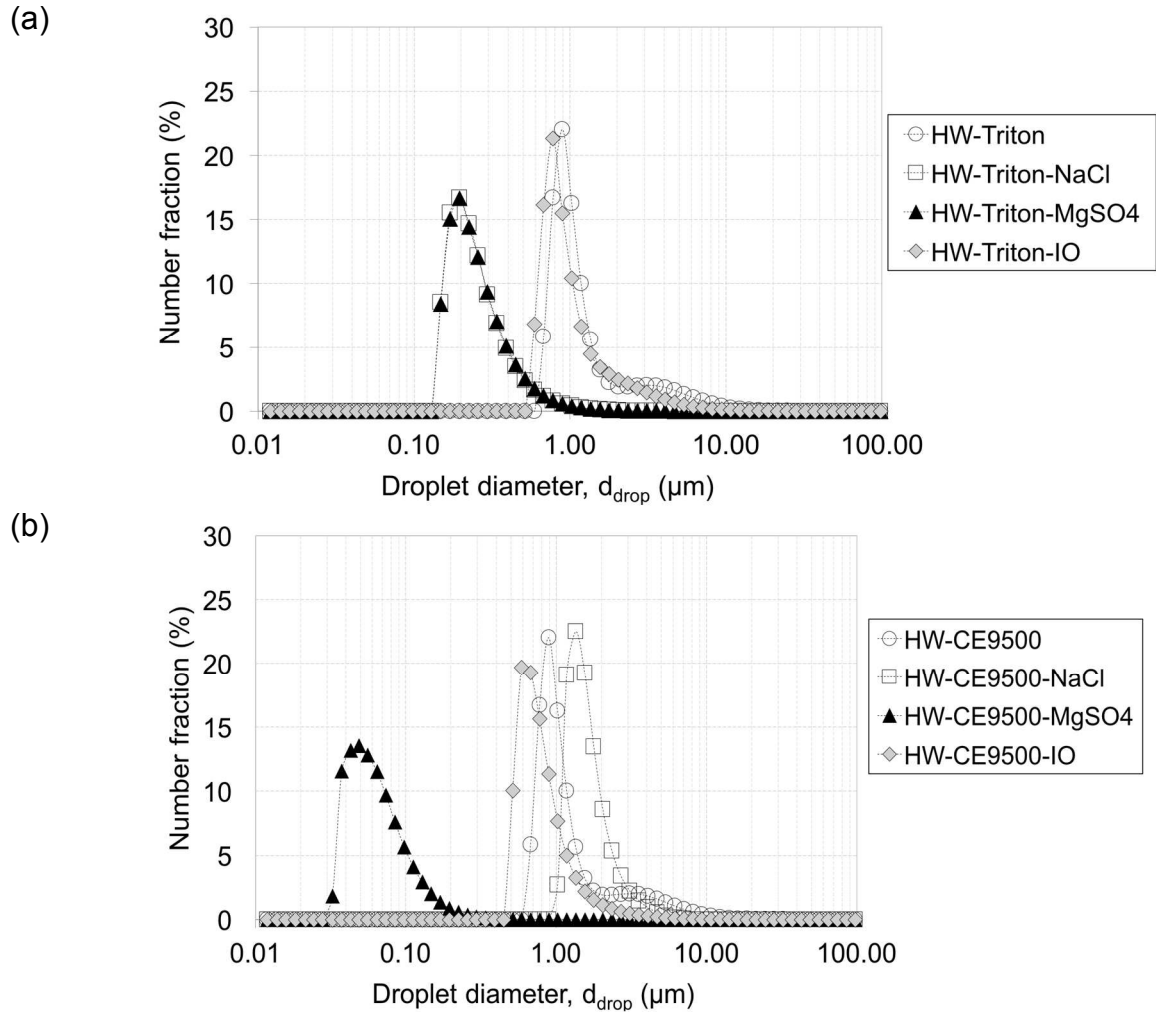


Figure 11. Effect of salt type on the number-based droplet size distributions stabilized by Triton (a) and CE9500 (b). Lines are added to guide the eye. Fig. 4 shows the corresponding volume-based distribution.

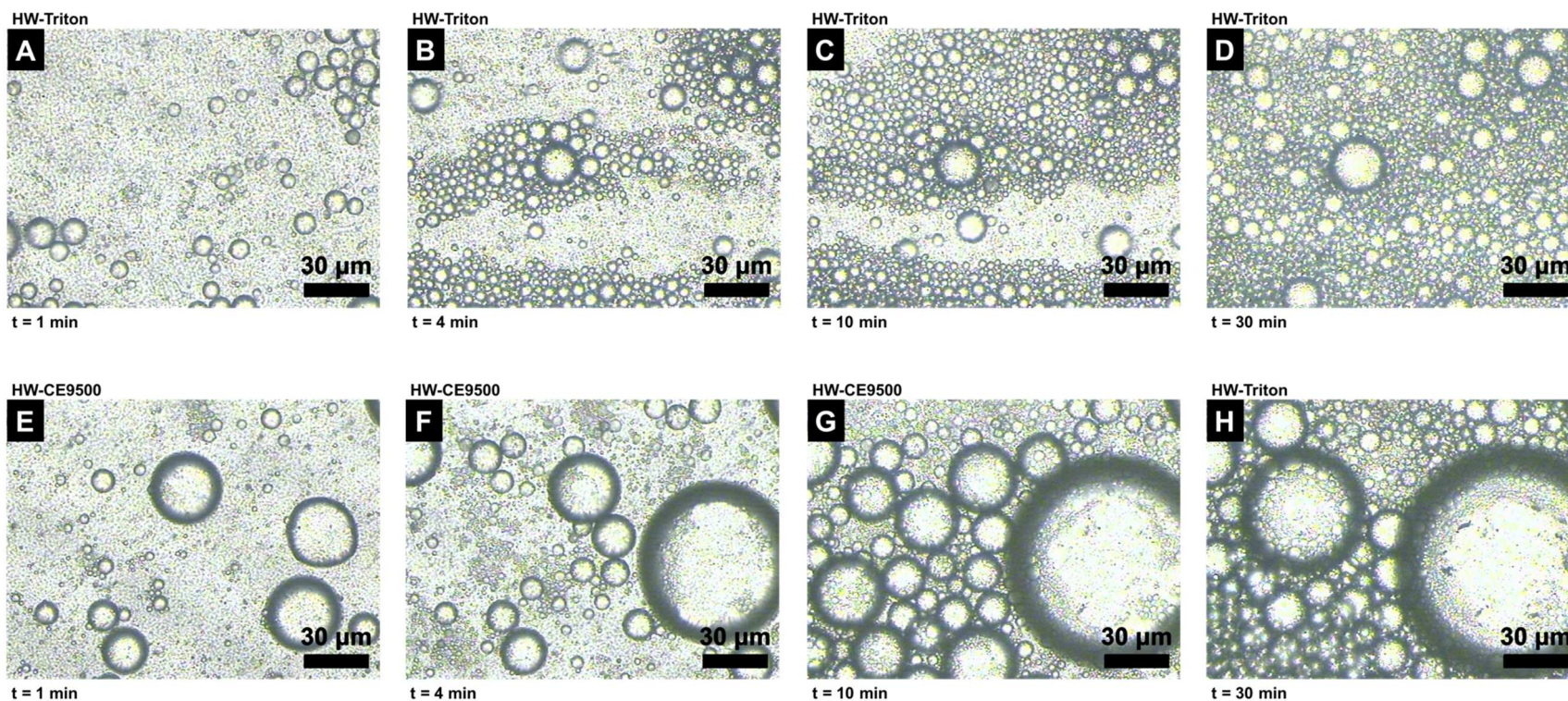


Figure 12. Transient behavior of oil droplets at the surface of Anopore membrane ($d_{\text{pore}}=0.02 \mu\text{m}$) during crossflow ultrafiltration of hexadecane-water emulsions stabilized by different surfactants: Triton (A-D) and CE9500 (E-H). Each row represents a separate DOTM experiment and each column corresponds to the same filtration time to aid with direct comparison of fouling patterns.

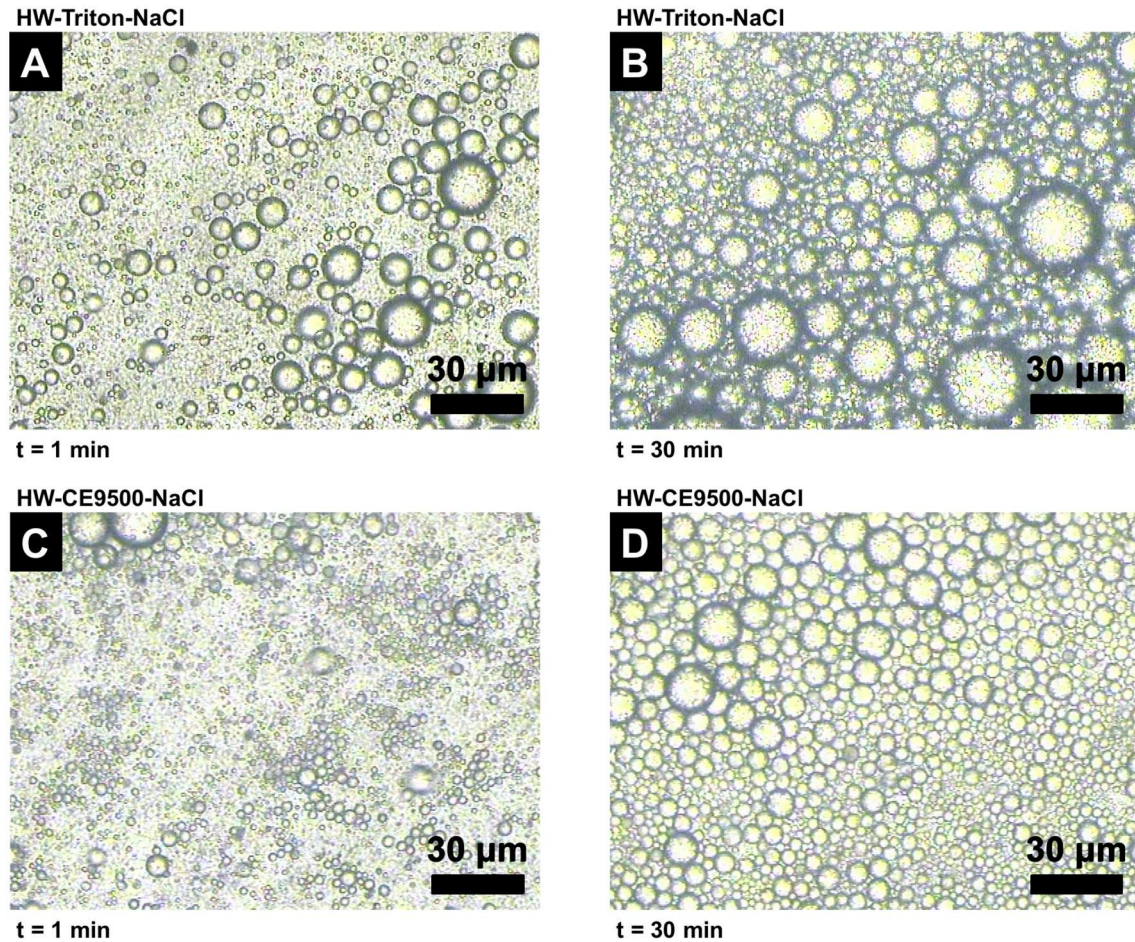
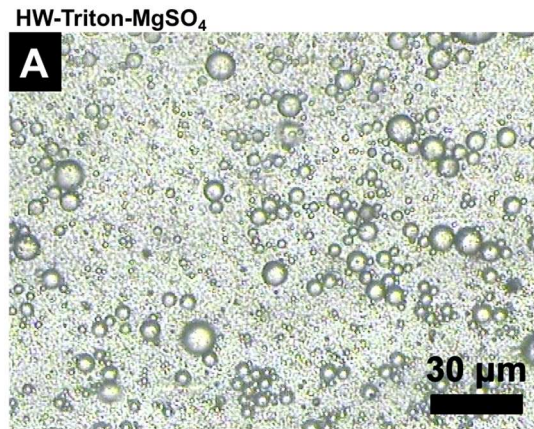
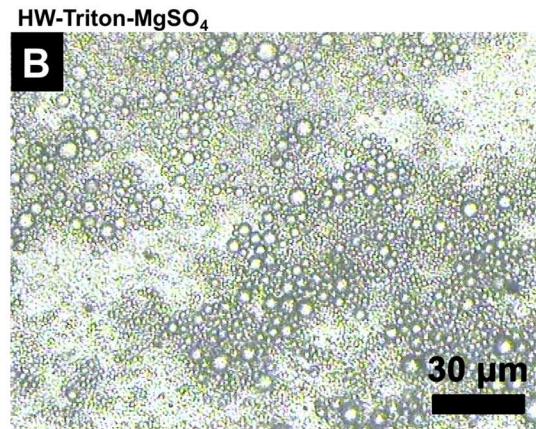


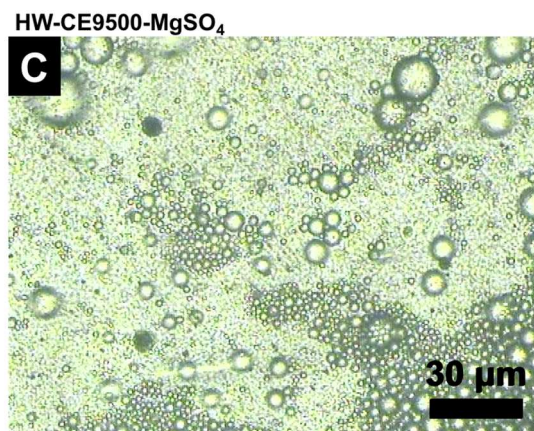
Figure 13. Effect of NaCl addition on fouling behavior of hexadecane-water emulsions. Each row represents a separate DOTM experiment: Test 2 (A, B); Test 6 (C, D). Each column corresponds to the same filtration time (1 min, 30 min).



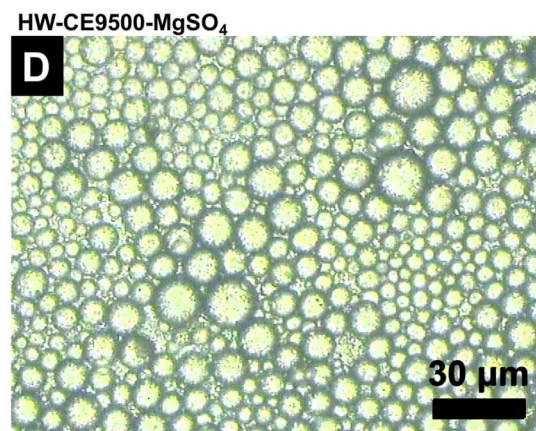
t = 1 min



t = 30 min



t = 1 min



t = 30 min

Figure 14. Effect of MgSO₄ addition on fouling behavior of hexadecane-water emulsions. Each row represents a separate DOTM experiment: Test 3 (A, B); Test 7 (C, D). Each column corresponds to the same filtration time (1 min, 30 min).

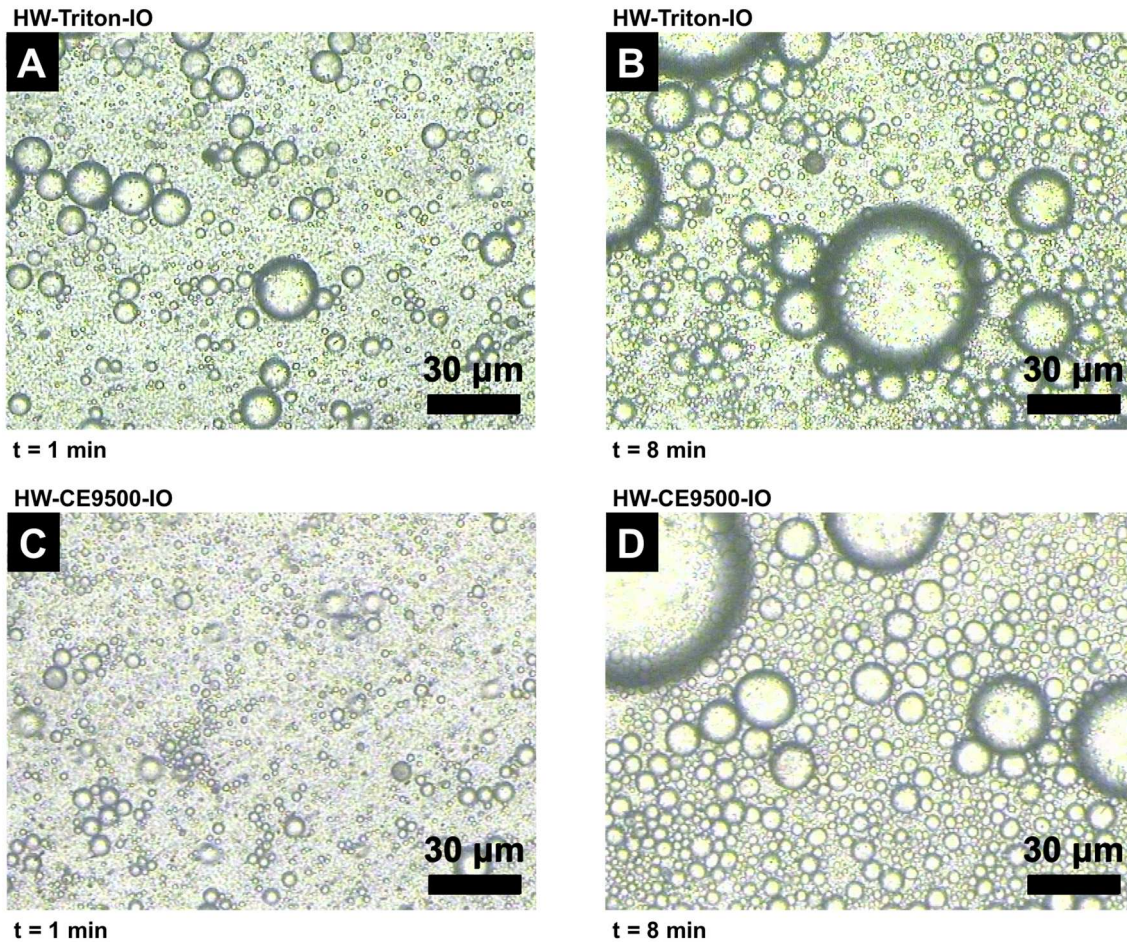


Figure 15. Effect of IO on fouling behavior of hexadecane-water emulsions. Each row represents a separate DOTM experiment: Test 4 (A, B); Test 8 (C, D). Each column corresponds to the same filtration time (1 min, 8 min).

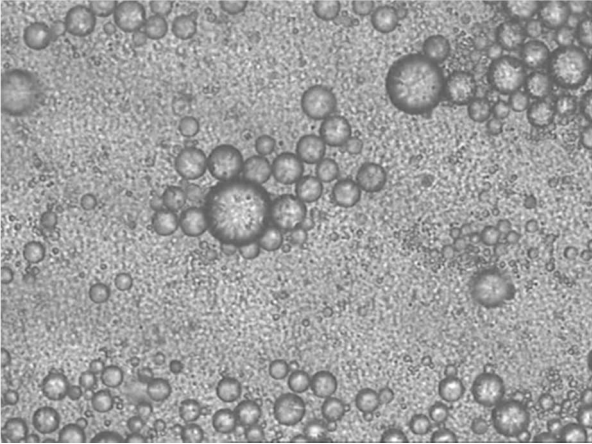


Figure 16. (video 1) DOTM Test 1 with HW-Triton emulsion. The recording starts 1 min into the test. Collective movement of droplets and detachment are observed at timestamps ~2 s, ~6 s, ~11 s, ~15 s, ~17 s, ~24 s, ~27 s and 33 s into the video.

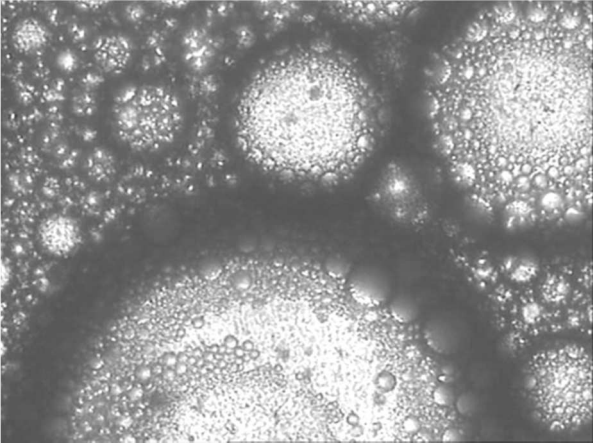


Figure 17. (video 2) DOTM Test 1 with HW-Triton emulsion. The recording starts 3600 s (60 min) into the test. Survey of the membrane surface shows full coverage by clusters of small oil droplets and occasional larger ones.

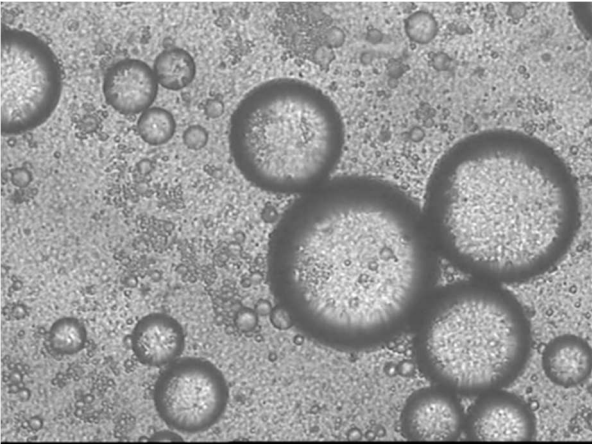


Figure 18. (video 3) DOTM Test 5 with HW-CE9500 emulsion. The recording starts 1 min into the experiment. Coalescence events are observed at time stamps of ~1 min 44s, 1 min 50 s, and 1 min 57 s into the video.

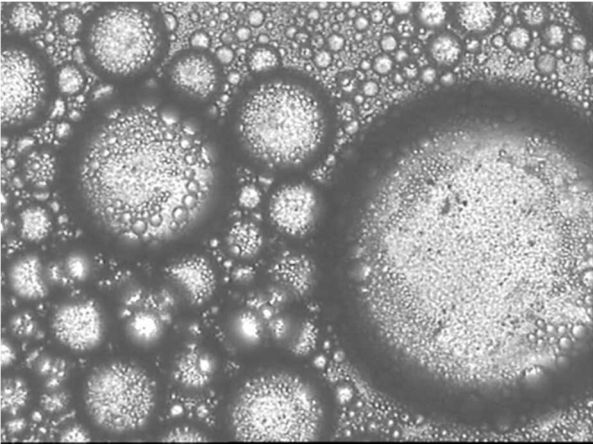


Figure 19. (video 4) DOTM Test 5 with HW-CE9500 emulsion. The recording starts 14 min into the experiment. Coalescence events are observed at time stamps of ~1 min 5 s and 1 min 7 s into the video.

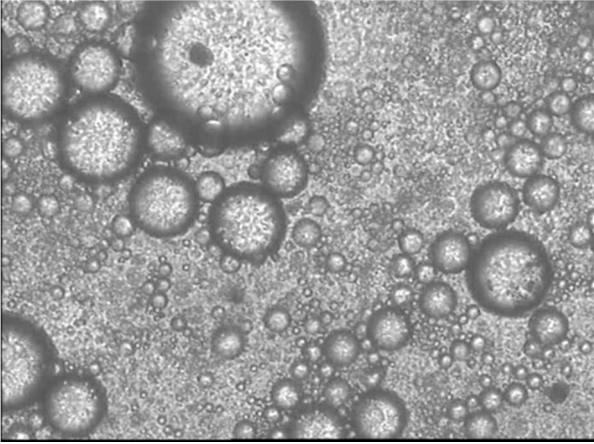


Figure 20. (video 5) DOTM Test 5 with HW-CE9500 emulsion. Membrane survey shows that the majority of the membrane is covered with a dark veil along with clusters of small oil droplets and large droplets. The membrane coverage by oil was sparse as some areas remained oil-free.

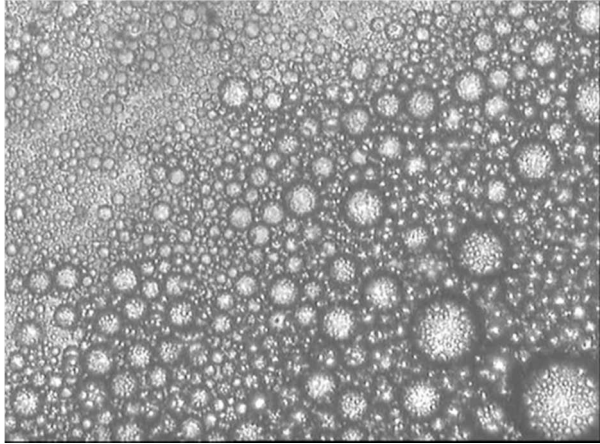


Figure 21. (video 6) DOTM Test 2 with HW-Triton-NaCl emulsion. The recording starts 13 min into the DOTM test. Multiple coalescence events were observed at the following timestamps ~12 s, ~17 s and ~46 s.

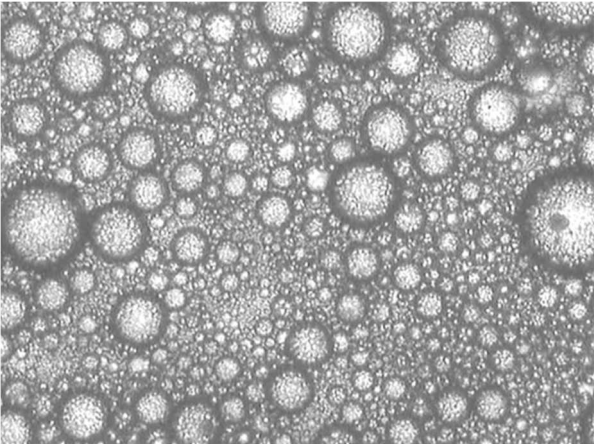


Figure 22. (video 7) Membrane survey 61 min into DOTM Test 2 shows that the membrane is completely covered by a monolayer of oil droplets.

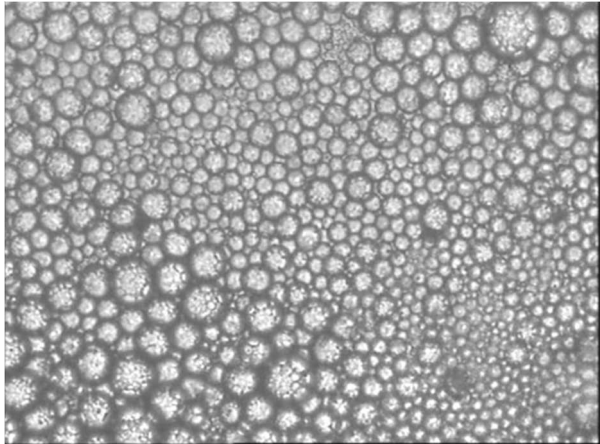


Figure 23. (video 8) DOTM Test 6 with HW-CE9500-NaCl emulsion. Membrane survey conducted 61 min into the experiment shows a monolayer coverage of droplets.

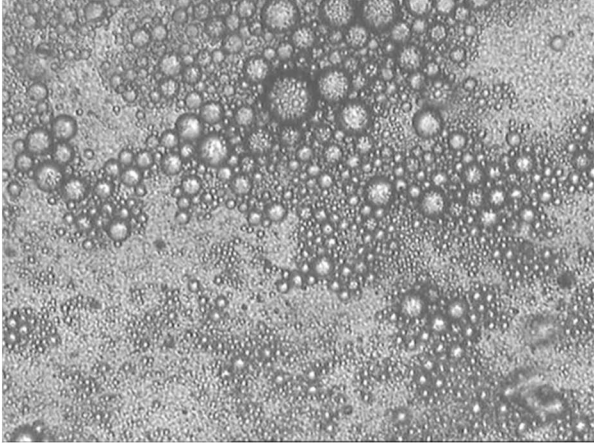


Figure 24. (video 9) DOTM Test 3 with HW-Triton-MgSO₄ emulsion. The recording starts 11 min into the experiment. Coalescence was observed at the following timestamps ~4 s, ~6 s, ~8 s, ~11 s, ~18 s, ~42 s, ~44 s, and ~46 s.

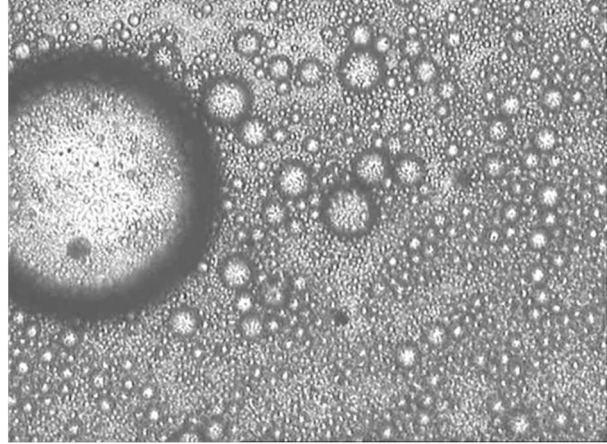


Figure 25. (video 10) Membrane survey 61 min into DOTM Test 3 shows that the membrane is covered with clusters of small droplets along with larger ones. Many areas of the membrane remained oil-free and available for water permeation.

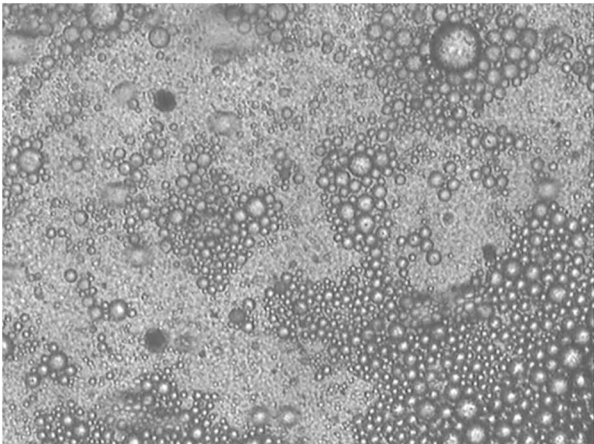


Figure 26. (video 11) DOTM Test 7 with HW-CE9500-MgSO₄ emulsion. The recording starts 3 min in to the experiment.

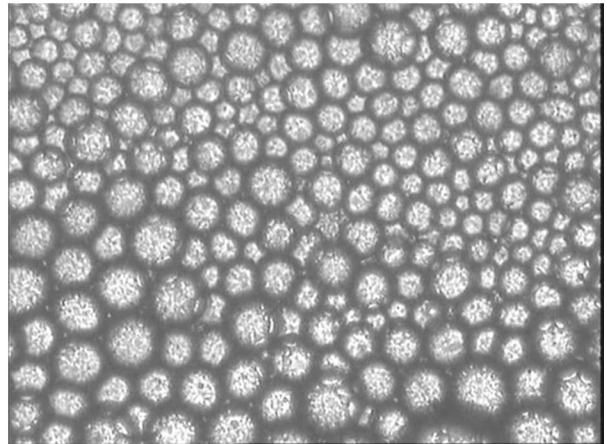


Figure 27. (video 12) DOTM Test 7 with HW-CE9500- MgSO₄ emulsion. The membrane was surveyed 60 min into the experiment showing complete oil coverage by a monolayer of droplets.

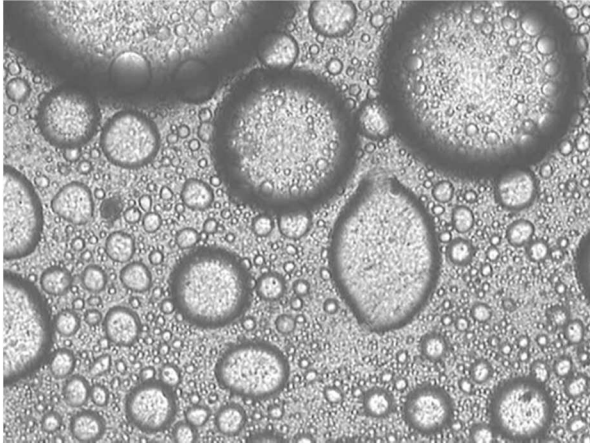


Figure 28. (video 13) DOTM Test 4 with HW-Triton-IO emulsion. The recording starts 36 min into the experiment. Multiple coalescence events were observed at the following timestamps ~2 s, ~8 s, ~18 s, ~25 s, ~30 s, ~48 s, ~55 s, ~1 min 1 s, ~1 min 15 s, ~1 min 25 s, ~1 min 34 s, ~1 min 46 s, ~1 min 55 s and ~2 min 1 s. 2 min into the video, droplet deformation is observed.

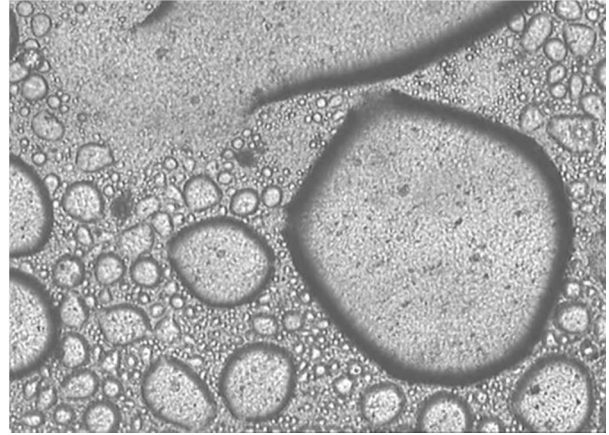


Figure 29. (video 14) DOTM Test 4 with HW-Triton-IO emulsion. The recording starts 40 min into the experiment.

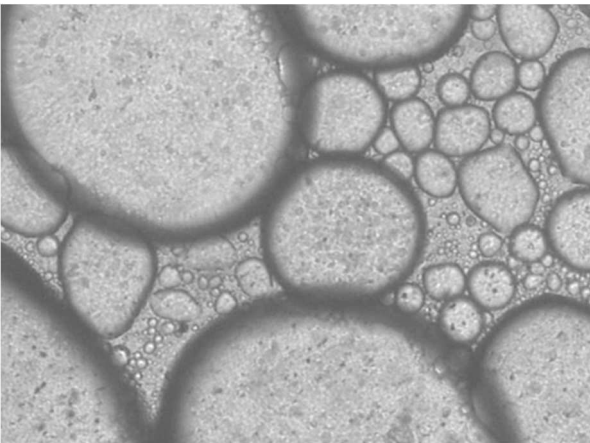


Figure 30. (video 15) DOTM Test 8 with HW-CE9500-IO emulsion. The recording starts 15 min into the experiment. Droplet coalescence was followed by droplet deformation and film formation.

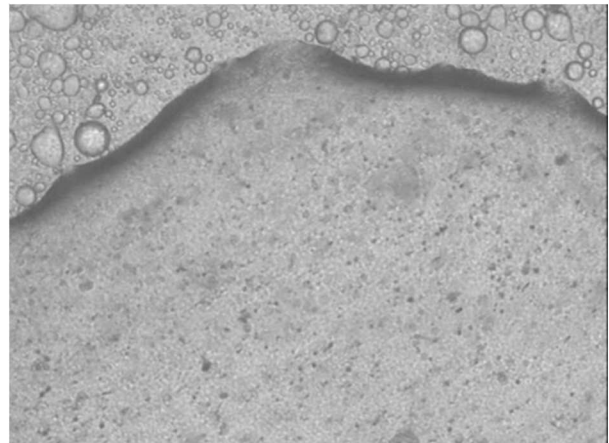


Figure 31. (video 16) DOTM Test 8 with HW-CE9500-IO emulsion. The recording starts 17 min into the experiment. Oil film quickly grew and spread over the entire focus area.

CHAPTER FOUR

Nanofiltration of saline oil-water emulsions: Combined effect of salt concentration polarization and fouling by oil*

*Published on September 1, 2020, *J. Membr. Sci.*, DOI: 10.1016/j.memsci.2020.118607

Abstract

The study employed NF270 nanofiltration membranes and SDS-stabilized hexadecane to identify mechanisms of membrane fouling by highly saline oil-water emulsions. Concentration dependencies of NaCl reflection coefficient σ and NaCl permeability coefficient ω were measured and used to determine separate contributions of osmotic pressure and fouling to the overall flux decline. The NaCl permeability coefficient asymptotically converged to the same steady state value across a range of feed salinities and concentration polarization conditions. The measured near-hyperbolic dependence of the reflection coefficient on the transmembrane concentration differential ($\sigma\Delta\pi_m \approx \text{const}$) negated the effect of concentration polarization on permeate flux. Oil caused an abrupt decrease in permeate flux but only for more saline feeds (seawater level and higher), which was interpreted as a result of membrane surface sealing by coalesced oil. Headloss analysis showed that over the longer term, the additional hydraulic resistance due to a layer of oil droplets on the membrane surface became the dominant fouling mechanism.

4.1. Introduction

The increase in energy demand has driven the rise in oil and gas production that taps into unconventional sources such as tar sands and oil shale [177]. The exploration and production of oil generates large volumes of oily wastewater known as produced water. In 2012, the total volume of produced water in the U.S. alone was estimated to be 21.2 billion barrels [178]. Produced water composition varies significantly depending on the type of hydrocarbon product generated, the geographic location of the field, and the amount of time the water remains in contact with the geological formation [143, 179, 180]. A major constituent of produced water is suspended oil (100 to 5000 mg/L) [181], of which a significant fraction can be present in emulsified form (i. e. in droplets smaller than 20 μm) requiring membrane filtration for effective separation [182, 183]. Produced water salinity is a site-specific variable covering a broad range from <500 mg/L (U.S. EPA's limit for drinking water) to values typical brines (> 300,000 mg/L [180]). For example, waters from U.S. production facilities in the Central Valley of California, the North Slope of Alaska, coastal Texas, and central Mississippi have salinities ranging from 18 to 320 g/L [184]. If not properly treated prior to discharge, produced water can pose significant environmental risks.

A number of treatment technologies (e.g. gravity separators, hydrocyclones, media filters, centrifuges, mesh coalescers, and flotation systems) can be used to treat produced water but their efficiency declines with a decrease in oil droplet size [185]. As a result, a fraction of emulsified and dissolved oil can persist through treatment. If downstream softening or desalination is required for beneficial reuse (e.g. irrigation, fire control systems, vehicle washing, and as power plant makeup water [179, 186]) such

oil-containing feeds can foul nanofiltration (NF) or reverse osmosis (RO) membranes. While numerous studies have evaluated MF and UF as alternative treatment options for produced water [78, 158-160, 166, 187-201], only a limited number of studies have assessed NF of oily feed waters [202-206]. This is likely because MF and UF are effective at removing micron-sized droplets at lower pressures. As a pretreatment for RO, NF removes macromolecules and multivalent cations without the penalty of a high osmotic pressure differential. This is important, for example, for implementing zero liquid discharge when processing saline brines, a common byproduct of produced water treatment. Nanofiltration, however, may also suffer from fouling by oil that persists through pretreatment especially if it is not membrane-based. These considerations point to the practical significance of understanding NF membrane fouling by oil.

Most of the published work on NF of oily feeds has focused on designing the membrane surface to resist fouling by oil and increase oil rejection [205-207]. For example, McCloskey et al. [205] developed a fouling-resistant membrane by modifying a commercial polyamide NF membrane with polydopamine (PD) and poly (ethylene glycol) (PEG). When challenged with soybean oil-in-water emulsion stabilized by a non-ionic surfactant, the PD-g-PEG modified NF membrane showed the highest resistance to fouling by oil. Muppalla et al. developed a composite membrane by modifying a polysulfone UF membrane with penta-block copolymer and achieved flux recovery up to 95% - much higher than 35% measured for unmodified polysulfone membrane [206]. An even smaller subset of the published work discusses membrane fouling by oil from a mechanistic perspective. Zhu et al. studied the effect of surfactant type and charge on the fouling of polyamide NF membranes [151]. Exponential fouling was observed for all

surfactant types used to stabilize the emulsion. Constant flux NF tests and theoretical calculations showed that cake layer formation is responsible for the initial stages of membrane fouling by emulsified oil. Tummons et al. investigated the behavior of oil droplets on model NF membrane surfaces and found that emulsion stability and electrical charge together with membrane's affinity for oil govern droplet attachment to the membrane surface [208].

There has not been a mechanistic study of NF membrane fouling by saline oily feeds. Of particular interest are the interactions between the fouling and concentration polarization processes [209-211]. In RO tests with NaCl solutions containing colloidal SiO₂ a two-way coupling was observed: rejected salt affects the hydraulic resistance of the colloidal cake on the membrane surface while the cake enhances concentration polarization of salt leading to high osmotic pressure differential across the membrane [212]. In the case of fouling by emulsified oil, one expects the coupling to be more complex because of deformability of oil droplets and the dependence of oil droplet stability on the ionic makeup of the continuous phase [213].

The present work aims at identifying dominant fouling mechanisms during nanofiltration of saline oil-in-water emulsions. It is hypothesized that a layer of oil droplets at the membrane surface enhances concentration polarization of salt while the rejected salt screens repulsive interactions between oil droplets leading to a closer-packed oil layer with a higher hydraulic resistance. Such two-way coupling should result in an increase in osmotic pressure, lower permeate flux, and a decreased rejection of salt. To test the hypothesis, the study was designed to identify individual contributions of membrane fouling and concentration polarization to the overall flux decline. The approach

is based on measuring membrane transport coefficients and their dependence on the concentration of salt.

4.2. Approach

4.2.1. Background

The volumetric permeate flux of solvent, J ($\text{m}^3/(\text{m}^2\cdot\text{s})$) is given by:

$$J = \frac{\Delta P - \sigma \Delta \pi_m}{\mu(R_m + R_f)} \quad (1)$$

where ΔP is the transmembrane pressure differential, μ is the dynamic viscosity, R_m is the hydraulic resistance of the clean membrane, R_f is the added hydraulic resistance due to fouling, σ is the reflection coefficient, and $\Delta \pi_m$ is the osmotic pressure differential across the membrane. Eq. (1) can be recast to show individual contributions of R_m , $\sigma \Delta \pi_m$ and R_f to the overall headloss, manifested in a constant pressure test as a permeate flux decline [212] :

$$\frac{\Delta P_m}{\Delta P} + \frac{\Delta P_f}{\Delta P} + \frac{\sigma \Delta \pi_m}{\Delta P} = 1$$

where $\Delta P_m = \mu J R_m$ and $\Delta P_f = \mu J R_f$. For ideal solutions, the value of $\Delta \pi_m$ can be approximated by van't Hoff's equation:

$$\Delta \pi_m = iRT(C_m - C_p) \quad (2)$$

where i is the van't Hoff's factor ($i = 2$ for 1:1 electrolyte), R is the universal gas constant, T is the temperature of the solution, C_m is the molar concentration of solute in the immediate vicinity of the membrane surface, and C_p is the molar concentration of solute in the permeate. Thin film theory [214] can be used to predict C_m :

$$\frac{C_m - C_p}{C_f - C_p} = \exp\left(\frac{J}{k_{cp}}\right) \quad (3)$$

where k_{cp} is the mass transfer coefficient, which can be estimated using a Sherwood correlation [215]. For a laminar flow in a rectangular channel, Sherwood correlation is:

$$\frac{k_{cp} \cdot d_h}{D} = \left(3.66^3 + 1.61^3 \cdot Re \cdot Sc \cdot \frac{d_h}{L}\right)^{\frac{1}{3}} \quad (4)$$

where L is the length of the channel, D is the solute's diffusion coefficient, d_h is the hydraulic diameter of the channel, Re is the Reynolds number, and Sc is the Schmidt number. Eq. (4) applies when $0.1 < Re \cdot Sc \cdot \frac{d_h}{L} < 10,000$ and when the channel is not constricted by a fouling layer on the membrane. The mass flux of solute across the membrane, J_s (kg/(m²·s)), is given by [216, 217]

$$J_s = B(C_m - C_p) + J(1 - \sigma)(C_m - C_p) \ln^{-1}\left(\frac{C_m}{C_p}\right) \quad (5)$$

where B (m/s) is the solute permeability coefficient. Both B and σ are generally concentration-dependent although an opposite assumption is often made to estimate these coefficients from flux and rejection data.

4.2.2. Quantifying separate contributions of membrane fouling and osmotic pressure to permeate flux decline

The present study aims at determining separate contributions of membrane fouling and concentration polarization to the overall flux decline. The methodology extends the approach used in our earlier studies on ion separation by salt rejecting membranes under conditions of colloidal fouling [212, 216] wherein the reflection coefficient was assumed to be equal to unity. The present work relaxes this assumption and assumes that both σ and B are concentration dependent. The following description details the three steps that lead to an unequivocal identification of individual contributions of $\sigma\Delta\pi_m$ and R_m to the overall flux decline.

Step 1: Determine reflection coefficient as a function of the solute concentration: $\sigma(C_m)$

Measurements during step 1 are performed at the membrane conditioning stage where NaCl is the only component of the feed solution. With no foulants in the feed ($R_f = 0$), equations (1), (2) and (3) are combined to give:

$$J = \frac{1}{\mu R_m} \left[\Delta P - 2\sigma RT(C_f - C_p) \exp\left(\frac{J}{k_{cp}}\right) \right] \quad (6)$$

In eq. (6), J and C_p are measured during the conditioning state, R_m is determined at the end of the compression stage, while ΔP and C_f are known (maintained constant). With viscosity and temperature known and k_{cp} determined from eq. (4), eq. (6) can be solved for σ . By performing conditioning tests with different values of C_f (to scan a range

of concentration polarization conditions and C_m values), the concentration dependence of the reflection coefficient, $\sigma(C_m)$, is determined.

Step 2: *Determine solute permeability coefficient as a function of the solute concentration: $\omega(C_m)$*

The rejected salt may interact with rejected oil droplets making it difficult to factor out the individual contributions of $\Delta\pi_m$ and R_f to the flux decline. In the presence of a fouling layer on the membrane surface, eq. (5) for the mass transfer coefficient, B , is not applicable. An alternative approach is taken instead. Given that $J_s = JC_p$, eq. (6) can be written as follows:

$$JC_p = B(C_m - C_p) + J(1 - \sigma(C_m))(C_m - C_p)\ln^{-1}\left(\frac{C_m}{C_p}\right) \quad (7)$$

With $\sigma(C_m)$ known (obtained at step 1), eq. (7) can be solved for B . As in step 1, C_m is determined from eqs (3) and (4) based on flux and rejection data during membrane conditioning tests with NaCl solution in the feed. Data from the set of conditioning tests used to determine (C_m) in step 1, can be employed once again: this time by solving eq. (7) for ω and determining its concentration dependence, $B(C_m)$.

Step 3: *Determine added resistance due to fouling (R_f) and osmotic pressure ($\Delta\pi_m$) as functions of time*

Eq. (7) can be applied to data from the fouling tests with both NaCl and emulsified oil (the foulant) in the feed. Based on known $\sigma(C_m)$ and $B(C_m)$ dependencies (determined at step 1 and step 2, respectively) and on measured values of J and C_p , eq. (7) can be solved for C_m as the only unknown. The obtained value of C_m can then be plugged into

eq. (2) to calculate the osmotic pressure differential $\Delta\pi_m$ during membrane fouling by oil. Finally, after determining $\Delta\pi_m$, eq. (1) can be used to compute R_f .

4.3. Materials and Methods

4.3.1. Reagents

Hexadecane (99%), sodium dodecyl sulfate (SDS, $\geq 98.5\%$), and sodium chloride (NaCl, $\geq 99\%$) were purchased from Sigma-Aldrich and used as received. DI water was supplied by a Milli-Q ultrapure water system (Integral 10, Millipore) equipped with a terminal 0.2 μm microfilter (MilliPak, Millipore); water resistivity was $\sim 18 \text{ M}\Omega\cdot\text{cm}$.

4.3.2. Oil-water emulsion preparation and characterization

Hexadecane-in-water emulsions were prepared by adding NaCl and SDS to 10 L of DI water prior to the addition of 0.1% v/v hexadecane (773 mg/L). The emulsion was prepared by mixing the solution using a digital stand mixer (RW 20 digital dual-range mixer, IKA) at 2154 rpm for 20 min. In all the emulsions, the concentration of SDS was set at 0.1 mM while NaCl concentration was either 100 mM (5.8 g/L), 469 mM (27.4 g/L), or 1711 mM (100.0 mg/L). For these concentrations, the errors in the osmotic pressure calculation (eq. (2)) that assumes an ideal solution, are 0.18%, 0.84%, and 3.06%, respectively. The errors are calculated by comparing osmotic pressure values computed using van't Hoff's equation for a 1:1 electrolyte and Gibbs equation: $\pi = \frac{RT}{\tilde{V}_w} \ln(\chi_w)$, where \tilde{V}_w and χ_w are the molar volume and molar fraction of the solvent. The 100 mM NaCl based on the in situ observation of minimal droplet attachment to a negatively charged NF membrane [208]. The 469 mM (27.4 g/L) NaCl solution matched the ionic strength of a typical seawater while 1711 mM (100 g/L) NaCl solution represented brine.

Laser diffractometry (Mastersizer 2000, Malvern Instruments) was used to determine the oil droplet size distribution in the bulk for each feed emulsion. The emulsion was continuously circulated through the optical unit of the Mastersizer using a peristaltic pump (Masterflux model, Cole-Parmer) installed downstream from the Mastersizer and operating at a flow rate of 70 mL/min. The interfacial tension of hexadecane with the three aqueous solutions was measured using a standard goniometer (model 250-F4, ramé-hart instrument) at 20 °C. A detailed procedure for interfacial tension measurement is described elsewhere [158, 194].

4.3.3. Crossflow filtration system

The crossflow filtration system has been described in detail previously [212]. Briefly, the crossflow cell is a SEPA CF II filtration cell (Sterlitech). The setup includes a positive displacement pump (M-03 hydra-cell) equipped with a 2 HP DC motor speed control (Penta Power KBMD-240D). The inlet of the pump is connected to a feed tank and the outlet of the pump is connected to a pulsation dampener (model H1020V, Blacoh Fluid Control) to reduce flow vibration and data noise. All tubing is made from stainless steel and rated for high pressure. A pressure gage is attached to the concentrate outlet to monitor the pressure inside the cell. A backpressure valve is installed in the concentrate line to regulate the pressure in the system. A flow-through glass cell is installed in the permeate line and operates as the holder of the conductivity probe. The conductivity probe (Vernier Lab Data Logger Pro) records conductivity of the permeate as a function of time. The permeate is directed to a beaker positioned on a mass balance (Adventurer Pro AV812, OHAUS). Values of permeate conductivity and permeate mass are

automatically logged into a computer. The feed solution is maintained at a constant temperature of 20 °C using a circulating chiller.

4.3.4. Experimental protocol

The experimental protocol includes of four stages: membrane compaction with DI water, membrane conditioning with NaCl solution, membrane conditioning with solution of surfactant and NaCl, and filtration of surfactant-stabilized emulsion of oil in NaCl solution as the continuous phase. In all stages, the crossflow velocity and transmembrane pressure were set constant at 0.1 m/s and 200 psi (1.38 MPa), respectively. Permeate mass was collected and conductivity of the permeate was measured during each stage.

Stage 1: Compaction. At the beginning of each experiment, DI water was filtered through the membrane to ensure that irreversible compaction does not contribute to the permeate flux decline. The membrane was compacted for 24 h at 200 psi (1.38 MPa). After compaction, the hydraulic resistance of the clean membrane was determined.

Stage 2: Conditioning with salt. NaCl was added to the feed tank to condition the membrane with the solution of the same ionic strength that will be used in the following stages. The conditioning was performed until steady permeate flux and NaCl rejection were achieved. During this stage, a flux change of less than 3% over 10 minutes ($\frac{dJ}{dt} \frac{1}{J} < 0.02 \text{ min}^{-1}$) as used as the criterion for achieving steady state flux.

Stage 3: Conditioning with surfactant. SDS was added to the feed tank and the membrane was conditioned until permeate flux and salt rejection achieved steady state values.

Stage 4: Fouling. The feed solution was replaced with the saline hexadecane-water emulsion. During the fouling stage, permeate samples were collected to determine

oil concentration in the permeate using gas chromatography. The detailed procedure for these measurements has been described elsewhere [164].

4.4. Results and Discussion

4.4.1. Oil-water emulsions: Droplet size and interfacial tension

Oil droplet size distribution and oil-water interfacial tension are key parameters that affect permeate flux and selectivity of separation [218, 219]. A droplet of diameter d_{drop} can enter a pore of diameter d_{pore} even if $d_{drop} > d_{pore}$ with the critical pressure (i.e. entry pressure) depending on both d_{drop} and d_{pore} [218]. For nanofiltration membranes, droplet size and stability affect droplet behavior at the membrane surface and, by extension, type and dynamics of membrane fouling by oil [208]. As shown in **Figure 37** (see Appendix), increasing ionic strength shifted the emulsion droplet size distribution towards larger sizes. The volume-weighted mean diameter for HD-0.1SDS-100NaCl, HD-0.1SDS-469NaCl, and HD-0.1SDS-1711NaCl emulsions was 22 μm , 37 μm , and 396 μm , respectively. The corresponding number-based mean diameters were 0.8 μm , 0.8 μm , and 1 μm . Based on the measured droplet size distribution, we expect complete rejection of oil by NF270 membrane.

Increasing the salinity of the continuous phase led to a decrease in the interfacial tension in accordance with earlier studies [151, 158, 166, 208]. In 100 mM NaCl solution, the interfacial tension of the SDS-stabilized emulsion was 19.7 ± 0.5 mN/m, decreasing to 19.2 ± 0.6 mN/m in 469 mM NaCl and to 13 ± 0.2 mN/m in 1711 mM NaCl. The decrease in interfacial tension at higher ionic strengths is caused by a combination of two effects: a shift in the equilibrium partitioning of the surfactant between dissolved and oil

phases towards oil (i.e. “salting out” of the surfactant), and screening of the surfactant charge, allowing for a higher density of surfactant at the oil-water interface [158, 166].

4.4.2. Determining concentration dependence of NF transport coefficients

Generally, σ and B are concentration dependent [220, 221]. Their values for select concentrations of NaCl have been reported in the literature. Boussouga and Lhassani [222] determined σ to be 0.22 and 0.53 in tests with 100 mM NaCl and 1 mM NaCl feeds, respectively. The values, however, were obtained based on the relationship that results from integrating eq. (1) in the assumption of concentration-independent B and σ [217]. Using the same approach, Nair et al. [223] correlated the reflection and permeability coefficients for different ions with the pure water permeability for a range of membranes including NF270.

4.4.2.1. NaCl reflection coefficient, σ , as a function of NaCl concentration

To determine σ , membrane conditioning tests with NaCl were performed at ΔP of 200 psi (1.38 MPa) with different feed concentrations C_f of NaCl in the feed. The reflection coefficient σ was determined using eq. (6). As expected, increasing C_f led to a decrease in permeate flux and intrinsic rejection, $R_{int} = 1 - \frac{C_p}{C_m}$. Similarly, the observed rejection, $R_{obs} = 1 - \frac{C_p}{C_f}$, decreased with an increase in C_f (see Appendix, **Figure 38**).

The dependence of the reflection coefficient, σ , on NaCl concentration at the membrane surface, C_m , did not show an identifiable trend (see Appendix, **Figure 39**). However, when plotted against the concentration *difference* across the membrane, the dependence was found to closely follow a power law. The trend was observed across all NF270 membranes tested and across all concentration polarization conditions for each

NF270 membrane. **Figure 32** shows the dependence of σ on the transmembrane difference in solute concentration expressed in terms of the osmotic pressure differential,

$$\Delta\pi_m = 2RT(C_m - C_p):$$

$$\sigma = a(\Delta\pi_m)^{-b} \quad (9)$$

where a and b are empirical constants. Using a linear regression of $\ln(\sigma)$ against $\ln(\Delta\pi_m)$, the values of a and b were determined. For the three NF270 membranes tested and when expressing $\Delta\pi_m$ in units of MPa, the values of a were $(5.44 \pm 0.07) \cdot 10^{-1}$, $(4.11 \pm 0.04) \cdot 10^{-1}$, and $(5.99 \pm 0.02) \cdot 10^{-1}$. The corresponding values of b were 1.26 ± 0.02 , 1.18 ± 0.02 , and 1.04 ± 0.01 . The error estimates are standard deviations computed based on linear regressions ($r^2 = 0.95$, 0.93 , and 0.99 , respectively) (**Figure 40**). Values of a and b for the merged dataset were $(5.57 \pm 0.03) \cdot 10^{-1}$ and 1.18 ± 0.01 (**Figure 41**). Given that b is close to unity, one can expect the *effective* osmotic pressure differential (i.e. $\sigma(C_m - C_p)$) to remain relatively constant during nanofiltration:

$$\sigma\Delta\pi_m = a\Delta\pi_m^{1-b} \cong a.$$

4.4.2.2. NaCl permeability coefficient, B , as a function of NaCl concentration

A separate set of conditioning tests was conducted to measure the salt permeability coefficient, B . Crossflow velocity was maintained constant (0.1 m/s) and transmembrane pressure was adjusted to achieve different values of C_m . With σ known from eq. (6), ω was determined using eq. (7). In these measurements, C_f was either 400 mM or 500 mM and ΔP was set at 100 psi, 140 psi, 200 psi, 240 psi, or 300 psi (at 0.69, 0.97, 1.38, 1.65 or 2.07 MPa). At the lowest ΔP tested (0.69 MPa), ω was negligible ($\omega \ll J(1 - \sigma)\ln^{-1}(C_m/C_p)$).

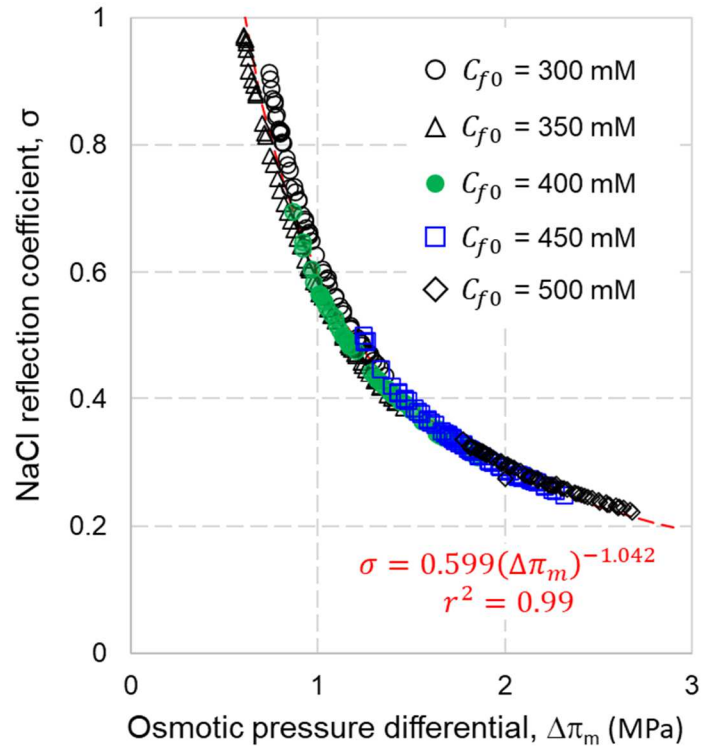


Figure 32. Dependence of NaCl reflection coefficient of an NF270 membrane on the osmotic pressure differential. Different segments of the dependence correspond to tests with different initial feed concentrations, C_{f0} , of NaCl. Results of replicate measurements with different initial feed concentrations, C_{f0} , of NaCl. Results of replicate measurements with two other NF270 membranes are shown in Appendix, Figure 24.

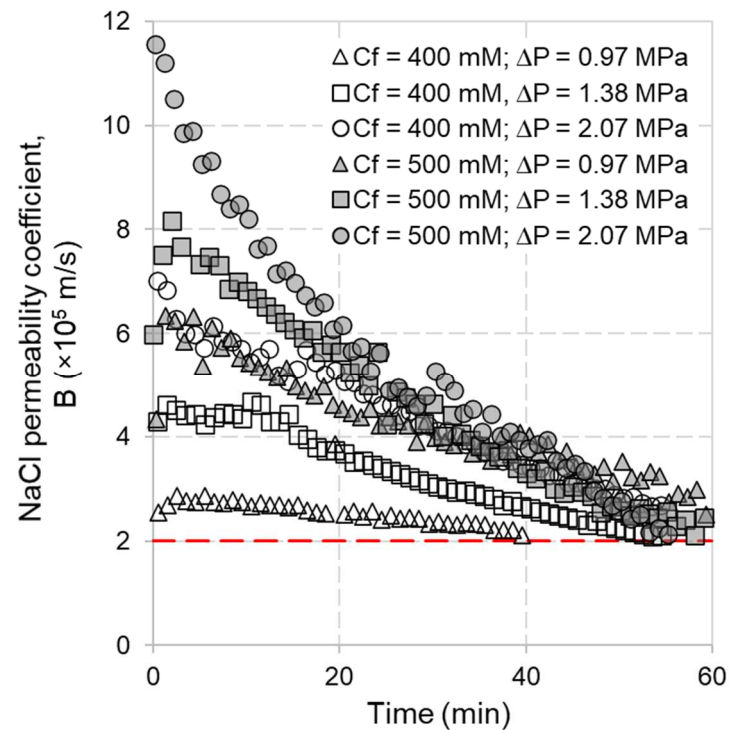


Figure 33. NaCl permeability coefficient of NF270 membrane during salt conditioning tests with different initial feed concentrations C_{f0} , of NaCl and different concentration polarization conditions. The dashed red line is the asymptote to which $B(t)$ dependence appears to converge. Each test was terminated once a steady state permeate flux was achieved: $\frac{dJ}{dt} \frac{1}{J} < 0.02 \text{ min}^{-1}$.

Figure 33 shows B for $C_f = 400$ mM at different transmembrane pressures, which corresponded to different J and C_m values. In all tests, B gradually decreased with time with larger decreases observed for higher ΔP . In all tests and across all conditions tested (feed concentration of salt and concentration polarization modules), B appeared to asymptotically approach the same steady-state value of ~ 20 $\mu\text{m/s}$. Differences in the duration of experiments performed to determine B were due to the fact that tests were run until a steady-state permeate flux was achieved and the time to steady-state was different in different tests.

4.4.3. Oil fouling experiments: Permeate flux and salt rejection at different ionic strengths

After compaction with DI water, the membrane was conditioned by filtering NaCl and SDS at $\Delta P = 200$ psi (1.38 MPa) and $v_{cf} = 0.1$ m/s (**Figure 41**). First NaCl was introduced into the feed of the compacted membrane. The resulting decline in permeate flux matched the value calculated based on the osmotic pressure. During the follow up step of conditioning with SDS, no permeate flux decline was observed. Because the conditioning stage lasted until permeate flux and NaCl rejection reached steady state, any changes in these metrics observed when oil is added to the feed, can be interpreted as a consequence of membrane fouling. **Figure 34** illustrates the permeate flux decline during the fouling stage where NF270 membrane is challenged an SDS-stabilized hexadecane-water emulsions. Steady state values reached after 3 h of filtration were similar in tests with different feeds: $9 \pm 3\%$, $15\% \pm 4\%$ and $16\% \pm 1\%$ of the initial flux in experiments with 10 mM NaCl, 469 mM NaCl and 1711 mM NaCl respectively. The rate of the flux decline was different, however, suggesting that different fouling mechanisms dominated the initial flux decline.

The fastest flux decline was observed in tests with HD-SDS-1711NaCl emulsion that had the lowest stability. In this case, oil droplets deposited on the membrane surface and formed contiguous oil films extending over large areas of the membrane surface thereby reducing the surface area available for permeation. The HD-SDS- 100NaCl emulsion had the highest stability compared to the other emulsions as indicated by lower values of the interfacial tension and volume-based weighed mean diameter. The smaller droplets pack tightly together to form a low porosity cake with high hydraulic resistance. The denser packing was due to smaller size and not droplet deformation: under experimental conditions of this work, the Capillary numbers corresponding to permeate and crossflow drags were both very small ($Ca_{pf} = \mu_w j / \sigma < 10^{-6}$, $Ca_{cf} = \mu_w \dot{\gamma} d_{drop} / \sigma < 10^{-3}$) indicating that droplet deformation was minimal. The slowest flux decline was observed with the HD-SDS-469NaCl emulsion that has intermediate stability. We hypothesize that surface coalescence occurred between a droplet passing in the direction of crossflow and other attached droplets to reach a critical size and the resulting large droplet is swept off the membrane by the crossflow shear. In this case, oil accumulation at the membrane surface is minimized as oil droplets can be removed by the crossflow shear prior to forming contiguous oil films.

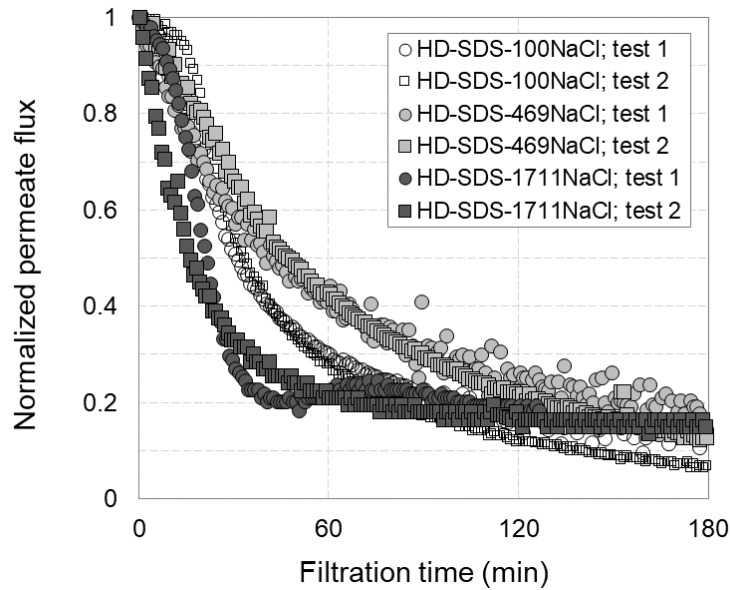


Figure 34. Permeate flux behavior in crossflow nanofiltration tests with SDS-stabilized saline emulsions of hexadecane as a function of NaCl concentration (100 mM, 469 mM, or 1711 mM). The experiments were performed at $\Delta P = 200$ psi (1.38 MPa) and with a constant crossflow velocity ($v_{cf} = 0.1$ m/s). Initial permeate fluxes and hydraulic resistance of clean membranes for all filtration tests are given in Appendix. Different symbols of the same shade correspond to different tests (each test was performed in duplicate).

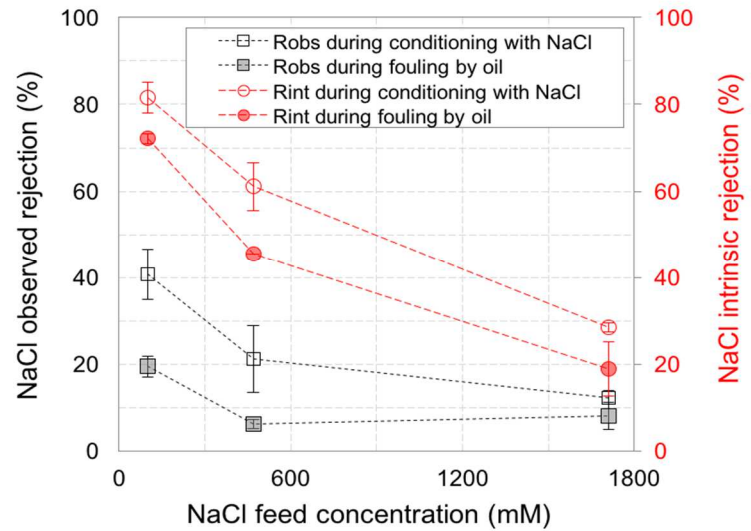


Figure 35. Steady state values of the observed (a) and intrinsic (b) rejection of NaCl by NF270 in conditioning tests (feed: NaCl and SDS) and in fouling tests (feed: NaCl, SDS, hexadecane). Lines are added to guide the eye. The (very weak) dependence of R_{obs} and R_{int} on time is shown in Appendix, Figure 27.

As expected, the oil rejection by the NF270 membrane was high: 99.99% ± 0.02 % for the HD-SDS-100NaCl emulsion, 100% ± 0.01% for the HD-SDS-469NaCl, and 99.98% ± 0.03% for the HD-SDS-1711NaCl emulsion, respectively. The introduction of the SDS-stabilized oil to the feed (fouling stage) resulted in a decrease in observed rejection of NaCl at all ionic strengths due to a decrease in permeate flux (**Figure 35**). Intrinsic rejection also decreased with the introduction of oil. The decrease is caused by fouling-induced changes in C_m that, in turn affect values of ω and σ . The dependence of R_{int} on ω and σ (and therefore, indirectly, on C_m) can be expressed by rearranging eq. (7) as follows:

$$J(1 - R_{int}) = BR_{int} - J(1 - \sigma)R_{int} \ln^{-1}(1 - R_{int}) \quad (10)$$

For $R_{int} \ll 1$, $\ln(1 - R_{int}) \cong -R_{int}$ and eq. (14) is simplified to give R_{int} as an explicit function of ω and σ :

$$R_{int} = \frac{1 + (1 - \sigma)}{1 + \frac{B}{J}} \quad (11)$$

When coupling between solute and solvent transport is minimal ($\sigma \cong 1$), eq. (11)

reduces to a familiar expression for R_{int} : $R_{int} = \left(1 + \frac{B}{J}\right)^{-1} \cong \frac{J}{B}$.

4.4.4. Headloss analysis. Implications for practice.

4.4.4.1. Instantaneous flux decline

In experiments with HD-0.1SDS-100NaCl, introduction of oil into the solution of NaCl led to a short term (~ 1 min) increase in permeate flux which was attributed to oil-induced changes in water permeability of the membrane. The fouling resistance has increased steadily (**Figure 36a**). In contrast, experiments with HD-0.1SDS-469NaCl and HD-0.1SDS-1711 NaCl showed precipitous decline in permeate flux upon the introduction of oil into the feed. For the highest ionic strength, the decline in flux was the highest corresponding to ~ 41% of the overall headloss. We attribute this instantaneous drop in flux to membrane surface sealing by oil. Indeed, such films were observed in our earlier studies on direct visualization of membrane fouling by oil and are typical for high ionic strength feeds [158, 208].

If instantaneous blockage of membrane area occurs, then a portion of the flux decline is caused by a decrease in the total membrane surface area available for permeation. Denoting the fraction of the membrane area blocked as $\eta(t)$ the effective membrane area is given by $A = A_0(1 - \eta)$ and the permeate flow rate, Q , can be described by a modified version of eq. (1):

$$Q = jA = \frac{\Delta P - \sigma \Delta \pi_m}{\mu R_m} A_0(1 - \eta) \quad (12)$$

One can define R_s as the added hydraulic resistance due to surface sealing so that:

$$Q = \frac{\Delta P - \sigma \Delta \pi_m}{\mu(R_m + R_s)} \quad (13)$$

A comparison of eq. (12) and eq. (13) shows that

$$R_s = R_m \frac{\eta}{1 - \eta} \quad (14)$$

Thus, in the presence of blockage, the transient headloss is given by a modified version of eq. (1):

$$\frac{\Delta P_m}{\Delta P} + \frac{\Delta P_s}{\Delta P} + \frac{\Delta P_f}{\Delta P} + \frac{\sigma \Delta \pi_m}{\Delta P} = 1 \quad (15)$$

where $\Delta P_s = \mu j R_s = \mu j R_m \frac{\eta}{1 - \eta}$.

The value of η was determined using the following algorithm: at the very start of the fouling stage, R_f was assumed to be zero, $\sigma \Delta \pi_m$ was assumed to match the value predicted value ($2RT\sigma(C_m - C_p)$) and R_s was calculated by selecting a value of η to explain the observed drop in flux. The calculation gave $\eta \approx 0.18$ and $\eta \approx 0.64$ in tests with NaCl concentrations of 469 mM and 1711 mM, respectively.

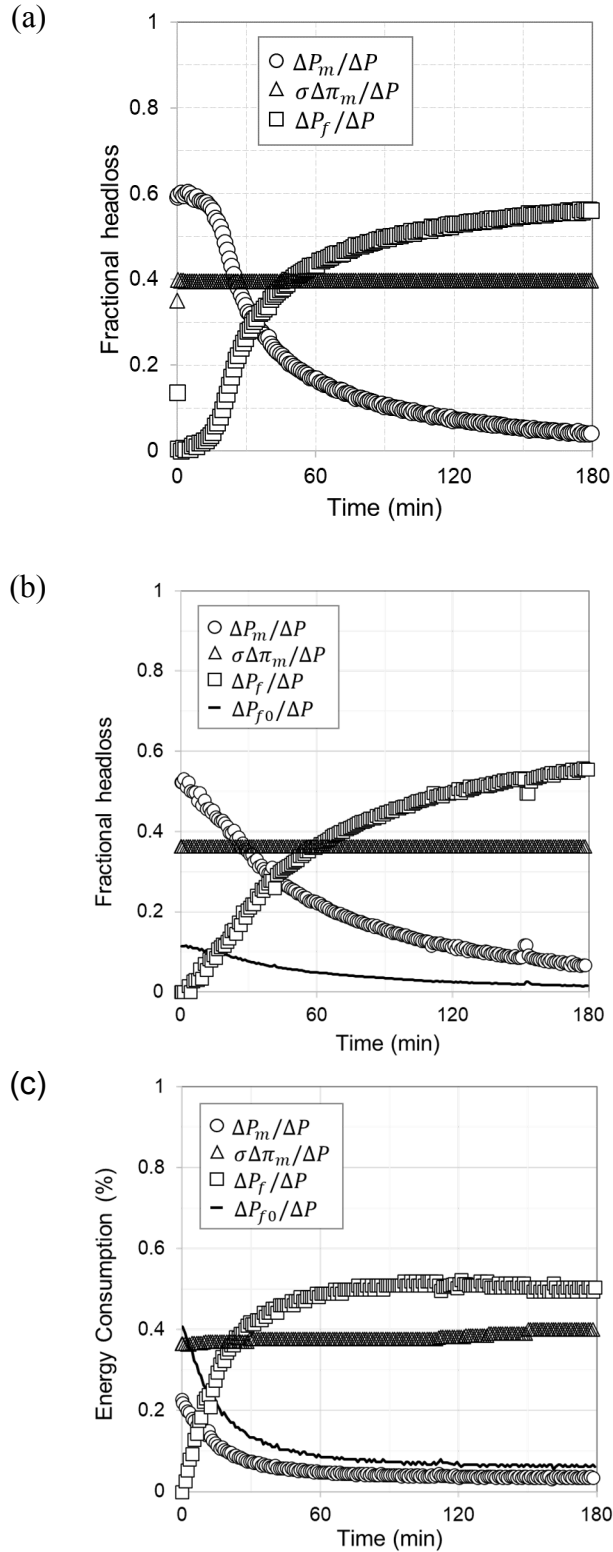


Figure 36. Headloss distribution across four different sources of hydraulic resistance in nanofiltration tests with SDS-stabilized saline emulsions of hexadecane as a function of NaCl concentration: a) 100 mM; (b) 469 mM; and (c) 1711 mM.

4.4.4.2 Headloss analysis: Relative contributions fouling and osmotic pressure to flux decline

The striking feature of NF270 membrane is the near-hyperbolic dependence of the reflection coefficient σ on the concentration differential across the membrane, $C_m - C_p$ (**Figure 32**). As a result, the term $\sigma\Delta\pi_m$ remains practically constant throughout the filtration process (**Figure 36**). As concentration polarization increases due to the buildup of the fouling layer that hinders back-diffusion of NaCl, σ decreases and more NaCl is transported across the membrane. Under conditions of the near constant $\sigma\Delta\pi_m$, the kinetics of permeate flux decline was determined by changes in R_f . Indeed, the slowest decline in flux was observed for the intermediate ionic strengths that had the slowest increase in R_f (**Figure 36b**). In sum, the analysis presented in sections 4.2. (approach) and 4.4.4 (results) confirms the hypothesis that NF270 fouling by emulsified oil indeed enhances concentration polarization of rejected NaCl. However, because the concentration-dependence of the reflection coefficient ($\sigma\Delta\pi_m \cong 0.56\Delta\pi_m^{-0.18}$) the enhancement does not lead to higher osmotic pressure differential. Higher C_m lead to lower σ that is to a stronger coupling between solvent (water) and solute (NaCl) transport across the membrane. As a result, rejection of NaCl decreases while flux remains relatively unchanged.

4.4.4.3. Implications for practice

Future work should explore how the rejection of multivalent cations depends on the ionic strength of the feed. If the ability of NF270 to reject larger ions is not affected, the enhanced “leaking” of NaCl at higher ionic strengths would bode well for pretreatment of brines prior to desalination. Lower osmotic pressure due to rejected NaCl would be

avoided while softening, removal of emulsified oil and, presumably, dissolved organics, can be maintained at high level to avoid fouling during downstream desalination by reverse osmosis or other means. The results on concentration dependence of σ and B are specific to the selected salt/membrane combination (NaCl/NF270). While the coupon-to-coupon consistency of the data is encouraging, the dependences can be different for other nanofiltration membranes. The proposed algorithm of determining $\sigma(C)$ and $B(C)$ should apply though.

A virtually immediate (within 1 min since the introduction of oil into the feed) and significant decrease of hydraulic permeability was observed during nanofiltration of highly saline emulsions (seawater level and higher). When interpreted as the fraction of membrane area “sealed” by oil, this precipitous decline in flux corresponded to the loss of 14% and 64% of the total membrane area available for permeation at the feed ionic strength of 469 mM and 1711 mM, respectively. Based on direct visualization data, we attribute this loss of permeability to spreading of oil films at the membrane surface. This calls for membrane materials or coatings that stunt the movement of the three-phase contact line to prevent oil film formation and spreading over the membrane surface. From the process engineering perspective, membrane surface sealing by oil films can be effectively managed by a hydraulic flush at zero transmembrane pressure.

Over the longer term, membrane fouling (R_f) becomes the dominant mechanism of flux decline. Specific fouling management strategies depend on the type of fouling with droplet stability playing an important role. Highly stable emulsions have small deformable droplets, which pack into low porosity and high hydraulic resistance layers. As **Figure 34** indicates, intermediate salinity appears to favor slower flux decline.

4.5. Conclusions

The study focused on membrane fouling mechanisms during nanofiltration of highly saline emulsions. Two parameters of the Spiegler-Kedem model – reflection coefficient σ and permeability coefficient ω - were measured as functions of solute concentration in 1:1 electrolyte feeds. Nanofiltration tests employed NF270 membranes and SDS-stabilized hexadecane emulsified in concentrated NaCl solutions (up to 100 g/L). For all membranes tested, σ followed a near hyperbolic dependence on the transmembrane concentration ($\sigma\Delta\pi_m \approx \text{const}$) while ω asymptotically converged to the same steady state value ($\sim 20 \mu\text{m/s}$) across a range of feed salinities and concentration polarization conditions. The results were used to determine separate contributions of osmotic pressure and fouling to the overall flux decline. Two salient features of the observed fouling dynamics and their practical implications were the following:

- 1) The decrease in σ with an increase C_m negated the effect of concentration polarization on permeate flux. Indeed, the contribution of osmotic pressure ($\sigma\Delta\pi_m$) to the overall headloss remained almost unchanged throughout different stages of membrane fouling. Future work should assess NF selectivity with respect to ions of difference valence in brine feeds. If higher rejections of multivalent ions can be maintained, the enhanced passage of NaCl at higher ionic strengths would support NF as a method of pretreating brines prior to desalination.
- 2) The initial decline of the permeate flux was a strong function of feed salinity. An abrupt drop in flux upon the introduction of oil into the feeds of high salinity (seawater level and higher) was interpreted as resulting from membrane surface sealing by coalesced oil films. For the 100 g(NaCl)/L feed, $\sim 64\%$ of the membrane

area was sealed within 1 min of membrane exposure to emulsified oil. Screened electrostatic repulsion between droplets at higher salinities leads to coalescence. When droplet-membrane interactions are favorable, this scenario leads to formation and growth of surface films. These considerations call for membrane materials or coatings that stunt the movement of the three-phase contact line to prevent oil film formation and spreading over the membrane surface.

In the longer term, the additional hydraulic resistance due to a layer of oil droplets on the membrane surface became the dominant mechanism of flux decline. The oil droplet layers are expected to have high specific resistance as the low interfacial tension typical for saline emulsions gives rise to small deformable droplets with high packing density.

APPENDIX

APPENDIX

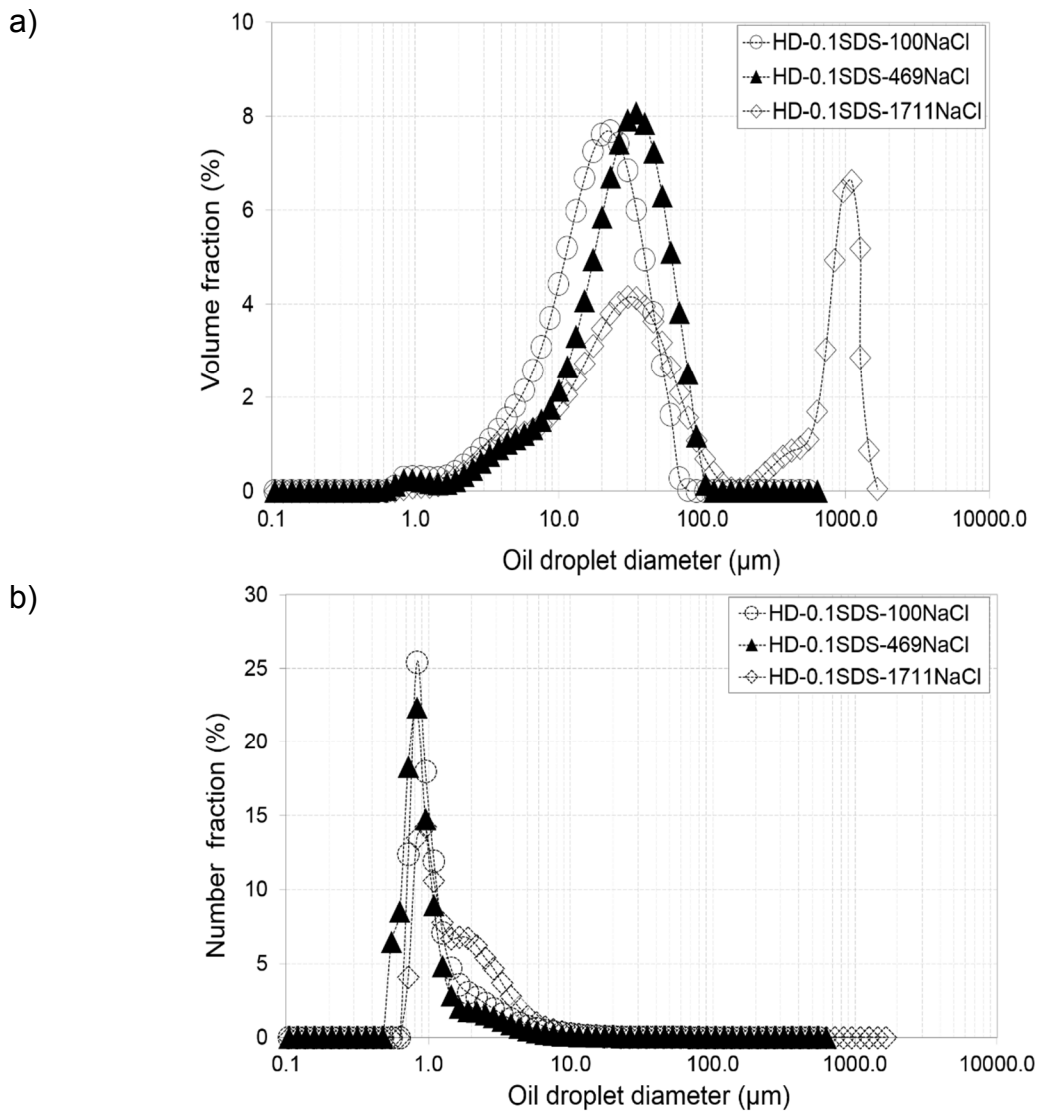


Figure 37. Volume-based (a) and number-based (b) droplet size distributions of SDS-stabilized hexadecane-in-water emulsion in the presence of salt (100 mM NaCl, 469 mM NaCl, or 1711 mM NaCl). The volume-based median diameter increased with an increase in the ionic strength from 20 μm to 32 μm to 49 μm for the HD-0.1SDS-100NaCl, HD-0.1SDS-469NaCl, and HD-0.1SDS-1711NaCl emulsions, respectively.

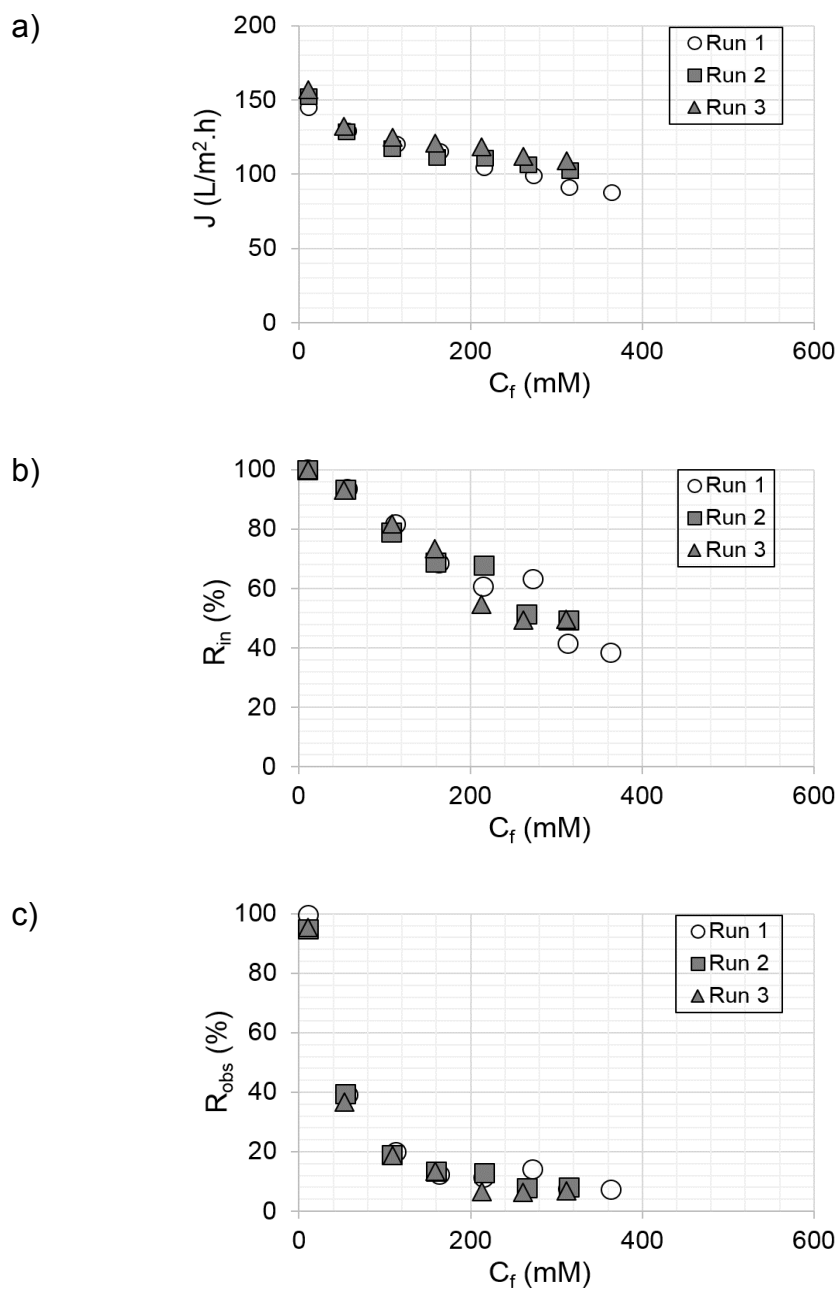


Figure 38. Permeate flux (a), intrinsic rejection of NaCl (b), and observed rejection of NaCl (c) by NF270 as functions of NaCl concentration in the feed.

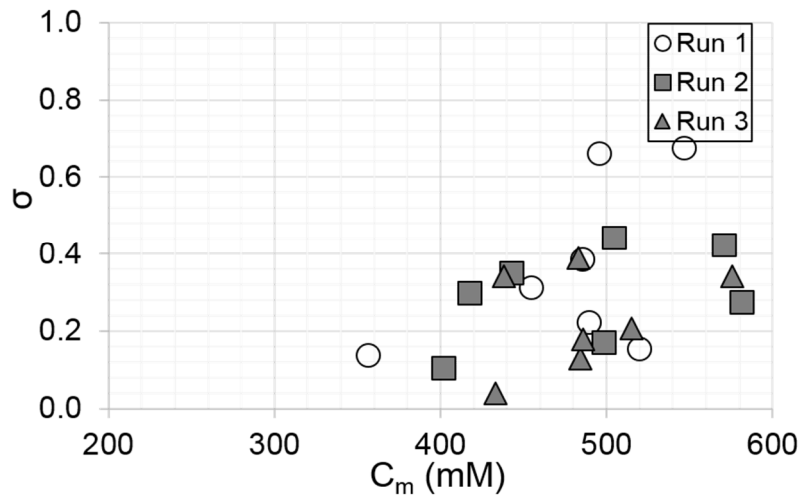


Figure 39. Dependence of reflection coefficient on NaCl concentration at the membrane surface

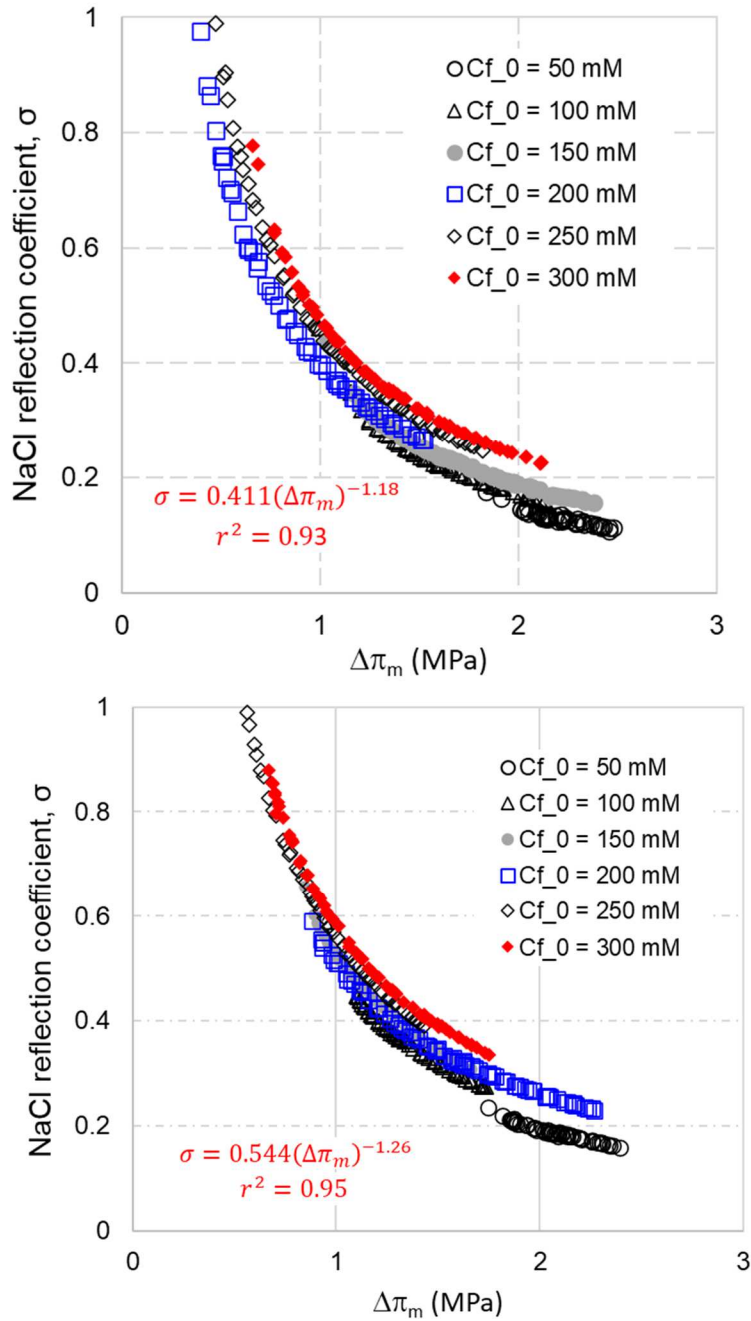


Figure 40. Dependence of NaCl reflection coefficient of NF270 membrane on the osmotic pressure differential. Different segments of the dependence correspond to tests with different initial feed concentrations, $C_{f,0}$, of NaCl. The two graphs are for two replicate measurements with two different NF270 membranes. The dependence for another NF270 membrane is shown in Figure 16.

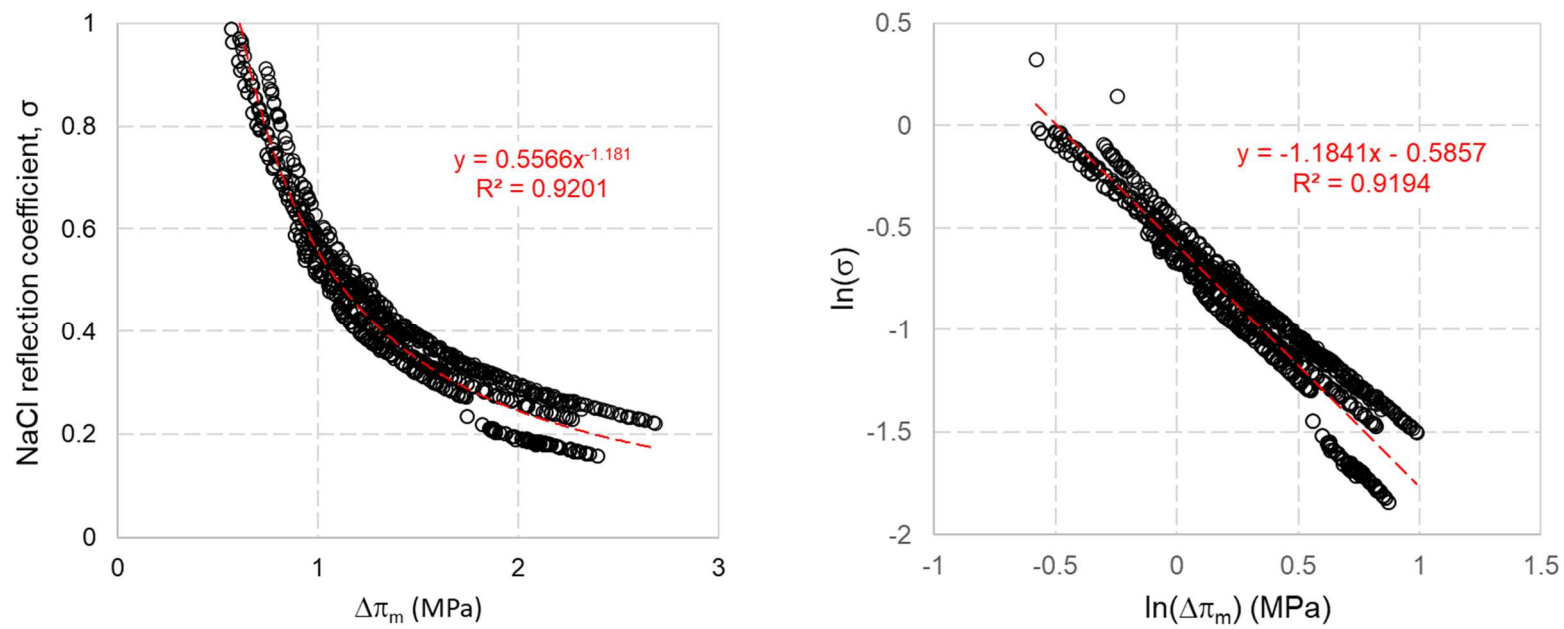


Figure 41. Dependence of NaCl reflection coefficient of NF270 membrane on the osmotic pressure differential. The power law provides the best fit (dashed red line). The data represent a merged dataset recorded in three separated tests with different NF270 membranes. Data set for each membrane consists of segments corresponding to different feed concentrations of NaCl (Figure 24).

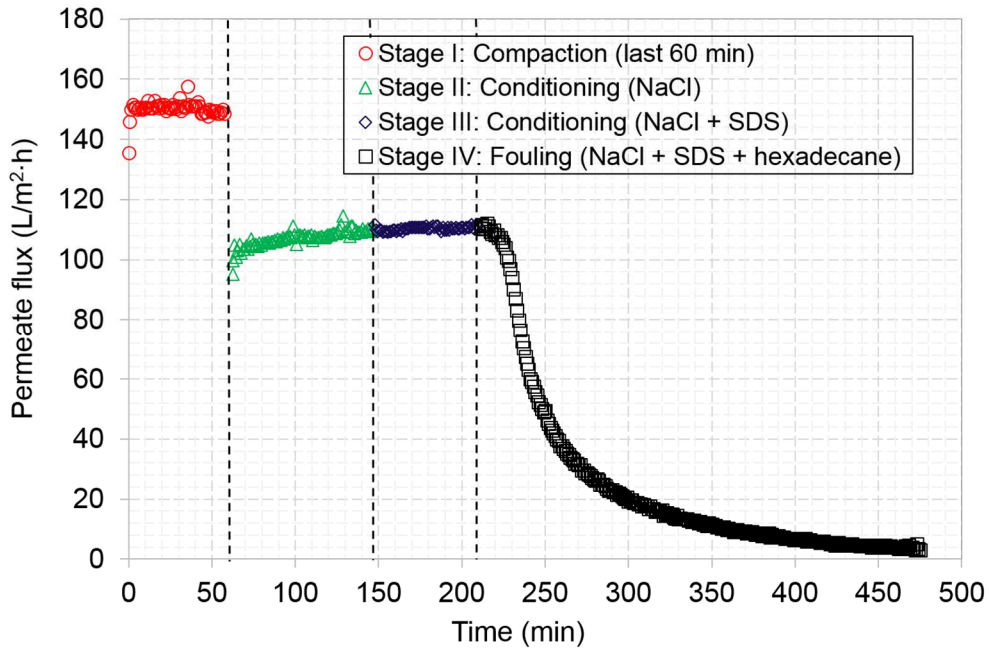


Figure 42. Permeate flux change during conditioning and fouling stages at $\Delta P = 200$ psi (1.38 MPa) and $C_{f0} = 100$ mM NaCl.

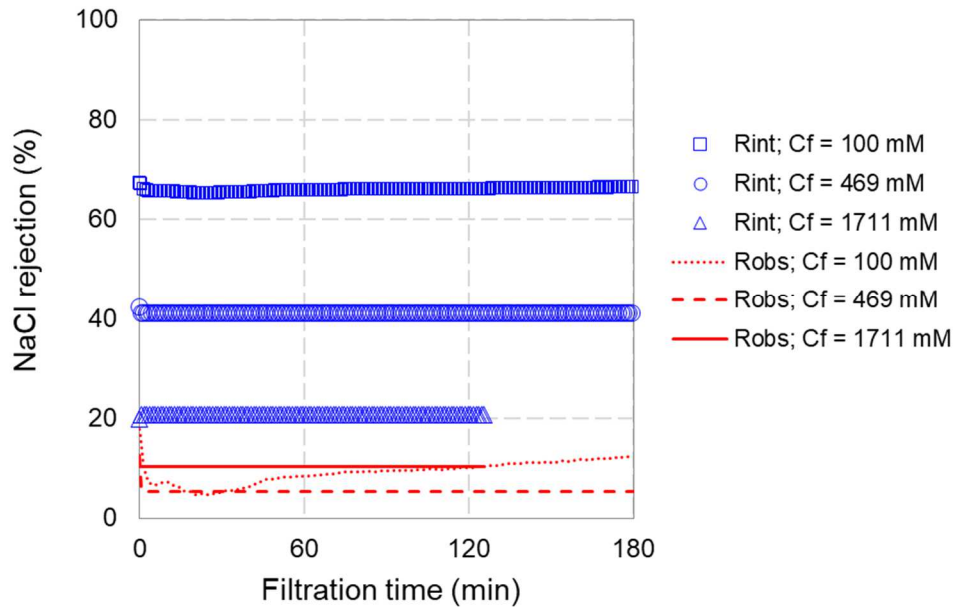


Figure 43. Observed and intrinsic rejections of NaCl by NF270 for SDS-stabilized hexadecane-in-water emulsion at different ionic strengths.

CHAPTER FIVE

Public perception of oil spills and pipelines

5.1. Introduction

The increase in the exploration, production, and consumption of oil and petroleum products has led to a higher threat of oil spills. In 2018, the United States consumed 7.5 billion barrels of petroleum products, which translates to 20.5 million barrels per day [224]. Approximately eighty million barrels of oil are transported daily from oil fields to consumers, which involves different modes of transportation such as tankers, pipelines, railcars, and tank trucks [225]. Accidents that lead to oil spills can occur at any stage of exploration, production, transportation, or storage.

Large oil spills such as the 1989 Exxon Valdez in Alaska and the 2010 Deepwater Horizon spill into the Gulf of Mexico have raised a global awareness of the related risks and their environmental and economic impacts. However, less attention has been given to potential spills as the existing regulations related to oil and gas industries are largely reactive rather than proactive. In other words, these policies are not designed to effectively prevent oil spills focusing, instead, on remediation once oil spills occur.

For now, oil and gas are considered indispensable sources of energy and transporting them is therefore generally seen as a necessary risk [226]. Clearly, there are real trade-offs resulting from the increased production and consumption of oil and gas (e.g. tradeoffs in security, economic benefits, energy dependence, environmental harm, health costs, and cultural consequences). Therefore, it is important to know how well

policymakers and the public understand the costs and benefits of such a commitment to oil.

To date, there have been no studies that have assessed U.S. residents' knowledge and attitudes towards oil spills particularly due to pipeline failure. The purpose of this survey study is to understand the public knowledge about oil spills and their stance on pipelines.

5.2. Methods

5.2.1. Survey Design

Data was obtained by surveying a national convenience sample of 630 American adults using *Qualtrics*. The survey utilized quotas to ensure that the final sample approximated national trends on key demographics as reported in the 2010 Census (age, gender, race, education, and rural/urban primary residence) and, for political affiliation, a 2019 poll conducted by Gallup. This survey module was part of a longer survey designed by a group of doctoral students in an Environmental Science and Policy Program class at Michigan State University. The module consisted of five knowledge-based questions (**Table 8**) one vignette (**Table 9**), four behavioral intention questions (**Table 10**), and one question related to their willingness to pay (WTP) (**Table 11**). The “knowledge-based” questions were designed to obtain general information of how much people know about oil spills and pipelines. It is important to note that the first three questions (Q1 through Q3) allowed multiple response options including “Don’t know”. However, the last two questions in this set, were binary; thus the participants were forced to answer whether they believed the answer to be “true” or “false”.

For the vignette, the participants read a scenario in which the governor of their

state asked for public input regarding the future of an oil pipeline in their state. Participants were told that, although the pipeline was not in imminent danger of spilling, there was some risk. Participants then reported whether their preferred response was shutting down the pipeline and losing the possible economic benefit to their state, shutting down the pipeline temporarily and paying higher taxes to replace the pipeline with safer materials, or keeping the pipeline open and risking an oil spill.

Regarding the attitudinal questions, participants were asked to indicate the extent to which they agreed with a certain statement (e.g. oil spills are a serious environmental issue) on a seven-point, Likert-like scale ranging from “Strongly Disagree” to “Strongly Agree” (**Table 10**). The WTP question tested the participant’s willingness to pay in terms of percentage increase in annual property taxes to transition their community from oil and gas to renewable energy such as wind, solar, or geothermal.

The participants also responded to demographic questions about age, gender, race, education, and political ideology, and completed the Assessment of Sustainability Knowledge (ASK) and the Sustainability Attitudes Scale (SAS) [227].

Knowledge and attitudes were used as response variables measured across several demographic parameters (education level, political affiliation, employment status, and race and ethnicity).

5.2.2. Data Analysis

Participant responses were analyzed quantitatively. The five questions that tested the participant’s knowledge about oil spills were first analyzed by evaluating the number of correct responses for each question. The next step was to test whether the accuracy on each individual question was related to the educational background of the participant

(coded as 2 x 2) using Pearson's chi-squared test. Education was recoded as dichotomous and was grouped into two categories: precollege (i.e. didn't finish high school and high school degree) and post-college (some college, associate or other 2-year, Bachelor's, and graduate degree). The chi-squared test was intended to test how likely it is that an observed distribution was due to chance. In other words, it measured how well the observed distribution of data fitted with the distribution that was expected if the variables (education level and outcome of the question) were independent.

For the vignette portion, Chi-squared test was used to measure whether the participant's preferences regarding the pipeline (shutdown vs kept open) depended on their race, education level, and political affiliation. Similar to education level, race was recoded as a dichotomous variable: White or Caucasian vs everyone else (i.e. Black or African American, Hispanic, Asian, American Indian or Alaska Native, Native Hawaiian, other Middle Eastern, multiracial, and Arab). Political affiliation was also recoded as two categories: Republicans vs everyone else (i.e. Democrats, Independent, and Other).

The next set of analysis was for the behavioral intention questions. Spearman's rank-order correlation was used to measure the strength and direction of association between the different ranked statements (e.g oil spills are a serious environmental issue vs. oil spills won't necessary affect my community). Moreover, a modified chi-squared test known as "Pearson's chi-squared test for count data" was used to evaluate whether the outcome of the vignette was related to the ranking chosen in the matrix. The outcome of the vignette was recoded as dichotomous: shutdown the pipeline vs kept open.

For the WTP question, a chi-squared test was used to evaluate whether the percentage chosen depends on the participant's political affiliation and employment

status. The percentage increase in taxes was regrouped into two categories, where the first category includes 0% to 4% and the second one is 6% to 10%. Similar to other demographic parameters, the employment status was recoded as a dichotomous variable (full-time employment vs. part-time and unemployed).

5.3. Results and Discussion

5.3.1. Summary Statistics

The respondent pool was almost equally divided among gender lines with 51.9% female (n=327/630), 47.9% male (n=302/630), and 0.2% other (n=1/630). The average age of the participants was nearly 47 years of age, and it varied between 19 and 93. In addition, 65.71% (n=414/630) of the participants were White or Caucasian, approximating the national trends based on the 2010 Census data.

Eighty-seven percent of those surveyed had at least finished high school with 57% indicating that they have completed some college. Nearly 34% of the participants indicated that they work full-time (32 hours or more per week). The average participant had a low sustainability knowledge but a generally positive attitude toward sustainability. For the ASK, none of the participants were able to answer all questions and only one participant was able to answer 11 out of the 12 questions correctly.

5.3.2. Knowledge-based Questions

Figure 44 shows the number of participants who answered the knowledge-based questions correctly. The majority of the respondents (51.90%; n=327/630) were able to answer two out of the five questions correctly. However, only 1.59% of the respondents (n=10/630) were able to answer all five questions. Overall, the participants were least

accurate regarding questions Q1 (What percentage of oil and gas does the U.S. consume?) and Q3 (How much do you think is the average cleanup cost for 1 gallon of oil spilled?) For Q1, 37.1% (n=234/630) of the respondents chose the “Don’t know” option and only 13.2% (n=83/630) answered correctly. Similarly, for the Q3, the majority of the participants (38.41%) chose the “Don’t know” option and only 27.5% chose the correct answer.

Regarding the true/false questions, most participants were notably more accurate. The majority of the respondents (69% and 74.4%, respectively) answered the following two questions correctly: Q4) cleaning up oil spilled under ice is no different than an oil spill in open water and Q5) in case of an oil spill, damages to the ecosystem can last longer in cold weather compared to temperate climate. Another possible explanation is that those questions were binary and “Don’t know” wasn’t an option; thus the participants were forced to answer. Although this suggests that participants were more accurate, it is important to note that they were required to respond and so would likely have been more accurate simply by chance.

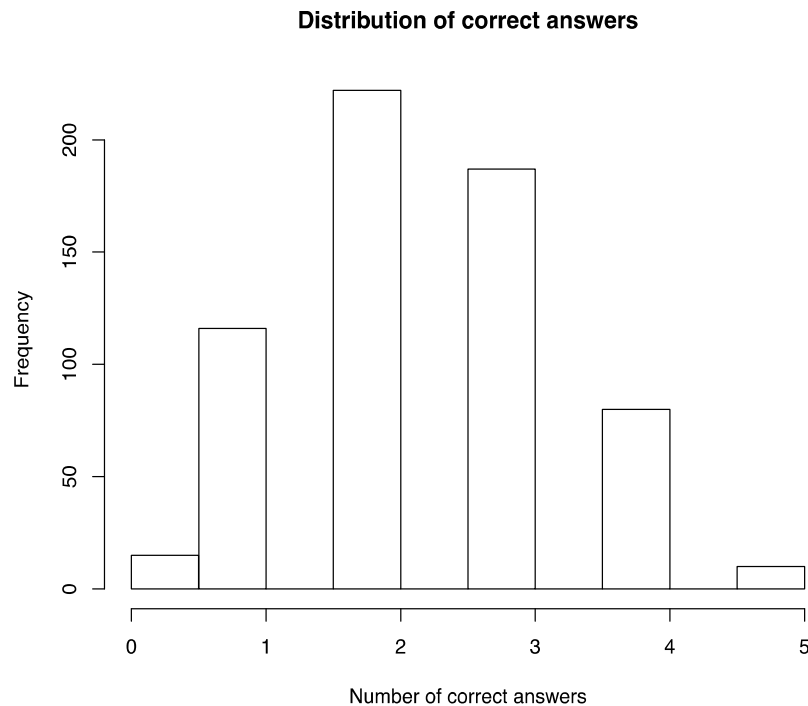


Figure 44. Number of respondents as a function of correct answers (n=630)

Having univariately evaluated the knowledge question responses, we next moved to test their association with education. The first chi-squared tests evaluated the independence of accuracy on each knowledge-based question and the respondent's education level (pre-college vs. post college). In this case, the null hypothesis was that the question outcome and education level were independent of one another. The alternative hypothesis was that the two variables have a strong relationship. For the multiple choice questions (Q1 through Q3), there seemed to be a strong relationship between education and the question outcome as the probability value (p-value) was below 0.05. However, the null hypothesis could not be rejected for the true/false questions (Q4 and Q5).

Next we assessed whether there is a relationship between getting all three multiple choice questions correct and the participant’s level of education. The null hypothesis (that the variables are independent) couldn’t be rejected as the p-value was significantly greater than 0.05 (p-value=0.10). Therefore, education level and getting all three answers correctly appear to be independent.

The last set of analysis focused on testing the relationship between choosing the “Don’t know” option for Q1 through Q3 and the participant’s level of education. Chi-squared test showed that there’s a dependence, but only for Q1 where $p < 0.001$.

Table 6. Chi-squared test for knowledge-based question outcome as a function of education level

Question	X ²	df	p-value
Q1.What percentage of oil and gas does the U.S. consume?	70.27	20	<0.001
Q2.How do you think most of the oil and gas is transported in the U.S.?	28.50	15	0.02
Q3.What do you think is the average cleanup cost for 1 gallon of oil spilled?	37.10	20	0.01

From **Table 6**, it can be seen that there were significant dependencies between the outcomes for questions 1-3 and education. The fact that this is not true for questions 4 and 5 reflects the noise in those questions since people were forced to guess (which means that some right answers mean accuracy [which should relate to education] and some mean lucky guesses [which should be random]).

The results therefore suggest that participants’ knowledge about oil spills was dependent of their educational background. This is consistent with other studies that have

examined the public's environmental knowledge and found that education was a major correlate [228-230]. However, we realize that education is only one of the factors contributing to learning and thinking in a cognitive learning process [231].

5.3.3. Vignette

Three chi-squared tests were used to measure whether the participant's preferred pipeline option is related to their race, political affiliation, and education level. Recent research related to environmental injustice have shown that perceived risk is closely related to race as white stand out for their uniformly low perceptions of environmental health risks compared to non-white respondents [232]. Therefore, for the vignette, we would expect minorities to choose the "safer" option. As mentioned earlier race and the preferred options were recoded as dichotomous variables. The preferred options were grouped into two categories: shutdown the pipeline and keep the pipeline open. In the first test, the null hypothesis was that the chosen pipeline option is independent from race. The null hypothesis couldn't be rejected as the p-value was greater than 0.05, but the test did achieve marginal significance ($p = 0.07$).

Political affiliation is one of the major predictors of environmental attitude and support for an environmental policy [233]. Numerous studies have found that political conservatives or republicans are less concerned about environmental issues, less supportive of environmental policy, and less likely to engage in individual environmental behavior [234-236]. This is consistent with our chi-squared test results that showed that the preferred option strongly depends on the political affiliation ($p < 0.001$). More republicans were willing to risk an oil spill by keeping the pipeline open. The final test

related to education level, returned a p-value of 0.03, which is less than 0.05, meaning that the preferred pipeline option also correlates with education.

5.3.4. Willingness to Pay (WTP)

Political affiliation and income are strong indicators for WTP [237]. Two chi-squared tests were performed to evaluate whether the participant's willingness to pay as percentage increase in annual property tax to transition their community from oil and gas to renewable energy depends on their political affiliation and employment status. Participants affiliated with the Democratic Party are willing to pay higher taxes for renewable energy compared to republicans. The political affiliation variable was coded as a dichotomous variable (republicans vs others). The chi-squared test shows that the percentage increase in tax and political affiliation are independent of each other (p-value=0.289).

The income data was unreliable in our survey; thus employment status (employed vs unemployed) was used instead. Participants who work full-time were willing to pay higher taxes for renewable energy. This was confirmed by the chi-squared test stating that employment status and participant's willingness to pay have a strong relationship (p-value < 0.001).

5.3.5. Behavioral Intention Questions

Spearman's rank-order correlation was used to measure the correlation strength between the different ranked statements (**Table 7**). In the first row, participants who consider oil spills to be a serious environmental issue are likely to disagree that oil spills won't affect their community. As expected, the spearman's correlation coefficient (-0.32) indicated a significant negative relationship between these two rank-order? statements.

On the other hand, participants who agree that the environmental risk associated with oil spills is worth the economic benefit are likely to agree that oil spills won't affect their community. The spearman's correlation coefficient of 0.33 indicate a significant positive relationship between these two ranked statements. In the last row, participants who disagreed that oil spills won't affect their community also disagreed that having an oil spill under ice is beneficial. This was indicated by a strong positive relationship (0.41) between the ranked statements.

Table 7. Spearman's rank-order correlation (significant associations are in bold)

	Q7.	Q8.	Q9.	Q10.
Q7. Oil spills are a serious environmental issue.		-0.06	-0.32 p<0.001	-0.16
Q8. The environmental risk associated with oil pipelines is worth the economic benefit it provides.			0.33 p<0.001	0.26
Q9. Oil spills won't necessary affect my community.				0.41 p<0.001
Q10. Having an oil spill under ice is beneficial as it restricts the spread of oil.				

5.3.6. Vignette and Behavioral Intention Questions

Modified chi-squared tests were used to assess whether the participant's preferred pipeline option is related to the ranking chosen in the matrix. First, we tested whether

there's a correlation between the ranking of "oil spills are a serious environmental issue" and the pipeline option chosen (shutdown pipeline vs keep pipeline open). The chi-squared test indicated that there is a strong relationship between the ranking and the chosen option as the p-value was significantly lower than 0.001. In the second test, we tested whether there's a dependence between the ranking of "oil spills won't necessary affect my community" and the preferred pipeline option. A p-value of 2.611e-08 indicating that the null hypothesis couldn't be rejected and the two variable are strongly dependent.

5.4. Conclusions

Oil spills are a serious environmental issue that can't be solely solved by technological innovation. The public are the main consumers of oil and gas, so it is important to understand how much the public knows about the costs and benefits of such a commitment to oil. This study evaluated public knowledge about oil spills, their attitudes and relevant behavioral intention.

The participants' knowledge about oil spills was found to be dependent on their educational level. This result is consistent other environmental studies that found education to be a main contributor to the public's environmental knowledge. A better predictor could have been educational background (social science vs. natural science) instead of educational level. However, we do realize that education is only one of the factors contributing to learning and thinking in a cognitive learning process.

The participant's attitude toward oil pipeline was found to be a strong function of political affiliation and educational level. Most republicans supported having an oil pipeline and were willing to take the risk of an oil spill. On the other hand, the participant's perceived risk depended on their education rather than their race/ethnicity. The findings

from this survey will have critical implications for identifying best practices and developing spill remediation policy in the U.S.

APPENDIX

APPENDIX

Table 8. Questions assessing knowledge related to energy (the correct answer is shown in bold along with the percentage of respondents for each option)

<p>Q1.What percentage of oil and gas does the U.S. consume?</p> <ul style="list-style-type: none">a. 10% of the world's consumption (3.01%)b. 20% of the world's consumption (13.2%)c. 30% of the world's consumption (20.96%)d. 40% of the world's consumption (25.73%)e. Don't know (37.1%)
<p>Q2.How do you think most of the oil and gas is transported in the U.S.?</p> <ul style="list-style-type: none">a. Rail (train) (11.61%)b. Semi-truck (17.15%)c. Pipeline (52.50%)d. Don't know (18.74%)
<p>Q3.What do you think is the average cleanup cost for 1 gallon of oil spilled?</p> <ul style="list-style-type: none">a. \$50 (5.39%)b. \$100 (13.0%)c. \$500 (15.71%)d. \$1000 (27.5%)e. Don't know (38.42%)
<p>Q4.Cleaning up oil spilled under ice is no different than an oil spill in open water.</p> <ul style="list-style-type: none">a. True (31%)b. False (69%)
<p>Q5.In case of an oil spill, damages to the ecosystem can last longer in cold weather compared to temperate climate.</p> <ul style="list-style-type: none">a. True (74.4%)b. False (25.6%)

Table 9. Vignette related to an oil pipeline in the respondent's state

Q6. Suppose that the state where you live has an oil pipeline. There is no immediate danger, but because of the nature of how the pipeline is built, it is very difficult to clean an oil spill if one were to occur. The governor has asked for public input regarding the pipeline.

Which of the following options would you prefer?

- a. Shutdown the pipeline and lose the possible economic benefit to your state
- b. Shutdown the pipeline temporarily and pay higher taxes to replace the pipeline.
- c. Keep the pipeline open and risk an oil spill.

Table 10. Attitudes and risk perception associated with oil spills (all items were set to 1-Strongly Disagree, to 7-Strongly Agree scale)

Q7. Oil spills are a serious environmental issue.

Q8. The environmental risk associated with oil pipelines is worth the economic benefit it provides.

Q9. Oil spills won't necessarily affect my community.

Q10. Having an oil spill under ice is beneficial as it restricts the spread of oil.

Table 11. Willingness to pay to switch to "greener" source of energy

Q11. What percentage increase in tax are you willing to pay to transition your community from oil and gas to renewable energy such as wind, solar, or geothermal?

- a. 0%
- b. 2%
- c. 4%
- d. 6%
- e. 8%
- f. 10%

CHAPTER SIX

Overarching conclusions and future work

Conclusions for each of the research projects were provided at the end of their corresponding chapters. Based on chapters 3 and 4 (visualization and permeability results), we can attribute the loss of membrane permeability to the spreading of oil films at the membrane surface. This calls for membrane materials or coatings that focus on tailoring affinity and pore space design to prevent oil film formation and spreading over the membrane surface. The material would need to have long-term durability in the presence of crossflow shear and more complex oily feeds.

Fouling mitigation strategies highly depend on the type of feed, specifically the stability of the oil emulsions. Highly stable emulsions have small deformable droplets, which pack into low porosity and high hydraulic resistance layers. Emulsion of intermediate stability appears to favor slower flux decline. Membrane cleaning strategies (hydraulic and chemical) will depend on the structure of the oil fouling layer.

Real-time direct visualization will continue to gain attention as it can provide early warnings of membrane fouling. This calls for coupling state-of-the-art techniques to develop higher resolution visualization techniques that can be valuable in diagnosing early stages of fouling.

Table 12 summarizes a few proposed experiments to gain additional insight into the mechanisms of membrane fouling by emulsified oil.

Table 12. Proposed experiments

Objectives	Proposed Experiments
Investigate the interaction of rejected emulsified oil and dissolved species in the vicinity of NF membrane and how membrane flux and salt rejection are impacted.	Constant pressure crossflow filtration tests with salt, surfactant solutions, and model emulsions stabilized by non-ionic or zwitterionic surfactants Variables: surfactant (type and concentration); salt (type and concentration)
Evaluate the filterability of Corexit-stabilized crude oil-water emulsions by practical ultra- and microfiltration membranes.	Constant pressure crossflow filtration tests with porous polymeric and ceramic membranes Variables: Corexit (concentration); salt (type and concentration); operational parameters (crossflow velocity and transmembrane pressure).
Evaluate efficiency of hydraulic and chemical cleaning for polymeric and ceramic membranes fouled by produced water or Corexit-stabilized crude oil emulsions.	Test membrane cleaning strategies hydraulic cleaning versus chemical cleaning Variables: cleaning solutions (surfactant or absorbent media); operational parameters (crossflow velocity, pH, temperature)
Measure kinetics of oil droplet deposition on surfaces of common membrane polymers with and without antifouling coatings.	Utilize Quartz Crystal Microbalance with Dissipation (QCM-D) to rank common membrane polymers in terms of their ability to resist fouling by nanoemulsions Variables: Sensor material (e.g. Al ₂ O ₃ , ZrO ₂ , and TiO ₂); PEM coating (e.g. number of [PSS/PAH] bilayers); surfactant (type and concentration)
Identify the mechanisms of membrane fouling by surfactant and nanoparticle-stabilized model emulsions.	Utilize the DOTM technique to visualize the evolution of the oil fouling layer on the membrane surface during crossflow filtration of model oil-water emulsions Variables: Nanoparticle (concentration); surfactant (type and concentration); oil (type); salt (type and concentration)
Assess different technologies for the pretreatment of produced water prior to using nanofiltration as a polishing step.	Compare the efficiency of several technologies (e.g. MF and hydrocyclones) in terms of oil removal, energy consumption, and throughput.

Based on this work, we can conclude that membrane technology complements rather than replaces conventional deoiling methods. The low values of steady state permeate flux and high pressure buildup during crossflow ultrafiltration and nanofiltration of hexadecane-water emulsions indicate that membrane separation is suitable as a polishing step rather than a standalone process. Oily industrial wastewater requires pretreatment by a high throughput deoiling unit such as hydrocyclones or flotation that can be later followed by membrane separation.

Ismail Serageldin, the Vice President of the World Bank in 1995, said: “If the wars of this century were fought over oil, the wars of the next century will be fought over water— unless we change our approach to managing this precious and vital resource” [1]. Water security can be achieved by leveraging on technologies and best management practices to meet the strong and growing water demand from both industrial and domestic sectors. One sustainable option is produced water reclamation, where it is treated to a water quality that makes it reusable and can augment current freshwater supplies.

REFERENCES

REFERENCES

- [1] N.M. Daud, S.R. Sheikh Abdullah, H. Abu Hasan, Z. Yaakob, Production of biodiesel and its wastewater treatment technologies: A review, *Process Safety and Environmental Protection*, 94 (2015) 487-508.
- [2] M. Cheryan, N. Rajagopalan, Membrane processing of oily streams. Wastewater treatment and waste reduction, *Journal of Membrane Science*, 151 (1998) 13-28.
- [3] M. Padaki, R. Surya Murali, M.S. Abdullah, N. Misdan, A. Moslehyani, M.A. Kassim, N. Hilal, A.F. Ismail, Membrane technology enhancement in oil–water separation. A review, *Desalination*, 357 (2015) 197-207.
- [4] J. Mueller, Y. Cen, R.H. Davis, Crossflow microfiltration of oily water, *Journal of Membrane Science*, 129 (1997) 221-235.
- [5] J. Neff, K. Lee, E.M. DeBlois, Produced Water: Overview of Composition, Fates, and Effects, in: K. Lee, J. Neff (Eds.) *Produced Water: Environmental Risks and Advances in Mitigation Technologies*, Springer New York, New York, NY, 2011, pp. 3-54.
- [6] A. Fakhru'l-Razi, A. Pendashteh, L.C. Abdullah, D.R.A. Biak, S.S. Madaeni, Z.Z. Abidin, Review of technologies for oil and gas produced water treatment, *Journal of Hazardous Materials*, 170 (2009) 530-551.
- [7] V. Mavrov, E. Bélières, Reduction of water consumption and wastewater quantities in the food industry by water recycling using membrane processes, *Desalination*, 131 (2000) 75-86.
- [8] S. Casani, M. Rouhany, S. Knøchel, A discussion paper on challenges and limitations to water reuse and hygiene in the food industry, *Water Research*, 39 (2005) 1134-1146.
- [9] M. Vourch, B. Balannec, B. Chaufer, G. Dorange, Treatment of dairy industry wastewater by reverse osmosis for water reuse, *Desalination*, 219 (2008) 190-202.
- [10] D.C. Seo, H.J. Lee, H.N. Hwang, M.R. Park, N.W. Kwak, I.J. Cho, J.S. Cho, J.Y. Seo, W.H. Joo, K.H. Park, J.S. Heo, Treatment of non-biodegradable cutting oil wastewater by ultrasonication-Fenton oxidation process, *Water science and technology : a journal of the International Association on Water Pollution Research*, 55 (2007) 251-259.
- [11] M. Perez, R. Rodriguez-Cano, L.I. Romero, D. Sales, Performance of anaerobic thermophilic fluidized bed in the treatment of cutting-oil wastewater, *Bioresource Technology*, 98 (2007) 3456-3463.

- [12] L. Yu, M. Han, F. He, A review of treating oily wastewater, *Arabian Journal of Chemistry*, 10 (2017) S1913-S1922.
- [13] J.M. Dickhout, J. Moreno, P.M. Biesheuvel, L. Boels, R.G.H. Lammertink, W.M. de Vos, Produced water treatment by membranes: A review from a colloidal perspective, *Journal of Colloid and Interface Science*, 487 (2017) 523-534.
- [14] R.G. Holdich, I.W. Cumming, I.D. Smith, Crossflow microfiltration of oil in water dispersions using surface filtration with imposed fluid rotation, *Journal of Membrane Science*, 143 (1998) 263-274.
- [15] A.S.C. Chen, J.T. Flynn, R.G. Cook, A.L. Casaday, Removal of Oil, Grease, and Suspended Solids From Produced Water With Ceramic Crossflow Microfiltration, *SPE-20291-PA*, 6 (1991) 131-136.
- [16] D. Vasanth, G. Pugazhenth, R. Uppaluri, Cross-flow microfiltration of oil-in-water emulsions using low cost ceramic membranes, *Desalination*, 320 (2013) 86-95.
- [17] J.S. Ho, L.N. Sim, R.D. Webster, B. Viswanath, H.G.L. Coster, A.G. Fane, Monitoring fouling behavior of reverse osmosis membranes using electrical impedance spectroscopy: A field trial study, *Desalination*, 407 (2017) 75-84.
- [18] A.I. Zouboulis, A. Avranas, Treatment of oil-in-water emulsions by coagulation and dissolved-air flotation, *Colloids and Surfaces A: Physicochemical and Engineering Aspects*, 172 (2000) 153-161.
- [19] S. Khoufi, F. Aloui, S. Sayadi, Treatment of olive oil mill wastewater by combined process electro-Fenton reaction and anaerobic digestion, *Water Research*, 40 (2006) 2007-2016.
- [20] K.-i. Suehara, Y. Kawamoto, E. Fujii, J. Kohda, Y. Nakano, T. Yano, Biological treatment of wastewater discharged from biodiesel fuel production plant with alkali-catalyzed transesterification, *Journal of Bioscience and Bioengineering*, 100 (2005) 437-442.
- [21] T. Frankiewicz, Understanding the Fundamentals of Water Treatment, the Dirty Dozen-12 Common Causes of Poor Water Quality, in: 11th Produced Water Seminar, Houston, TX, 2001.
- [22] P. Kajitvichyanukul, Y.T. Hung, L.K. Wang, *Membrane Technologies for Oil-Water Separation*, 2011.
- [23] Z. Yang, V.V. Tarabara, M.L. Bruening, Adsorption of Anionic or Cationic Surfactants in Polyanionic Brushes and Its Effect on Brush Swelling and Fouling Resistance during Emulsion Filtration, *Langmuir*, 31 (2015) 11790-11799.

- [24] A. Szep, R. Kohlheb, Water treatment technology for produced water, *Water Science and Technology*, 62 (2010) 2372-2380.
- [25] S. Mondal, S.R. Wickramasinghe, Produced water treatment by nanofiltration and reverse osmosis membranes, *Journal of Membrane Science*, 322 (2008) 162-170.
- [26] T. Bilstad, E. Espedal, Membrane separation of produced water, *Water Science and Technology*, 34 (1996) 239-246.
- [27] M. Gryta, K. Karakulski, The application of membrane distillation for the concentration of oil-water emulsions, *Desalination*, 121 (1999) 23-29.
- [28] S. Velioglu, L. Han, J.W. Chew, Understanding membrane pore-wetting in the membrane distillation of oil emulsions via molecular dynamics simulations, *Journal of Membrane Science*, 551 (2018) 76-84.
- [29] L. Han, Y.Z. Tan, T. Netke, A.G. Fane, J.W. Chew, Understanding oily wastewater treatment via membrane distillation, *Journal of Membrane Science*, 539 (2017) 284-294.
- [30] Y.Z. Tan, L. Han, W.H. Chow, A.G. Fane, J.W. Chew, Influence of module orientation and geometry in the membrane distillation of oily seawater, *Desalination*, 423 (2017) 111-123.
- [31] G.V.R. Inc., Produced Water Treatment Market Analysis By Production Source (Crude Oil, Natural Gas), By Technology (Primary Separation, Secondary Separation, Tertiary Separation), By Application (Onshore, Offshore) And Segment Forecasts To 2024, (2016).
- [32] F.S. Incorporated, Super Hydrophilic Membranes, in, 2016.
- [33] D.J. Miller, X.F. Huang, H. Li, S. Kasemset, A. Lee, D. Agnihotri, T. Hayes, D.R. Paul, B.D. Freeman, Fouling-resistant membranes for the treatment of flowback water from hydraulic shale fracturing: A pilot study, *Journal of Membrane Science*, 437 (2013) 265-275.
- [34] K. Loganathan, P. Chelme-Ayala, M.G. El-Din, Effects of different pretreatments on the performance of ceramic ultrafiltration membrane during the treatment of oil sands tailings pond recycle water: A pilot-scale study, *Journal of Environmental Management*, 151 (2015) 540-549.
- [35] R.W. Field, G.K. Pearce, Critical, sustainable and threshold fluxes for membrane filtration with water industry applications, *Advances in Colloid and Interface Science*, 164 (2011) 38-44.
- [36] G.O. Lenntech, Ultrafilic M-Series: Membrane Element for the Separation of Oil & Water, in, 2002.

- [37] A. Technologies, AkvoFloat™ Flotation-Filtration Process, in, 2017.
- [38] K.D. K. Guerra, S. Dundorf, Oil and Gas Produced Water Management and Beneficial Use in the Western United States, in, 2011.
- [39] Y. Pan, W. Wang, T. Wang, P. Yao, Fabrication of carbon membrane and microfiltration of oil-in-water emulsion: An investigation on fouling mechanisms, *Separation and Purification Technology*, 57 (2007) 388-393.
- [40] R. Del Colle, C.A. Fortulan, S.R. Fontes, Manufacture of ceramic membranes for application in demulsification process for cross-flow microfiltration, *Desalination*, 245 (2009) 527-532.
- [41] K. Masoudnia, A. Raisi, A. Aroujalian, M. Fathizadeh, Cross-Flow Microfiltration Oil-in-Water Emulsion Using Polyvinylidene fluoride Membrane, *Procedia Engineering*, 44 (2012) 1974-1976.
- [42] B. Hu, K. Scott, Microfiltration of water in oil emulsions and evaluation of fouling mechanism, *Chemical Engineering Journal*, 136 (2008) 210-220.
- [43] S.-H. Lee, K.-C. Chung, M.-C. Shin, J.-I. Dong, H.-S. Lee, K.H. Auh, Preparation of ceramic membrane and application to the crossflow microfiltration of soluble waste oil, *Materials Letters*, 52 (2002) 266-271.
- [44] A.B. Koltuniewicz, R.W. Field, Process factors during removal of oil-in-water emulsions with cross-flow microfiltration, *Desalination*, 105 (1996) 79-89.
- [45] X. Hu, Y. Yu, J. Zhou, Y. Wang, J. Liang, X. Zhang, Q. Chang, L. Song, The improved oil/water separation performance of graphene oxide modified Al₂O₃ microfiltration membrane, *Journal of Membrane Science*, 476 (2015) 200-204.
- [46] S.H.D. Silalahi, T. Leiknes, J. Ali, R. Sanderson, Ultrasonic time domain reflectometry for investigation of particle size effect in oil emulsion separation with crossflow microfiltration, *Desalination*, 236 (2009) 143-151.
- [47] L. Luo, G. Han, T.-S. Chung, M. Weber, C. Staudt, C. Maletzko, Oil/water separation via ultrafiltration by novel triangle-shape tri-bore hollow fiber membranes from sulfonated polyphenylenesulfone, *Journal of Membrane Science*, 476 (2015) 162-170.
- [48] A. Alpatova, E.-S. Kim, S. Dong, N. Sun, P. Chelme-Ayala, M. Gamal El-Din, Treatment of oil sands process-affected water with ceramic ultrafiltration membrane: Effects of operating conditions on membrane performance, *Separation and Purification Technology*, 122 (2014) 170-182.

- [49] A. Rezvanpour, R. Roostaazad, M. Hesampour, M. Nyström, C. Ghotbi, Effective factors in the treatment of kerosene–water emulsion by using UF membranes, *Journal of Hazardous Materials*, 161 (2009) 1216-1224.
- [50] B. Chakrabarty, A.K. Ghoshal, M.K. Purkait, Ultrafiltration of stable oil-in-water emulsion by polysulfone membrane, *Journal of Membrane Science*, 325 (2008) 427-437.
- [51] P.H.H. Duong, T.-S. Chung, Application of thin film composite membranes with forward osmosis technology for the separation of emulsified oil–water, *Journal of Membrane Science*, 452 (2014) 117-126.
- [52] X. Zhang, J. Tian, S. Gao, Z. Zhang, F. Cui, C.Y. Tang, In situ surface modification of thin film composite forward osmosis membranes with sulfonated poly(arylene ether sulfone) for anti-fouling in emulsified oil/water separation, *Journal of Membrane Science*, 527 (2017) 26-34.
- [53] H. Zhang, S. Fang, C. Ye, M. Wang, H. Cheng, H. Wen, X. Meng, Treatment of waste filtrate oil/water emulsion by combined demulsification and reverse osmosis, *Separation and Purification Technology*, 63 (2008) 264-268.
- [54] S. Kasemset, A. Lee, D.J. Miller, B.D. Freeman, M.M. Sharma, Effect of polydopamine deposition conditions on fouling resistance, physical properties, and permeation properties of reverse osmosis membranes in oil/water separation, *Journal of Membrane Science*, 425-426 (2013) 208-216.
- [55] L.R. Firman, N.A. Ochoa, J. Marchese, C.L. Pagliero, Deacidification and solvent recovery of soybean oil by nanofiltration membranes, *Journal of Membrane Science*, 431 (2013) 187-196.
- [56] X.B. Zhu, A. Dudchenko, X.T. Gu, D. Jassby, Surfactant-stabilized oil separation from water using ultrafiltration and nanofiltration, *Journal of Membrane Science*, 529 (2017) 159-169.
- [57] A. Fouladitajar, F.Z. Ashtiani, B. Valizadeh, S.B. Armand, R. Izadi, Application of gas/liquid two-phase flow in cross-flow microfiltration of oil-in-water emulsion; permeate flux and fouling mechanism analysis, *Desalination and Water Treatment*, 57 (2016) 4476-4486.
- [58] G. Ducom, H. Matamoros, C. Cabassud, Air sparging for flux enhancement in nanofiltration membranes: application to O/W stabilised and non-stabilised emulsions, *Journal of Membrane Science*, 204 (2002) 221-236.
- [59] K. Karakulski, A.W. Morawski, Treatment of spent emulsion from a cable factory by an integrated UF/NF membrane system, *Desalination*, 149 (2002) 163-167.

- [60] J. Zhong, X.J. Sun, C.L. Wang, Treatment of oily wastewater produced from refinery processes using flocculation and ceramic membrane filtration, *Separation and Purification Technology*, 32 (2003) 93-98.
- [61] J.K. Milic, E. Drazevic, K. Kosutic, M. Simonic, Microfiltration of cutting-oil emulsions enhanced by electrocoagulation, *Desalination and Water Treatment*, 57 (2016) 10959-10968.
- [62] Z.X. Wang, J. Jin, D.Y. Hou, S.H. Lin, Tailoring surface charge and wetting property for robust oil-fouling mitigation in membrane distillation, *Journal of Membrane Science*, 516 (2016) 113-122.
- [63] T. Mohammadi, A. Esmaelifar, Wastewater treatment of a vegetable oil factory by a hybrid ultrafiltration-activated carbon process, *Journal of Membrane Science*, 254 (2005) 129-137.
- [64] Y. Liu, Advanced treatment of biologically treated heavy oil wastewater for reuse as boiler feed-water by combining ultrafiltration and nanofiltration, *Desalination and Water Treatment*, 57 (2016) 13113-13119.
- [65] N. Hilal, G. Busca, N. Hankins, A.W. Mohammad, The use of ultrafiltration and nanofiltration membranes in the treatment of metal-working fluids, *Desalination*, 167 (2004) 227-238.
- [66] K. Karakulski, A. Kozlowski, A.W. Morawski, Purification of oily wastewater by ultrafiltration, *Separations Technology*, 5 (1995) 197-205.
- [67] U. Daiminger, W. Nitsch, P. Plucinski, S. Hoffmann, Novel techniques for oil-water separation, *Journal of Membrane Science*, 99 (1995) 197-203.
- [68] Y. Rasouli, M. Abbasi, S.A. Hashemifard, Oily wastewater treatment by adsorption–membrane filtration hybrid process using powdered activated carbon, natural zeolite powder and low cost ceramic membranes, *Water Science and Technology*, 76 (2017) 895-908.
- [69] X.-N. Cheng, Y.-W. Gong, Treatment of oily wastewater from cold-rolling mill through coagulation and integrated membrane processes, *Environmental Engineering Research*, 23 (2018) 159-163.
- [70] J. Rodrigues Pires da Silva, F. Merçon, L. Firmino da Silva, A. Andrade Cerqueira, P. Braz Ximango, M.R. da Costa Marques, Evaluation of electrocoagulation as pre-treatment of oil emulsions, followed by reverse osmosis, *Journal of Water Process Engineering*, 8 (2015) 126-135.
- [71] M. Cheryan, *Ultrafiltration and Microfiltration Handbook*, Taylor & Francis, 1998.

- [72] R.A. Dangel, D. Astraukis, J. Palmateer, Fatty acid separation from hydrolyzer wastewater by ultrafiltration, *Environmental progress*, 14 (1995) 65-68.
- [73] B.K. Nandi, R. Uppaluri, M.K. Purkait, Treatment of Oily Waste Water Using Low-Cost Ceramic Membrane: Flux Decline Mechanism and Economic Feasibility, *Separation Science and Technology*, 44 (2009) 2840-2869.
- [74] S.J. Judd, Membrane technology costs and me, *Water Research*, 122 (2017) 1-9.
- [75] A. Bick, L. Gillerman, Y. Manor, G. Oron, Economic Assessment of an Integrated Membrane System for Secondary Effluent Polishing for Unrestricted Reuse, *Water*, 4 (2012) 219.
- [76] J. Hermia, Constant pressure blocking filtration laws - application to power-law non-newtonian fluids, *Transactions of the Institution of Chemical Engineers*, 60 (1982) 183-187.
- [77] M. Abbasi, M.R. Sebzari, A. Salahi, S. Abbasi, T. Mohammadi, Flux decline and membrane fouling in cross-flow microfiltration of oil-in-water emulsions, *Desalination and Water Treatment*, 28 (2011) 1-7.
- [78] A. Salahi, M. Abbasi, T. Mohammadi, Permeate flux decline during UF of oily wastewater: Experimental and modeling, *Desalination*, 251 (2010) 153-160.
- [79] T. Mohammadi, M. Kazemimoghadam, M. Saadabadi, Modeling of membrane fouling and flux decline in reverse osmosis during separation of oil in water emulsions, *Desalination*, 157 (2003) 369-375.
- [80] H. Ohya, J.J. Kim, A. Chinen, M. Aihara, S.I. Semenova, Y. Negishi, O. Mori, M. Yasuda, Effects of pore size on separation mechanisms of microfiltration of oily water, using porous glass tubular membrane, *Journal of Membrane Science*, 145 (1998) 1-14.
- [81] A.B. Koltuniewicz, R.W. Field, T.C. Arnot, Cross-flow and dead-end microfiltration of oily-water emulsion. Part I: Experimental study and analysis of flux decline, *Journal of Membrane Science*, 102 (1995) 193-207.
- [82] Z.W. He, D.J. Miller, S. Kasemset, L. Wang, D.R. Paul, B.D. Freeman, Fouling propensity of a poly(vinylidene fluoride) microfiltration membrane to several model oil/water emulsions, *Journal of Membrane Science*, 514 (2016) 659-670.
- [83] Z. He, D.J. Miller, S. Kasemset, D.R. Paul, B.D. Freeman, The effect of permeate flux on membrane fouling during microfiltration of oily water, *Journal of Membrane Science*, 525 (2017) 25-34.

- [84] E.N. Tummons, V.V. Tarabara, Jia W. Chew, A.G. Fane, Behavior of oil droplets at the membrane surface during crossflow microfiltration of oil–water emulsions, *Journal of Membrane Science*, 500 (2016) 211-224.
- [85] Z. He, S. Kasemset, A.Y. Kirschner, Y.-H. Cheng, D.R. Paul, B.D. Freeman, The effects of salt concentration and foulant surface charge on hydrocarbon fouling of a poly(vinylidene fluoride) microfiltration membrane, *Water Research*, 117 (2017) 230-241.
- [86] M.B. Tanis-Kanbur, S. Veliöglu, H.J. Tanudjaja, X. Hu, J.W. Chew, Understanding membrane fouling by oil-in-water emulsion via experiments and molecular dynamics simulations, *Journal of Membrane Science*, 566 (2018) 140-150.
- [87] T.A. Trinh, W. Li, Q. Han, X. Liu, A.G. Fane, J.W. Chew, Analyzing external and internal membrane fouling by oil emulsions via 3D optical coherence tomography, *Journal of Membrane Science*, 548 (2018) 632-640.
- [88] S.J. Maguire-Boyle, A.R. Barron, A new functionalization strategy for oil/water separation membranes, *Journal of Membrane Science*, 382 (2011) 107-115.
- [89] N. Maximous, G. Nakhla, W. Wan, Comparative assessment of hydrophobic and hydrophilic membrane fouling in wastewater applications, *Journal of Membrane Science*, 339 (2009) 93-99.
- [90] B. Chakrabarty, A.K. Ghoshal, M.K. Purkait, Cross-flow ultrafiltration of stable oil-in-water emulsion using polysulfone membranes, *Chemical Engineering Journal*, 165 (2010) 447-456.
- [91] W.J. Chen, J.M. Peng, Y.L. Su, L.L. Zheng, L.J. Wang, Z.Y. Jiang, Separation of oil/water emulsion using Pluronic F127 modified polyethersulfone ultrafiltration membranes, *Separation and Purification Technology*, 66 (2009) 591-597.
- [92] N.A. Ochoa, M. Masuelli, J. Marchese, Effect of hydrophilicity on fouling of an emulsified oil wastewater with PVDF/PMMA membranes, *Journal of Membrane Science*, 226 (2003) 203-211.
- [93] Y. Zhan, S. He, X. Wan, S. Zhao, Y. Bai, Thermally and chemically stable poly(arylene ether nitrile)/halloysite nanotubes intercalated graphene oxide nanofibrous composite membranes for highly efficient oil/water emulsion separation in harsh environment, *Journal of Membrane Science*, 567 (2018) 76-88.
- [94] J. Wang, L.a. Hou, K. Yan, L. Zhang, Q.J. Yu, Polydopamine nanocluster decorated electrospun nanofibrous membrane for separation of oil/water emulsions, *Journal of Membrane Science*, 547 (2018) 156-162.

- [95] X. Li, H. Shan, M. Cao, B. Li, Mussel-inspired modification of PTFE membranes in a miscible THF-Tris buffer mixture for oil-in-water emulsions separation, *Journal of Membrane Science*, 555 (2018) 237-249.
- [96] Y. Hou, R. Li, J. Liang, Superhydrophilic nickel-coated meshes with controllable pore size prepared by electrodeposition from deep eutectic solvent for efficient oil/water separation, *Separation and Purification Technology*, 192 (2018) 21-29.
- [97] J. Li, Y. Long, C. Xu, H. Tian, Y. Wu, F. Zha, Continuous, high-flux and efficient oil/water separation assisted by an integrated system with opposite wettability, *Applied Surface Science*, 433 (2018) 374-380.
- [98] J. Mulder, M. Mulder, *Basic Principles of Membrane Technology*, Kluwer Acad. Publ., 2010.
- [99] J.K. Koh, Y.W. Kim, S.H. Ahn, B.R. Min, J.H. Kim, Antifouling Poly(vinylidene fluoride) Ultrafiltration Membranes Containing Amphiphilic Comb Polymer Additive, *Journal of Polymer Science Part B-Polymer Physics*, 48 (2010) 183-189.
- [100] J. Mansouri, S. Harrisson, V. Chen, Strategies for controlling biofouling in membrane filtration systems: challenges and opportunities, *Journal of Materials Chemistry*, 20 (2010) 4567-4586.
- [101] X. Hu, E. Bekassy-Molnar, G. Vatai, Analysis and characterization of membrane fouling of ultrafiltration separation for oil-in-water emulsion, *Chemical Papers-Chemicke Zvesti*, 57 (2003) 16-20.
- [102] R.J. Zhang, S.L. Yu, W.X. Shi, J.Y. Tian, L.M. Jin, B. Zhang, L. Li, Z.Q. Zhang, Optimization of a membrane cleaning strategy for advanced treatment of polymer flooding produced water by nanofiltration, *Rsc Advances*, 6 (2016) 28844-28853.
- [103] R.S. Juang, K.H. Lin, Flux recovery in the ultrafiltration of suspended solutions with ultrasound, *Journal of Membrane Science*, 243 (2004) 115-124.
- [104] S. Adham, A. Hussain, J. Minier-Matar, A. Janson, R. Sharma, Membrane applications and opportunities for water management in the oil & gas industry, *Desalination*, 440 (2018) 2-17.
- [105] R. Rautenbach, R. Albrecht, *Membrane Processes*, John Wiley & Sons Ltd, New York, 1989.
- [106] F.L. Wang, V.V. Tarabara, Coupled effects of colloidal deposition and salt concentration polarization on reverse osmosis membrane performance, *Journal of Membrane Science*, 293 (2007) 111-123.

- [107] T. Darvishzadeh, V.V. Tarabara, N.V. Priezjev, Oil droplet behavior at a pore entrance in the presence of crossflow: Implications for microfiltration of oil–water dispersions, *Journal of Membrane Science*, 447 (2013) 442-451.
- [108] T. Darvishzadeh, N.V. Priezjev, Effects of crossflow velocity and transmembrane pressure on microfiltration of oil-in-water emulsions, *Journal of Membrane Science*, 423-424 (2012) 468-476.
- [109] W. Zhou, S. Li, Y. Liu, Z. Xu, S. Wei, G. Wang, J. Lian, Q. Jiang, Dual Superlyophobic Copper Foam with Good Durability and Recyclability for High Flux, High Efficiency, and Continuous Oil–Water Separation, *ACS Applied Materials & Interfaces*, 10 (2018) 9841-9848.
- [110] Q. Chang, J.-e. Zhou, Y. Wang, J. Liang, X. Zhang, S. Cerneaux, X. Wang, Z. Zhu, Y. Dong, Application of ceramic microfiltration membrane modified by nano-TiO₂ coating in separation of a stable oil-in-water emulsion, *Journal of Membrane Science*, 456 (2014) 128-133.
- [111] S.G. Yiantsios, A.J. Karabelas, An assessment of the Silt Density Index based on RO membrane colloidal fouling experiments with iron oxide particles, *Desalination*, 151 (2003) 229-238.
- [112] C.-H. Wei, S. Laborie, R. Ben Aim, G. Amy, Full utilization of silt density index (SDI) measurements for seawater pre-treatment, *Journal of Membrane Science*, 405-406 (2012) 212-218.
- [113] N. Ghaffour, F. Wali, G.L. Amy, Assessment of silt density index (SDI) as fouling propensity parameter in reverse osmosis (RO) desalination systems AU - Rachman, R.M., *Desalination and Water Treatment*, 51 (2013) 1091-1103.
- [114] A. Alhadidi, A.J.B. Kemperman, J.C. Schippers, M. Wessling, W.G.J. van der Meer, The influence of membrane properties on the Silt Density Index, *Journal of Membrane Science*, 384 (2011) 205-218.
- [115] J.C. Schippers, J. Verdouw, Modified fouling index, a method of determining the fouling characteristics of water, *Desalination*, 32 (1980) 137-148.
- [116] J.S. Choi, T.M. Hwang, S. Lee, S. Hong, A systematic approach to determine the fouling index for a RO/NF membrane process, *Desalination*, 238 (2009) 117-127.
- [117] F. Zamani, H.J. Tanudjaja, E. Akhondi, W.B. Krantz, A.G. Fane, J.W. Chew, Flow-field mitigation of membrane fouling (FMMF) via manipulation of the convective flow in cross-flow membrane applications, *Journal of Membrane Science*, 526 (2017) 377-386.

- [118] H.J. Tanudjaja, V.V. Tarabara, A.G. Fane, J.W. Chew, Effect of cross-flow velocity, oil concentration and salinity on the critical flux of an oil-in-water emulsion in microfiltration, *Journal of Membrane Science*, 530 (2017) 11-19.
- [119] H.J. Tanudjaja, W. Pee, A.G. Fane, J.W. Chew, Effect of spacer and crossflow velocity on the critical flux of bidisperse suspensions in microfiltration, *Journal of Membrane Science*, 513 (2016) 101-107.
- [120] F. Zamani, A. Ullah, E. Akhondi, H.J. Tanudjaja, E.R. Cornelissen, A. Honciuc, A.G. Fane, J.W. Chew, Impact of the surface energy of particulate foulants on membrane fouling, *Journal of Membrane Science*, 510 (2016) 101-111.
- [121] F. Wicaksana, A.G. Fane, P. Pongpairoj, R.W. Field, Microfiltration of algae (*Chlorella sorokiniana*): Critical flux, fouling and transmission, *Journal of Membrane Science*, 387–388 (2012) 83-92.
- [122] Y.P. Zhang, A.G. Fane, A.W.K. Law, Critical flux and particle deposition of fractal flocs during crossflow microfiltration, *Journal of Membrane Science*, 353 (2010) 28-35.
- [123] Y.P. Zhang, A.G. Fane, A.W.K. Law, Critical flux and particle deposition of bidisperse suspensions during crossflow microfiltration, *Journal of Membrane Science*, 282 (2006) 189-197.
- [124] P.R. Neal, H. Li, A.G. Fane, D.E. Wiley, The effect of filament orientation on critical flux and particle deposition in spacer-filled channels, *Journal of Membrane Science*, 214 (2003) 165-178.
- [125] H. Li, A.G. Fane, H.G.L. Coster, S. Vigneswaran, Observation of deposition and removal behaviour of submicron bacteria on the membrane surface during crossflow microfiltration, *Journal of Membrane Science*, 217 (2003) 29-41.
- [126] H. Li, A.G. Fane, H.G.L. Coster, S. Vigneswaran, An assessment of depolarisation models of crossflow microfiltration by direct observation through the membrane, *Journal of Membrane Science*, 172 (2000) 135-147.
- [127] H. Li, A.G. Fane, H.G.L. Coster, S. Vigneswaran, Direct observation of particle deposition on the membrane surface during crossflow microfiltration, *Journal of Membrane Science*, 149 (1998) 83-97.
- [128] H.J. Tanudjaja, M.B. Tanis-Kanbur, V.V. Tarabara, A.G. Fane, J.W. Chew, Striping phenomenon during cross-flow microfiltration of oil-in-water emulsions, *Separation and Purification Technology*, 207 (2018) 514-522.
- [129] H.J. Tanudjaja, J.W. Chew, Assessment of oil fouling by oil-membrane interaction energy analysis, *Journal of Membrane Science*, 560 (2018) 21-29.

- [130] E.N. Tummons, J.W. Chew, A.G. Fane, V.V. Tarabara, Ultrafiltration of saline oil-in-water emulsions stabilized by an anionic surfactant: Effect of surfactant concentration and divalent counterions, *Journal of Membrane Science*, 537 (2017) 384-395.
- [131] A. Subramani, X. Huang, E.M.V. Hoek, Direct observation of bacterial deposition onto clean and organic-fouled polyamide membranes, *Journal of Colloid and Interface Science*, 336 (2009) 13-20.
- [132] P.Z. Culfaz, M. Haddad, M. Wessling, R.G.H. Lammertink, Fouling behavior of microstructured hollow fibers in cross-flow filtrations: Critical flux determination and direct visual observation of particle deposition, *Journal of Membrane Science*, 372 (2011) 210-218.
- [133] W.D. Mores, R.H. Davis, Direct visual observation of yeast deposition and removal during microfiltration, *Journal of Membrane Science*, 189 (2001) 217-230.
- [134] S. Chang, A.G. Fane, Characteristics of microfiltration of suspensions with inter-fiber two-phase flow, *Journal of Chemical Technology & Biotechnology*, 75 (2000) 533-540.
- [135] D.W. R.W. Field, J.A. Howell, B.B. Gupta, Critical flux concept for microfiltration fouling, *Journal of Membrane Science*, 100 (1995) 259-272.
- [136] Y. Gao, S. Haavisto, C.Y. Tang, J. Salmela, W. Li, Characterization of fluid dynamics in spacer-filled channels for membrane filtration using Doppler optical coherence tomography, *Journal of Membrane Science*, 448 (2013) 198-208.
- [137] C. Dreszer, A.D. Wexler, S. Drusová, T. Overdijk, A. Zwijnenburg, H.C. Flemming, J.C. Kruithof, J.S. Vrouwenvelder, In-situ biofilm characterization in membrane systems using Optical Coherence Tomography: Formation, structure, detachment and impact of flux change, *Water Research*, 67 (2014) 243-254.
- [138] M. Xie, H.K. Shon, S.R. Gray, M. Elimelech, Membrane-based processes for wastewater nutrient recovery: Technology, challenges, and future direction, *Water Res.*, 89 (2016) 210-221.
- [139] M. Cheryan, N. Rajagopalan, Membrane processing of oily streams. Wastewater treatment and waste reduction, *J. Membr. Sci.*, 151 (1998) 13-28.
- [140] M. Padaki, R.S. Murali, M.S. Abdullah, N. Misdan, A. Moslehyani, M. Kassim, N. Hilal, A. Ismail, Membrane technology enhancement in oil–water separation: A review, *Desalination*, 357 (2015) 197-207.
- [141] N.M. Daud, S.R.S. Abdullah, H.A. Hasan, Z. Yaakob, Production of biodiesel and its wastewater treatment technologies: A review, *Process Saf. Environ.*, 94 (2015) 487-508.

- [142] S. Madaeni, A. Gheshlaghi, F. Rekabdar, Membrane treatment of oily wastewater from refinery processes, *Asia-Pac. J. Chem. Eng.*, 8 (2013) 45-53.
- [143] D. Wandera, S.R. Wickramasinghe, S.M. Husson, Modification and characterization of ultrafiltration membranes for treatment of produced water, *J. Membr. Sci.*, 373 (2011) 178-188.
- [144] S. Jiménez, M. Micó, M. Arnaldos, F. Medina, S. Contreras, State of the art of produced water treatment, *Chemosphere*, 192 (2018) 186-208.
- [145] P. Raffa, A.A. Broekhuis, F. Picchioni, Polymeric surfactants for enhanced oil recovery: A review, *J. Petrol. Sci. Eng.*, 145 (2016) 723-733.
- [146] S. Weschenfelder, M. Fonseca, B. Costa, C. Borges, Influence of the use of surfactants in the treatment of produced water by ceramic membranes, *J. Water Process Eng.*, 32 (2019) 100955.
- [147] J.M. Dickhout, J. Moreno, P. Biesheuvel, L. Boels, R.G. Lammertink, W.M. de Vos, Produced water treatment by membranes: A review from a colloidal perspective, *J. Colloid Interface Sci.*, 487 (2017) 523-534.
- [148] E. Tummons, H. Qi, H.J. Tanudjaja, C.A. Hejase, J.W. Chew, V.V. Tarabara, Membrane fouling by emulsified oil: A review, *Sep. Purif. Technol.*, (2020) 116919.
- [149] Z. Mai, V. Butin, M. Rakib, H. Zhu, M. Rabiller-Baudry, E. Couallier, Influence of bulk concentration on the organisation of molecules at a membrane surface and flux decline during reverse osmosis of an anionic surfactant, *J. Membr. Sci.*, 499 (2016) 257-268.
- [150] D. Lu, L. Dongwei, Z. Tao, M. Jun, Ceramic membrane fouling during ultrafiltration of oil/water emulsions: Roles played by stabilization surfactants of oil droplets, *Environ. Sci. Technol.*, 49 (2015) 4235-4244.
- [151] X. Zhu, A. Dudchenko, X. Gu, D. Jassby, Surfactant-stabilized oil separation from water using ultrafiltration and nanofiltration, *J. Membr. Sci.*, 529 (2017) 159-169.
- [152] J.M. Dickhout, E. Virga, R.G. Lammertink, W.M. de Vos, Surfactant specific ionic strength effects on membrane fouling during produced water treatment, *J. Colloid Interface Sci.*, 556 (2019) 12-23.
- [153] H. Nagasawa, T. Omura, T. Asai, M. Kanezashi, T. Tsuru, Filtration of surfactant-stabilized oil-in-water emulsions with porous ceramic membranes: Effects of membrane pore size and surface charge on fouling behavior, *J. Membr. Sci.*, (2020) 118210.

- [154] E. Virga, B. Bos, P. Biesheuvel, A. Nijmeijer, W.M. de Vos, Surfactant-dependent critical interfacial tension in silicon carbide membranes for produced water treatment, *J. Colloid Interface Sci.*, (2020).
- [155] Y.-M. Lin, G.C. Rutledge, Separation of oil-in-water emulsions stabilized by different types of surfactants using electrospun fiber membranes, *J. Membr. Sci.*, 563 (2018) 247-258.
- [156] M.B. Tanis-Kanbur, S. Veliöglu, H.J. Tanudjaja, X. Hu, J.W. Chew, Understanding membrane fouling by oil-in-water emulsion via experiments and molecular dynamics simulations, *J. Membr. Sci.*, 566 (2018) 140-150.
- [157] E.N. Tummons, V.V. Tarabara, Jia W. Chew, A.G. Fane, Behavior of oil droplets at the membrane surface during crossflow microfiltration of oil–water emulsions, *J. Membr. Sci.*, 500 (2016) 211-224.
- [158] E.N. Tummons, J.W. Chew, A.G. Fane, V.V. Tarabara, Ultrafiltration of saline oil-in-water emulsions stabilized by an anionic surfactant: Effect of surfactant concentration and divalent counterions, *J. Membr. Sci.*, 537 (2017) 384-395.
- [159] H.J. Tanudjaja, M.B. Tanis-Kanbur, V.V. Tarabara, A.G. Fane, J.W. Chew, Striping phenomenon during cross-flow microfiltration of oil-in-water emulsions, *Sep. Purif. Technol.*, 207 (2018) 514-522.
- [160] H.J. Tanudjaja, J.W. Chew, Assessment of oil fouling by oil-membrane interaction energy analysis, *J. Membr. Sci.*, 560 (2018) 21-29.
- [161] E.N. Tummons, C.A. Hejase, Z. Yang, J.W. Chew, M.L. Bruening, V.V. Tarabara, Oil droplet behavior on model nanofiltration membrane surfaces under conditions of hydrodynamic shear and salinity, *J. Colloid Interface Sci.*, 560 (2020) 247-259.
- [162] P. Venkataraman, J. Tang, E. Frenkel, G.L. McPherson, J. He, S.R. Raghavan, V. Kolesnichenko, A. Bose, V.T. John, Attachment of a hydrophobically modified biopolymer at the oil–water interface in the treatment of oil spills, *ACS Appl. Mater. Interfaces*, 5 (2013) 3572-3580.
- [163] B.J. Place, M.J. Perkins, E. Sinclair, A.L. Barsamian, Trace analysis of surfactants in Corexit oil dispersant formulations and seawater, *Deep-Sea Res. II*, 129 (2016) 273-281.
- [164] S. Kucuk, Membrane filtration of crude oil emulsions stabilized by corexit 9500 dispersant, Michigan State University. Environmental Engineering, 2018.
- [165] H. Li, A.G. Fane, H.G.L. Coster, S. Vigneswaran, Direct observation of particle deposition on the membrane surface during crossflow microfiltration, *J. Membr. Sci.*, 149 (1998) 83-97.

- [166] J.M. Dickhout, J.M. Kleijn, R.G.H. Lammertink, W.M. de Vos, Adhesion of emulsified oil droplets to hydrophilic and hydrophobic surfaces - effect of surfactant charge, surfactant concentration and ionic strength, *Soft Matter*, 14 (2018) 5452-5460.
- [167] Z. He, S. Kasemset, A.Y. Kirschner, Y.-H. Cheng, D.R. Paul, B.D. Freeman, The effects of salt concentration and foulant surface charge on hydrocarbon fouling of a poly(vinylidene fluoride) microfiltration membrane, *Water Res.*, 117 (2017) 230-241.
- [168] H.J. Tanudjaja, V.V. Tarabara, A.G. Fane, J.W. Chew, Effect of cross-flow velocity, oil concentration and salinity on the critical flux of an oil-in-water emulsion in microfiltration, *J. Membr. Sci.*, 530 (2017) 11-19.
- [169] N.G.P. Chew, S. Zhao, C.H. Loh, N. Permogorov, R. Wang, Surfactant effects on water recovery from produced water via direct-contact membrane distillation, *J. Membr. Sci.*, 528 (2017) 126-134.
- [170] M.L. Corrin, W.D. Harkins, The effect of salts on the critical concentration for the formation of micelles in colloidal electrolytes, *JACS*, 69 (1947) 683-688.
- [171] H. Iyota, T. Tomimitsu, M. Aratono, Miscibility of calcium chloride and sodium dodecyl sulfate in the adsorbed film and aggregates, *Colloid Polym. Sci.* 288 (2010) 1313-1320.
- [172] P. Somasundaran, K.P. Ananthapadmanabhan, M.S. Celik, E.D. Manev, A thermodynamic model of redissolution of calcium sulfonate precipitates in NaCl solutions, *Soc. Petrol. Eng. J.*, 24 (1984) 667-676.
- [173] K.L. Stellner, J.F. Scamehorn, Surfactant precipitation in aqueous solutions containing mixtures of anionic and nonionic surfactants, *J. AM. Chem. Soc.*, 63 (1986) 566-574.
- [174] K.C. Powell, A. Chauhan, Dynamic interfacial tension and dilational rheology of dispersant Corexit 9500, *Colloid Surface A*, 497 (2016) 352-361.
- [175] J. Keurentjes, M.C. Stuart, D. Brinkman, C. Schroën, K. Van't Riet, Surfactant-induced wetting transitions: role of surface hydrophobicity and effect on oil permeability of ultrafiltration membranes, *Colloid Surface*, 51 (1990) 189-205.
- [176] R. Pichot, F. Spyropoulos, I. Norton, Competitive adsorption of surfactants and hydrophilic silica particles at the oil–water interface: Interfacial tension and contact angle studies, *J. Colloid Interface Sci.*, 377 (2012) 396-405.
- [177] M. Çakmakce, N. Kayaalp, I. Koyuncu, Desalination of produced water from oil production fields by membrane processes, *Desalination*, 222 (2008) 176-186.

- [178] J. Veil, U.S. Produced Water Volumes and Management Practices in 2012, in, Prepared for the Ground Water Protection Council, 2015.
- [179] J.A. Veil, M.G. Puder, D. Elcock, R.J.J. Redweik, A white paper describing produced water from production of crude oil, natural gas, and coal bed methane, in, 2004.
- [180] J.M. Neff, Bioaccumulation in Marine Organisms: Effect of Contaminants from Oil Well Produced Water, Elsevier, 2002.
- [181] TORR Canada's presentation, in: 14th International Petroleum Environmental Conference, Houston Texas, 2007.
- [182] M. Padaki, R.S. Murali, M.S. Abdullah, N. Misdan, A. Moslehyani, M.A. Kassim, N. Hilal, A.F. Ismail, Membrane technology enhancement in oil-water separation. A review, *Desalination*, 357 (2015) 197-207.
- [183] H.J. Tanudjaja, C.A. Hejase, V.V. Tarabara, A.G. Fane, J.W. Chew, Membrane-based separation for oily wastewater: A practical perspective, *Water Res.*, 156 (2019) 347-365.
- [184] Y.K. Kharaka, J.J. Thordsen, A. G., Environmental degradation associated with exploration for a production of energy sources in USA, in: Y.K.K.a. O.V., Chudaev (Eds.) *Water-Rock Interaction*, Rotterdam, 1995, pp. 25-30.
- [185] T. Frankiewicz, Understanding the fundamentals of water treatment. The dirty dozen - 12 common causes of poor water quality, in: 11th Produced Water Seminar, Houston, TX, 2001.
- [186] F.I.-R. Ahmadun, A. Pendashteh, L.C. Abdullah, D.R.A. Biak, S.S. Madaeni, Z.Z. Abidin, Review of technologies for oil and gas produced water treatment, *J. Haz. Mater.*, 170 (2009) 530-551.
- [187] A. Salahi, A. Gheshlaghi, T. Mohammadi, S.S. Madaeni, Experimental performance evaluation of polymeric membranes for treatment of an industrial oily wastewater, *Desalination*, 262 (2010) 235-242.
- [188] V. Singh, M.K. Purkait, C. Das, Cross-flow microfiltration of industrial oily wastewater: Experimental and theoretical consideration, *Sep. Sci. Technol.*, 46 (2011) 1213-1223.
- [189] M.H. Al-Malack, Treatment of petroleum refinery wastewater using crossflow and immersed membrane processes, *Desalin. Water Treat.*, 51 (2013) 6985-6993.
- [190] J. Zhong, X.J. Sun, C.L. Wang, Treatment of oily wastewater produced from refinery processes using flocculation and ceramic membrane filtration, *Sep. Purif. Technol.*, 32 (2003) 93-98.

- [191] R.J. Lahiere, K.P. Goodboy, Ceramic membrane treatment of petrochemical wastewater *Environ. Prog.*, 12 (1993) 86-96.
- [192] Y.S. Li, L. Yan, C.B. Xiang, L.J. Hong, Treatment of oily wastewater by organic-inorganic composite tubular ultrafiltration (UF) membranes, *Desalination*, 196 (2006) 76-83.
- [193] A. Deriszadeh, M.M. Husein, T.G. Harding, Produced water treatment by micellar-enhanced ultrafiltration, *Environ. Sci. Technol.*, 44 (2010) 1767-1772.
- [194] E.N. Tummons, V.V. Tarabara, J.W. Chew, A.G. Fane, Behavior of oil droplets at the membrane surface during crossflow microfiltration of oil-water emulsions, *J. Membr. Sci.*, 500 (2016) 211-224.
- [195] D. Lu, T. Zhang, J. Ma, Ceramic membrane fouling during ultrafiltration of oil/water emulsions: Roles played by stabilization surfactants of oil droplets, *Environ. Sci. Technol.*, 49 (2015) 4235-4244.
- [196] G. Fux, G.Z. Ramon, Microscale dynamics of oil droplets at a membrane surface: Deformation, reversibility, and implications for fouling, *Environ. Sci. Technol.*, 51 (2017) 13842-13849.
- [197] A. Ullah, V.M. Starov, M. Naeem, R.G. Holdich, Microfiltration of deforming oil droplets on a slotted pore membrane and sustainable flux rates, *J. Membr. Sci.*, 382 (2011) 271-277.
- [198] T. Darvishzadeh, V.V. Tarabara, N.V. Priezjev, Oil droplet behavior at a pore entrance in the presence of crossflow: Implications for microfiltration of oil-water dispersions, *J. Membr. Sci.*, 447 (2013) 442-451.
- [199] B. Chakrabarty, A.K. Ghoshal, M.K. Purkait, Ultrafiltration of stable oil-in-water emulsion by polysulfone membrane, *J. Membr. Sci.*, 325 (2008) 427-437.
- [200] B. Chakrabarty, A.K. Ghoshal, M.K. Purkait, Cross-flow ultrafiltration of stable oil-in-water emulsion using polysulfone membranes, *Chem. Eng. J.*, 165 (2010) 447-456.
- [201] B.K. Nandi, R. Uppaluri, M.K. Purkait, Microfiltration of stable oil-in-water emulsions using kaolin based ceramic membrane and evaluation of fouling mechanism, *Desalin. Water Treat.*, 22 (2010) 133-145.
- [202] A. Rahimpour, B. Rajaeian, A. Hosienzadeh, S.S. Madaeni, F. Ghoreishi, Treatment of oily wastewater produced by washing of gasoline reserving tanks using self-made and commercial nanofiltration membranes, *Desalination*, 265 (2011) 190-198.
- [203] A. Orecki, M. Tomaszewska, The oily wastewater treatment using the nanofiltration process, *Pol. J. Chem. Technol.*, 9 (2007) 40-42.

- [204] S. Mondal, S.R. Wickramasinghe, Produced water treatment by nanofiltration and reverse osmosis membranes, *J. Membr. Sci.*, 322 (2008) 162-170.
- [205] B.D. McCloskey, H.B. Park, H. Ju, B.W. Rowe, D.J. Miller, B.D. Freeman, A bioinspired fouling-resistant surface modification for water purification membranes, *J. Membr. Sci.*, 413 (2012) 82-90.
- [206] R. Muppalla, S.K. Jewrajka, A. Reddy, Fouling resistant nanofiltration membranes for the separation of oil–water emulsion and micropollutants from water, *Sep. Purif. Technol.*, 143 (2015) 125-134.
- [207] A. Vu, N.S. Mark, G.Z. Ramon, X. Qian, A. Sengupta, S.R. Wickramasinghe, Oil deposition on polymer brush-coated NF membranes, *Membranes*, 9 (2019) 168.
- [208] E.N. Tummons, C.A. Hejase, Z. Yang, J.W. Chew, M.L. Bruening, V.V. Tarabara, Oil droplet behavior on model nanofiltration membrane surfaces under conditions of hydrodynamic shear and salinity, *J. Colloid Interface Sci.*, 560 (2019) 247-259.
- [209] E.M.V. Hoek, A.S. Kim, M. Elimelech, Influence of crossflow membrane filter geometry on colloidal fouling of reverse osmosis membranes, *Environ. Eng. Sci.*, 19 (2002) 357-372.
- [210] E.M.V. Hoek, M. Elimelech, Cake-enhanced concentration polarization: A new fouling mechanism for salt-rejecting membranes, *Environ. Sci. Technol.*, 37 (2003) 5581-5588.
- [211] A. Azaïs, J. Mendret, E. Petit, S. Brosillon, Evidence of solute-solute interactions and cake enhanced concentration polarization during removal of pharmaceuticals from urban wastewater by nanofiltration, *Water Res.*, 104 (2016) 156-167.
- [212] F. Wang, V.V. Tarabara, Coupled effects of colloidal deposition and salt concentration polarization on reverse osmosis membrane performance, *J. Membr. Sci.*, 293 (2007) 111-123.
- [213] A.S. Kim, H. Chen, Diffusive tortuosity factor of solid and soft cake layers: A random walk simulation approach, *J. Membr. Sci.*, 279 (2006) 129-139.
- [214] J. Mulder, *Basic Principles of Membrane Technology*, Springer Science & Business Media, 2012.
- [215] R. Rautenbach, *Membrane Processes*, John Wiley & Sons Ltd., New York, 1989.
- [216] W. Shan, P. Bacchin, P. Aimar, M.L. Bruening, V.V. Tarabara, Polyelectrolyte multilayer films as backflushable nanofiltration membranes with tunable hydrophilicity and surface charge, *J. Membr. Sci.*, 349 (2010) 268-278.[217] K.S. Spiegler, O. Kedem,

Thermodynamics of hyperfiltration (reverse osmosis): criteria for efficient membranes, *Desalination*, 1 (1966) 311.

[218] F.F. Nazzal, M.R. Wiesner, Microfiltration of oil-in-water emulsions, *Water Environ. Res.*, 68 (1996) 1187-1191.

[219] E.N. Tummons, H. Qi, H. Tanudjaja, C.A. Hejase, J.W. Chew, V.V. Tarabara, Membrane fouling by emulsified oil: A review, *Separ. Purif. Technol.* , Accepted (2020).

[220] O. Kedem, V. Freger, Determination of concentration-dependent transport coefficients in nanofiltration: Defining an optimal set of coefficients, *J. Membr. Sci.*, 310 (2008) 586-593.

[221] S. Bason, O. Kedem, V. Freger, Determination of concentration-dependent transport coefficients in nanofiltration: Experimental evaluation of coefficients, *J. Membr. Sci.*, 326 (2009) 197-204.

[222] Y. Boussouga, A. Lhassani, Study of mass transfer mechanisms for reverse osmosis and nanofiltration membranes intended for desalination, *J. Environ. Sci.*, 8 (2017) 1128-1138.

[223] R. Nair, E. Protasova, S. Strand, T. Bilstad, Implementation of Spiegler–Kedem and steric hindrance pore models for analyzing nanofiltration membrane performance for smart water production, *Membranes*, 8 (2018) 78.

[224] M. Fingas, *The basics of oil spill cleanup*, CRC press, 2012.

[225] J. Michel, M. Fingas, Oil Spills: Causes, consequences, prevention, and countermeasures, in: *Fossil Fuels: Current Status and Future Directions*, World Scientific, 2016, pp. 159-201.

[226] N.P. Ventikos, F.S. Sotiropoulos, Disutility analysis of oil spills: Graphs and trends, *Mar. Pollut. Bull.*, 81 (2014) 116-123.

[227] A. Zwickle, K. Jones, Sustainability knowledge and attitudes: Assessing latent constructs, in: *Handbook of sustainability and social science research*, Springer, 2018, pp. 435-451.

[228] T.A. Arcury, T.P. Johnson, Public environmental knowledge: A statewide survey, *J. Environ. Educ.*, 18 (1987) 31-37.

[229] J.C. Bradley, T.M. Waliczek, J.M. Zajicek, Relationship between environmental knowledge and environmental attitude of high school students, *J. Environ. Educ.*, 30 (1999) 17-21.

- [230] P.M. Tikka, M.T. Kuitunen, S.M. Tynys, Effects of educational background on students' attitudes, activity levels, and knowledge concerning the environment, *J. Environ. Educ.*, 31 (2000) 12-19.
- [231] J.J. Jenkins, Four points to remember: A tetrahedral model of memory experiments, 1979.
- [232] T.A. Satterfield, C. Mertz, P. Slovic, Discrimination, vulnerability, and justice in the face of risk, *Risk analysis: An international journal*, 24 (2004) 115-129.
- [233] F.M. Buttel, W.L. Flinn, The politics of environmental concern: The impacts of party identification and political ideology on environmental attitudes, *Environ. Behav.*, 10 (1978) 17-36.
- [234] A. Leiserowitz, Climate change risk perception and policy preferences: The role of affect, imagery, and values, *Climatic change*, 77 (2006) 45-72.
- [235] T. Dietz, A. Dan, R. Shwom, Support for climate change policy: Social psychological and social structural influences, *Rural Sociol.*, 72 (2007) 185-214.
- [236] A.M. McCright, R.E. Dunlap, C. Xiao, Perceived scientific agreement and support for government action on climate change in the USA, *Climatic Change*, 119 (2013) 511-518.
- [237] J.E. Aldy, M.J. Kotchen, A.A. Leiserowitz, Willingness to pay and political support for a US national clean energy standard, *Nat. Clim. Change*, 2 (2012) 596-599.